SINGHAL, RUCHI GUPTA. Transport Properties of Hectorite Based Nanocomposite Single-ion Conductors. (Under the direction of Dr. Peter S. Fedkiw and Dr. Saad A. Khan.)

Lithium-ion batteries are an important power source for small electronic technologies because of desirable characteristics including high-energy density, low weight, and excellent cycle performance. We investigated the electrochemical and rheological effects of clay nanocomposite fillers in lithium-ion battery electrolytes. Nanocomposite hectorite, a non-reactive smectite clay filler, was used in this study. Hectorite and other 2:1 layered clays (smectites) are unique in that they are characterized by a large negatively charged plate-like structure (~250-nm diameter) with exchangeable counter cations sandwiched between thin platelets (~1 nm). For lithium battery application, the native sodium cations on hectorite are exchanged for lithium ions and the plate-like particles are dispersed in high-dielectric solvents (e.g., ethylene carbonate (EC) and propylene carbonate (PC)) to create a physically gelled structure. The cation mobility is considerable relative to the mobility of the large anion clay platelets. Lithium-ion transference numbers of Li-hectorite in carbonate solvent have shown near unity values indicating efficient Li^+ movement in a cell.

Conductivity in our electrolytes is not as high as $LiPF_6$ liquid electrolytes used in today's market, however, we hypothesized that the addition of low-molecular weight polymer compounds would improve conductivity. Our objective was to show improved conductivity in Li-hectorite/ethylene carbonate electrolytes with the addition of polyethylene glycol di-methyl ether (PEG-dm, 250 MW). Several combinations of clay

and polymer loading are studied in an attempt to find an electrolyte with the highest conductivity. Finally, a preliminary comparison between hydroxyl terminated PEO (PEG) and PEG-dm as a polymer co-solvent with EC, is made with regards to rheological properties.

We find all samples to exhibit gel-like behavior with room temperature conductivities of order 0.1 mS/cm. A maximum in conductivity is observed with increasing clay concentration. A maximum in clay basal spacing is also observed in the same concentration range, suggesting a direct correlation between conductivity and basal spacing. G′ and yield stress increased by two orders of magnitude with increasing clay concentration and conductivity increased by one order of magnitude (from 5 to 25% clay), indicating clearly clay concentration to be the primary factor in determining the characteristics of these single ion conductors. Addition of PEG-dm to the base EC electrolyte shows moderate improvement in conductivity; the elastic modulus and yield stress also increase by a factor of three. Clay concentration had a dominating effect on all results including rheology results, when compared to solvent composition. PEG-dm electrolytes yielded a stronger gel sample when compared to PEG electrolytes. In addition, we found an interesting correlation between clay basal spacing and conductivity as a function of clay concentration.

TRANSPORT PROPERTIES OF HECTORITE BASED NANOCOMPOSITE SINGLE-ION CONDUCTORS

by

RUCHI GUPTA SINGHAL

A thesis submitted to the Graduate Faculty of
North Carolina Sate University
in partial fulfillment of the Degree of
Master of Science

DEPARTMENT OF CHEMICAL ENGINEERING

Raleigh
April 2003

APPROVED BY:

Dr. Peter S. Fedkiw
Chairman, Advisory Committee

Dr. Saad A. Khan
Co-Chairman, Advisory Committee

Dr. Jan Genzer

Biography

Ruchi Gupta Singhal, was born in Conyers, Georgia on May 29, 1978 to Dr. and Mrs. Rakesh and Rama Gupta. She received her secondary education in Conyers in the public schooling systems. She graduated as valedictorian of her class at Salem High School in June, 1996 and accepted two distinguished scholarships for her future education: Georgia HOPE Scholarship and Georgia Governor's Scholarship.

Ruchi began her studies as a chemical engineer at the Georgia Institute of Technology in October 1996, where she accepted an additional scholarship sponsored by AMD. While at Georgia Tech, the author experienced three summer internships, two with Hercules Inc. and one with Proctor and Gamble Inc., starting from 1996 to 1998. In the summer of 1999, she participated in a chemical engineering unit operation laboratory program in the University of London. During her senior year at Georgia Tech, she worked on an independent research project, under the guidance of Dr. Cliff Henderson, studying the effect of various salts on the dissolution of photoresist layers on semiconductor wafers. She was on the dean's list for all her years at Georgia Tech, and graduated in May, 2000 with high honors.

The author enrolled in the chemical engineering masters program at North Carolina State University in August, 2000. She was given the distinguished GAANN (Graduate Assistance in Areas of National Need) fellowship by the Department of Education and she won first place in the Schoenborn Poster Presentation, in November, 2002. Her master's thesis research was conducted under the advisement of Dr. Peter S. Fedkiw and Dr. Saad A. Khan.

Acknowledgements

I would like to thank my dear husband, Sameer Singhal, for his support throughout my graduate studies. He was extremely patient and helpful during the writing of this thesis. I would also like to thank my parents, Rakesh and Rama Gupta, for their guidance throughout my life and direction toward the field of science. I also want to thank Sameer's parents, Ashok and Sangeeta Singhal, for their insight and guidance. My friends have also been a great support for me namely, Aysa Akad, Arthi Jayaraman, Kathie Lee Burns and Tori Brannan. And a special thanks to all of the Fedkiw and Khan group members, especially Mike Riley, Jeff Yerian, Jian Zhou, and Angelica Sanchez.

I would like to thank Dr. Genzer and Dr. Martin, for their advice and expertise. A special thanks goes to my advisors, Dr. Peter S. Fedkiw and Dr. Saad A. Khan, who were kind enough to guide me through my master's research. Finally, I would like to thank the Department of Education for sponsoring me with the GAANN fellowship, without which I would not have been able to conduct my research.

Contents

List of Tables

List of Figures

Chapter 1: Introduction

1.1 Motivation of Research

Rechargeable lithium-ion batteries are an important component in today's small-electronics technology because of desirable characteristics that include high energy density, low weight, and excellent cycle performance. For instance, in 1997 alone, sales of lithium battery systems exceeded 200 billion dollars[1]. Because of governmental mandates for electric vehicles and the ever-increasing demand for portable power sources, lithium batteries are expected to grow more than 20% per year[2,3]. Lithium-ion batteries in particular are predicted to last the lifetime of a car because of their high energy and power density[4,5]. However, several factors in lithium-ion batteries, especially in the electrolyte, have limited commercial usage. Most lithium-ion batteries use a liquid electrolyte, which requires the use of a microporous polymeric membrane to separate the electrodes. As an alternative our group[6] is attempting to avoid a separator by using a gel electrolyte with high mechanical strength. These gel electrolytes must still possess comparable electrochemical properties to liquid electrolytes such as conductivity, lithium transference number, and electrode/electrolyte interfacial stability. The technological impact of developing an electrolyte with improved conductivity and strong mechanical strength is significant and warrants further exploration.

The study of composite polymer electrolytes (CPE) is increasing considerably because they possess desirable properties of both liquid and solid electrolytes. Nano-size fillers such as TiO_2, SiO_2, or Al_2O_3 have shown many advantageous effects on electrochemical properties, (e.g., conductivity and transference number) of CPEs[7-9]. The benefit of fillers when added to a liquid solvent is their ability to create a gel-like matrix

making an open-channel structure for ion transport. However, most fillers are passive, and contribute only to the battery electrolyte as a structural skeleton. We focus on an active filler, lithium-hectorite, where the nano-material participates in the ion-transport and improves mechanical strength.

Hectorite and other 2:1 layered clays (smectites) are unique in that they are characterized by a large negatively charged plate-like structure (~250-nm diameter) with exchangeable counter cations sandwiched between thin platelets (~1 nm). For lithium battery application, the native sodium cations on hectorite are exchanged for lithium ions and the plate-like particles are dispersed in high-dielectric solvents (e.g., ethylene carbonate (EC) and propylene carbonate (PC)) to create a physically gelled structure. The cation mobility is considerable relative to the mobility of the large anion clay platelets.

Lithium-ion transference numbers in carbonate solvents with hectorite were shown to be near unity, which indicates predominantly lithium-ion mobility[10]. Conductivity at room temperature, however, in these electrolytes is around 10^{-4} S/cm, whereas the conductivity in a typical non-polymeric Li-ion battery electrolyte ($LiPF_6$ + EC + PC) is around 10^{-2} S/cm. The use of high-molecular weight polyethylene oxide (PEO) has been shown to increase basal spacing of clay platelets[11], however, the ionic conductivity (10^{-6} S/cm) remains several orders of magnitude below non-polymer electrolytes. We intend to show that low-molecular weight methyl terminated PEO, polyethylene glycol di-methyl ether (PEG-dm), with a carbonate co-solvent and Li-hectorite will yield higher ionic conductivities than carbonate electrolytes without PEG-dm. Our hypothesis is that low-molecular weight PEG-dm (250 MW) will increase basal

spacing of the clay platelets, which will create channels for lithium ions to travel more freely through the electrolyte.

1.2 Objectives

The objective of this research is to investigate the effect of PEG-dm on conductivity, basal spacing of platelets, and rheological properties in hectorite/carbonate electrolytes. Conductivity is measured using impedance spectroscopy to quantify ion motion. The microscopic structure of hectorite clay platelets is analyzed using x-ray diffraction (XRD) to find platelet spacing after dispersion into solution. Rheological properties are investigated, in order to find the intrinsic mechanical properties, such as gel modulus and yield stress of the electrolyte. Several combinations of clay and polymer loading are studied in an attempt to find an electrolyte with the highest conductivity. Finally, a preliminary comparison between hydroxyl terminated PEO (PEG) and PEG-dm as a polymer co-solvent with EC is made with regards to rheological properties.

1.3 Outline of Thesis

Five chapters form this thesis: introduction, literature review, experimental materials and methods, results and discussion, and conclusions and recommendations. Following these chapters are three appendixes: the first addresses experimental methods used in making the electrolytes, the second discusses supplemental rheology experiments of Na-hectorite, and the third is an order of magnitude estimation of polymer coverage on hectorite platelets.

1.4 References

1. R. J. Brood, "Recent Developments in Batteries for Portable Consumer Electronics Applications", *Interface*, **8**, 20-23 (1999).

2. L. Xie, D. Fouchard, and S. Megahed *Material Requirements for Lithium-Ion Batteries*; Mater. Res. Soc. Symp. Proc.: San Francisco, CA, 1995; Vol. 393, pp 285-304.

3. A. Tether *Scientist Helping America*; http://safe.sysplan.com/scihelpamerica/ad.html, 2002.

4. L. Gaines and R. Cuenca "Costs of Lithium-Ion Batteries for Vehicles," Transportation Technology R&D Center, May 2000.

5. M. Wakihara, "Recent developments in lithium ion batteries", *Materials Science & Engineering R-Reports*, **33**, 109-134 (2001).

6. S. R. Raghavan, M. W. Riley, P. S. Fedkiw, and S. A. Khan, "Composite Polymer Electrolytes Based on Poly(ethylene glycol) and Hydrophobic Fumed Silica:Dynamic Rheology and Microstructure", *Chemistry of Materials*, **10**, 244-251 (1997).

7. Y. X. Li, P. S. Fedkiw, and S. A. Khan, "Lithium/V_6O_{13} cells using silica nanoparticle-based composite electrolyte", *Electrochimica Acta*, **47**, 3853-3861 (2002).

8. J. Fan, S. R. Raghavan, X. Y. Yu, S. A. Khan, P. S. Fedkiw, J. Hou, and G. L. Baker, "Composite polymer electrolytes using surface-modified fumed silicas: conductivity and rheology", *Solid State Ionics*, **111**, 117-123 (1998).

9. H. J. Walls, J. Zhou, J. A. Yerian, P. S. Fedkiw, S. A. Khan, M. K. Stowe, and G. L. Baker, "Fumed silica-based composite polymer electrolytes: synthesis, rheology, and electrochemistry", *Journal of Power Sources*, **89**, 156-162 (2000).

10. M. Riley, P. Fedkiw, and S. Khan, "Transport Properties of Lithium Hectorite-Based Composite Electrolytes", *Journal of Electrochemical Society*, (2001).

11. P. Aranda and E. Ruiz-Hitzky, "Poly(ethylene oxide)/NH^{4+}-smectite nanocomposites", *Applied Clay Science*, **15**, 119-135 (1999).

Chapter 2: Literature Review

2.1 Battery Background

2.1.1 Battery Basics

Batteries are a form of an electrochemical power source, which are noted for their energy efficiency when compared to other power sources. There are three types of electrochemical cells: primary, secondary, and fuel cells. In this chapter, we will focus on secondary cells, specifically rechargeable lithium batteries. Certain parameters are key in order to assess a battery: terminal voltage, cell discharge capacity, cycle life, and specific energy. Battery components also have important characteristics such as electrode interfacial reactivity and electrolyte conductivity[1].

The main components of a battery are a positive electrode (cathode), negative electrode (anode), and the electrolyte. The cathode is the electron acceptor, the anode is the electron donor, and the electrolyte is the medium for which these electrons, as ions travel. Complex oxides of lithium such as $LiCoO_2$, $LiNiO_2$, and $LiMn_2O_4$ are used as positive electrodes for lithium and lithium-ion batteries. Negative electrodes vary for lithium and lithium-ion batteries. Lithium batteries have lithium metal for the anode, and lithium-ion batteries have Li-intercalated carbon as the anode. The electrolyte is an especially important component of batteries because it serves as a channel for ion flow and isolates the electrodes from each other. Lithium-ion battery electrolyte is the focus of our study and will be discussed in detail in the next sections. Figure 2.1 is a schematic of a button cell configuration that contains an anode, cathode, electrolyte, plus other small components.

2.1.2 Secondary Batteries

Unlike primary batteries, secondary batteries have the unique property of returning to their original state of charge upon passing current in the opposite direction. Hence, these batteries are also known as storage or rechargeable batteries. Secondary batteries are used as an energy storage devices for aircraft engines, emergency power sources, and automotive systems) or rechargeable devices (i.e. cell phones batteries, laptop batteries, and electric vehicle batteries). In energy storage devices, a primary energy source charges the device, and the device then delivers its energy to the load on demand. Rechargeable batteries differ from primary batteries because they are usually operated until complete discharge and can be recharged instead of discarded. Energy densities are usually lower for secondary batteries as opposed to primary batteries; however, capacity that is lost when the battery is not in use can be regained by recharging[2].

Rechargeable batteries such as nickel-cadmium, nickel-metal hydride, lithium-ion, and lithium metal are valuable because of their portable nature and high energy density. Lithium metal batteries in particular show better performance than nickel or lead based devices[3]. In lithium metal batteries the negative electrode is lithium metal, the electrolyte is a non-aqueous solution, and the positive electrode is a complex matrix structure (usually a transition metal oxide) made to release and accept lithium ions[4]. Lithium-ion batteries have a unique negative electrode made of lithiated carbon. With a lithiated carbon anode, interfacial reactions that occur with lithium metal anodes do not occur; however, lithiated carbon is a reactive substance.

2.1.3 Nickel and Lead Based Rechargeable Batteries

Nickel-based battery electrolytes are quite different from those used for lithium batteries. These batteries are found in many motor driven applications, and consume much of the small battery market. In nickel-cadmium and nickel-metal hydride batteries, oxidation of nickel hydroxide is the charging reaction at the positive electrode. Charging at the negative electrode is different for both batteries. Potassium hydroxide, the main component of the electrolyte, is dissolved in water. These batteries are very sensitive to the concentration of KOH, and can suffer significant ohmic loss. Lead-acid batteries also have water-based electrolytes but also contain sulfuric acid which is needed for the reactions at the electrodes. Lead-acid batteries have the highest power densities among the aqueous batteries, however capacity is not at the desired level[5].

2.1.4 Lithium metal and Lithium-ion Batteries

The previously described batteries have unimpressive energy to weight ratios (Figure 2.2)[6]. Active material in nickel and lead based battery are a small fraction of the battery's total mass, and usually is not as "active" as one would desire. Because of this issue, lithium is an obvious choice for future secondary batteries. Lithium has high electrochemical potential and low atomic weight. The one major concern with lithium metal is it's extremely high reactivity. This issue adds difficulty in making the battery because the procedure would need to be done in a non-reactive environment (i.e. water-free). Another concern is the formation of dendrites on lithium metal upon cycling[7].

The benefits of lithium-ion batteries make it a growing market for secondary batteries. Their composite electrodes make them non-hazardous and their "rocking chair technology" (RCT) makes them unique. RCT is the concept of lithium ions traveling

back and forth between composite electrodes during charge and discharge. As can be expected, the media through which these ions travel is very important.

Organic liquid solvents are very common electrolyte components for lithium batteries. Ethylene carbonate (EC) and propylene carbonate (PC) are examples of organic solvents, as are tetrahydrofuran (THF) and 2-methyl- tetrahydrofuran (2Me-THF)[8]. Salts can be $LiAsF_6$, $LiPF_6$, $LiBF_4$, $LiClO_4$, and $Li(CF_3SO_2)_2N$. Protective films form from interactions of lithium with the organic electrolyte solutions. The protective film is a lithium ion conductor and electron insulator. Impurities such as H_2O, O_2, and CO_2 react with organic lithium compounds in the protective films to form Li_2CO_3, Li_2O_2, Li_2O, and LiOH. However, these films will not form on composite lithiated substrates.

Currently, electrochemical windows for lithium batteries using $LiMn_2O_4$ or similar cathodes are between 3 and 4 V. Electrolytes in these batteries are aprotic solvents with Li salts, polymers (such as polyethylene oxide (PEO) and its derivatives) with Li salts, and polymers with aprotic solvents and Li salts. All three of these electrolyte mixtures are viable alternatives in lithium metal batteries. Research[9] is being done on lithium-ion batteries with non-reactive mixtures and polymers co-solvents.

2.2 Polymer Electrolyte Background

It was observed by Fenton et al. [10] that polyethylene oxide (PEO) in conjunction with alkali salts gave high-ion mobility. There are many derivatives of PEO by changing the backbone and end-groups of a chain. For low-molecular weight polymers, end groups have an influence on various properties of the polymer. Polyethylene glycol dimethyl ether (PEG-dm) is one example of such a polymer, as it possesses methyl groups instead of OH groups as found in PEO. Oligomeric PEG-dm has shown[11]

promising conductivities in electrolytes with fumed silica and lithium salt. Polymers electrolytes have shown[12] an increase in the dissociation of ions in an electrolyte, thereby leading to increased ionic conductivity. The addition of PEO oligomers to an electrolyte also reduces the vapor pressure of the total solvent, which in turns reduces the volatility of the battery upon overcharge.

Transport properties such as conductivity, salt diffusion coefficient, and cationic transference number have been investigated for PEO based electrolytes. Doeff et al.[13,14] found salt concentration has an effect on these properties for various types of salt/polymer combinations. In Figure 2.3, we can see their conductivity (σ) and transference number (t_+^o) with varying salt concentration. The opposite trends seen by conductivity and transference numbers reflected that negatively charged ionic aggregates are relatively immobilized by the host matrix but cation transport does not improve.

Polymer electrolytes can function as both separator and electrolyte, which would improve the energy density, volume, and weight of the battery[15]. However, even with improved ion conductivities, a few drawbacks were noticed[16] in the PEO/salt complexes. Slow deformation of polymer (polymer creeping), leading to higher interfacial resistance at the electrodes, is one major concern in lithium batteries. Adding plasticizers or fine oxide particles has been one avenue taken to reduce polymer creeping. Addition of ceramic powders to polymer matrices has been done extensively in the past[17-20], and adding fillers to polymer electrolytes is the same concept; nano-size fillers like TiO_2, SiO_2, or Al_2O_3 have shown many positive electrochemical effects on polymer electrolytes.

Other negative issues with polymer electrolytes are crystallinity, ion-pair formation, and high mobility of anions. Polymer electrolytes are useful at temperatures above T_m to avoid crystalline phase. Forsyth et al. studied how to inhibit phase change of PEO-based complexes with the addition of TiO_2. They found conductivity reaches a maximum at an optimum amount of filler. They also found through ^7Li NMR measurements a change in the lithium-ion environment with addition of filler, as noted from the relaxation time (T_2)[21]. Figure 2.4 shows both conductivity and NMR results found by Forsyth et al. From their data, they noticed polymer segmental motion was enhanced with the addition of low filler, at high concentration of filler, the enhancement diminished. Fumed silica particles, SiO_2, are promising fillers for composite polymer electrolytes (CPE). Conductivity in these CPE's can be as high as liquid electrolytes, however diffusion measurements indicate interactions are taking place among lithium ions, polymer chains and silica[22,23].

Aranda and Ruiz-Hitzky [24] found intercalating PEO in smectite clay, such as hectorite, reduced the crystallinity of the electrolyte and exfoliated the clay platelets as found from X-ray diffractometry. Stronger interactions were seen between NH_4^+ cations and the polymer than alkali metal cations, such as Li^+ and the polymer. Aranda and Ruiz-Hitzky observed from the X-Ray diffractograms a regular pattern corresponding to a unique phase. They concluded the polymer forms a helical structure between the layers of clay and "jump" to a planar zig-zag structure depending on the cation attached on the clay (Figure 2.5)[25]. Aranda and Ruiz-Hitzky also found ^1H NMR spectroscopy of PEO shows two distinct peaks representing two distinct phases: crystal and amorphous. The appearance of the two phases also causes helical jump motion within nanocomposites.

Solid electrolyte membranes and combination inorganic-organic polymer electrolytes are examples of current research. Many variations can be investigated with polymers in battery electrolytes, including crosslinked polymers and polyelectrolyte[26-32].

2.3 Hectorite Background

2.3.1 Hectorite Structure and Properties

Hectorite received its name from the city where it is mined, Hector, San Bernadina County, California. When mined it has a soft greasy texture, and is white in color. In the lab-use state the clay is dried and crushed and resembles a white odorless powder. Hectorite and other 2:1 layered clays (smectites) are unique in that they are characterized by a negatively charged plate-like structure with exchangeable associated cation counterion sandwiched between the plate-like layers (Figure 2.6). The negative charge comes from the divalent magnesium ions in hectorite that are substituted partially by monovalent lithium ions. Because of its unique properties in detergents and cosmetics, hectorite is an export for California and sells for $1/lb. We investigated the use of synthetic hectorite clay in battery electrolyte applications. For lithium battery application, the native sodium cations are exchanged for lithium ions[33]. The plate-like particles can be dispersed in high-dielectric solvents (e.g., ethylene carbonate and propylene carbonate) to create a physically gelled structure.

Smectite clays are characterized by their crystal structure. Within the layers, a two-dimensional ordering is apparent, and along the c-axis, periodicity is apparent. Some smectites are turbostratic, i.e. their layers are randomly rotated with respect to each other; however, there is still ordering in the c-direction. “Swelling” in this direction changes the

interlamellar spacing and is a useful parameter of clay materials. Water can cause extreme osmotic swelling in smectites with Na or Li divalent cations. Although non-aqueous battery systems have very low water content, understanding c-spacing due to swelling from water is very important. XRD and TEM (transmission electron spectroscopy) are common tools used to analyze the c-spacing structure of smectite clays (TEM results shown in Figure 2.7)[34,35]. Molecular simulation has also been utilized to examine local structure and phase behavior of "disk-like" smectite platelets[36].

H. van Olphen[37] was one of the first to describe the possibility of a three-dimensional structure created by electrostatic interactions of the negatively charged platelets[37,38]. In his research, the platelet structures are compared to a "house of cards" where the cards represented the charged platelets. Krishnamoorti[39] studied polymer layered silicates and developed a schematic of their achievable nanostructures. He categorizes the major structures as unmixed, intercalated, and exfoliated (Figure 2.8). Immiscible, or unmixed, nanocomposites form aggregates, which inhibit polymer from filling between the clay layers. Intercalated structures form when the stacks of platelets open up, to allow polymer in between, but still resemble a stacking configuration. Exfoliated platelets exists when layers are completely spread apart and dispersed well in the polymer solution[38,39]. The clay layers are anisotropic, according to Krishnamoorti, due to their long plate-like characteristics. Rheology and X-ray diffraction (XRD) are two main analytical methods Krishnamoorti uses to assess the type of structure in his system. Contrary to Krishnamoorti's nanocomposites, we use carbonate solvents in addition to polymers to help open the structure of the clay, however the basic nanocomposite system is the same.

2.3.2 Clays as Nanocomposite Fillers

Modified layered silicates have been incorporated with polymers extensively in hopes to improve mechanical stability of the polymer. Usually these silicates (clays for example) are added in small amounts and yet display dramatic change to barrier properties, as shown by Xu and Manias[40]. Organically modified clays are frequently biocompatible and are used in cosmetics, food supplements, stomach acid-reducing medicines, and blood sacs for artificial hearts. Xu and Manias have found that alkylammonium modified montmorillonite can significantly increase the modulus of their Poly(urethane urea) samples but not compromise its ductility[40]. Organically modified montmorillonite is an especially common type of clay found in polymer nanocomposites, due to its availability, inert nature, and cation exchange capacity. Hectorite and montmorillonite are of the same smectite group of clays; however, hectorite is a trioctohedral mineral and montmorillonite is a dioctohedral mineral[37]. Recent investigations of incorporating montmorillonite into polypropylene (PP) have shown improved modulus and barrier properties. One drawback with these systems is the extent of mixing necessary to disperse the clay and a decrease in thermal properties of the polymer with clay[41].

Al-Mukhtar et al.[42] studied the water uptake and swelling Na-Laponite, a synthetic hectorite, and Na-Hectorite clays. Hectorite has larger particle size than Laponite, however both are in smectites family. In Al-Mukhtar's study he found, through XRD, that adding pressure (up to 10 MPa) decreases the spacing between the clay layers. He also investigated the difference in spacing when the clay was saturated and unsaturated in water. In either case Laponite proved to be more exfoliated that hectorite,

with a basal spacing around 2.5 nm at 1 MPa compared to Hectorite layer spacing of 1.8 nm at the same pressure[42]. Another study by Conard et al. has shown that upon cation exchange water molecules form various polyhedra between spacing of layers[43]. When Li^+ is exchanged for the natural Na^+, the water molecules form a coordination triangle ($Li \cdot 3H_2O$) in the interlamellar space of the layers. XRD and IR spectroscopy were used to verify structures of exchangeable cations and water [43,44].

Polymer mechanical stability is a key issue in many chemical industries. Clays hold the unique feature of forming matrices within polymers thereby improving tensile strength of certain polymers. Once improved, these polymers can be used for heat resistant materials or product packaging material. Balazs et al.[45] formulated an analytical model, which simulated interactions between polymer chains and clay lattices. They looked at the effect of placing surfactants on the platelet and its interaction with polymer solutions. From the models they developed, they found it is possible to predict when clays can be exfoliated by polymers and when the opposite may occur[45,46]. Other models, describing molecular motion within clay-based nanocomposite, show ways to avoid crystalline behavior in polymers. Amorphous polymers, used in montmorillonite nanocomposites, have been predicted by Kwiatkowski and Whittaker to retain mechanical strength upon addition of copolymers or branched block copolymers[47].

Aranda and Ruiz-Hitzky's research, discussed in the previous section, confirmed an improvement in chemical and thermal stability when clays are added to polymers. Aranda and Ruiz-Hitzky's XRD patterns confirm clay (montmorillonite) layer spacing increases due to polymer chain intercalation (Figure 2.9). Impedance plots indicate

improved cationic conductivity for the same intercalated clay/polymer samples when compared to other montmorillonite samples without polymer (Figure 2.10)[25].

New studies are emerging on the topic of surfactants attached to clay surfaces. Beyer et al.[48] found that amine terminated polystyrene can be bound to montmorillonite by simple dispersion techniques. These modified clays were then added to polystyrene forming the desired polymer-layered silicate (PLS) nanocomposite. PLS type nanocomposites are created in three main ways: in situ polymerization of the matrix monomer in the presence of the modified clay, solution intercalation, or melt processing. Beyer et al. used TGA to find the amount surfactant attached to the clay surface and small–angle X-Ray scattering (SAXS) and transmission electron microscopy (TEM) to characterize morphology. Little change was noticed in their SAXS data when comparing modified clay to PLS nanocomposite (Figure 2.16). Surface initiated polymerization (SIP) is a technique that is being attempted for clay surfaces (Figure 2.17)[49]. This technique has not been used for electrolytes yet however, clay electrolytes could benefit from this method. SIP is further described in the recommendation section of this thesis.

Laponite, bentonite, stevensite, montmorillonite, and hectorite are examples of types of clay added to various polymer materials. Surface and intergallery poly(methylmethacrylate) (PMMA) formations in various forms of hectorite are studied using SEM and ESR[50,51]. Shear response of polymer with the addition of clays has been another important area of research. In order to address the ongoing problem of shear-induced polymer structure change, clays have been added to provide an ordered network for the polymer[38,39,52]. Although these studies do not focus on the potential of these

nanocomposites as electrolytes, they show interesting properties of nanocomposites for other applications[53-57].

2.3.3 Clay/Polymer Electrolytes

Battery electrolytes in gel form are a new focus for the battery research. In order to make a gel electrolyte, plasticizers, like SiO_2 and other oxide nano-fillers, are added to PEO solvent mixtures. Clay is a good plasticizer for low hydrophobic polymers because of the intercalating nature of the polymer with the clay, and because it sustains a high interfacial area[58]. The high interfacial area reduces the crystallinity of the polymer, which leads to higher ionic conductivity while keeping the beneficial mechanical properties of PEO. Chen et al.[59] investigated PEO and PMMA based electrolytes with montmorillonite. Montmorillonite and other clays, which are used as plasticizers, are modified with large bulky cations to tailor the electrolyte even further. Chen et al. modified montmorillonite with dimethyldioctadecylammonium chloride (Dclay) and found an increase in ionic conductivity for their lithium salt and polymer electrolyte (Figure 2.11). Their research also showed a difference in basal spacing among natural Na-montmorillonite, Dclay modified montmorillonite, and clay/polymer/salt complexes (Figure 2.12)[60-62].

One drawback to clay minerals for battery electrolytes is their intrinsic hydrophilic nature. Cation modification, as described above, is one way to avoid this issue. Researchers are exploring organic cations and their ability to make hydrophilic clays into organophilic compounds. The term organophilic implies that organically modified clays can be attracted to organic polymers. Hwang and Liu[63] show, through

XRD data, that organophilic clays have increased interlamellar spacing when added to PAN (polyacrylonitrile) polymer (Figure 2.13).

Fan *et al.*[64] have shown ionic conductivity results for electrolytes incorporating PEO, $LiClO_4$, and clay. Several modified forms of montmorillonite clay (sodium, lithium, dodecylamine) were investigated to ascertain their effect on ionic conductivity. Exchangeable cations on the clay surface, like dodecylamine, were found to affect basal spacing (an increase of 30%) as detected from X-Ray diffraction; however, the conductivity is little affected. The optimum concentration of non-modified clay, at which the conductivity is the highest, was determined to be around 5%. Both XRD and conductivity results of Fan et al. are shown in Figure 2.14 and 2.15.

2.4 References

1. J. O. Besenhard *Handbook of Battery Materials*; Wiley-VCH: New York, 1999.

2. D. Linden *Handbook of Batteries*; Second ed.; McGraw-Hill Inc.: New York, 1995.

3. S. Megahed and B. Scrosati, "Rechargeable Nonaqueous Batteries", *Interface*, 34-37 (1995).

4. B. Scrosati, "Challenge of portable power", *Nature*, **373**, 557-558 (1995).

5. P. D. Bennet, K. R. Bullock, and M. E. Fiorino, "Aqueous Rechargable Batteries", *Interface*, 26-30 (1995).

6. J. M. Tarascon and M. Armand, "Issues and challenges facing rechargeable lithium batteries", *Nature*, **414**, 359-367 (2001).

7. M. J. Riezenman, "The Search for Better Batteries", *IEEE Spectr.*, **32**, 51-56 (1995).

8. M. Wakihara and O. Yamamoto *Lithium-ion Batteries Fundamentals and Performance*; Wiley-VCH: New York, 1998.

9. D. Aurbach, "Review of selected electrode-solution interactions which determine the performance of Li and Li ion batteries", *J. Power Sources*, **89**, 206-218 (2000).

10. D. E. Fenton, J. M. Parker, and P. V. Wright, *Polymer*, **14**, 589 (1973).

11. J. Fan and P. S. Fedkiw, "Composite electrolytes prepared from fumed silica, polyethylene oxide oligomers, and lithium salt", *J. Electrochem. Soc.*, **144**, 399-408 (1997).

12. Y.-T. Kim and E. S. Smotkin, "The effect of plasticizers on transport and electrochemical properties of PEO-based electrolytes for lithium rechargeable batteries", *Solid State Ion.*, **149**, 29-37 (2002).

13. M. M. Doeff, L. Edman, S. E. Sloop, J. Kerr, and L. C. De Jonghe, "Transport properties of binary salt polymer electrolytes", *J. Power Sources*, **89**, 227-231 (2000).

14. M. M. Doeff and J. S. Reed, "Li ion conductors based on laponite/poly(ethylene oxide) composites", *Solid State Ion.*, **115**, 109-115 (1998).

15. G. B. Appetecchi, P. Romagnoli, and B. Scrosati, "Composite gel membranes: a new class of improved polymer electrolytes for lithium batteries", *Electrochem. Commun.*, **3**, 281-284 (2001).

16. D. Golodnitsky, G. Ardel, and E. Peled, "Effect of plasticizers on the CPE conductivity and on the Li- CPE interface", *Solid State Ion.*, **85**, 231-238 (1996).

17. H. J. Walls, J. Zhou, J. A. Yerian, P. S. Fedkiw, S. A. Khan, M. K. Stowe, and G. L. Baker, "Fumed silica-based composite polymer electrolytes: synthesis, rheology, and electrochemistry", *J. Power Sources*, **89**, 156-162 (2000).

18. Y. X. Li, P. S. Fedkiw, and S. A. Khan, "Lithium/V_6O_{13} cells using silica nanoparticle-based composite electrolyte", *Electrochimica Acta*, **47**, 3853-3861 (2002).

19. J. Fan, S. R. Raghavan, X. Y. Yu, S. A. Khan, P. S. Fedkiw, J. Hou, and G. L. Baker, "Composite polymer electrolytes using surface-modified fumed silicas: conductivity and rheology", *Solid State Ion.*, **111**, 117-123 (1998).

20. J. Zhou, P. S. Fedkiw, and S. A. Khan, "Interfacial Stability Between Lithium and Fumed Silica-Based Composite Electrolytes", *J. Electrochem. Soc.*, **149**, 1121-1126 (2002).

21. M. Forsyth, D. R. MacFarlane, A. Best, J. Adebahr, P. Jacobsson, and A. J. Hill, "The effect of nano-particle TiO2 fillers on structure and transport in polymer electrolytes", *Solid State Ion.*, **147**, 203-211 (2002).

22. Y. Aihara, G. B. Appetecchi, B. Scrosati, and K. Hayamizu, "Investigation of the ionic conduction mechanism of composite poly(ethyleneoxide) PEO-based polymer gel electrolytes including nano-size SiO_2", *Physical Chemistry Chemical Physics*, **4**, 3443-3447 (2002).

23. S. R. Raghavan, M. W. Riley, P. S. Fedkiw, and S. A. Khan, "Composite Polymer Electrolytes Based on Poly(ethylene glycol) and Hydrophobic Fumed Silica:Dynamic Rheology and Microstructure", *Chem. Mat.*, **10**, 244-251 (1997).

24. P. Aranda and E. Ruiz-Hitzky, "Poly(ethylene oxide)/NH^{4+}-smectite nanocomposites", *Appl. Clay Sci.*, **15**, 119-135 (1999).

25. P. Aranda and E. Ruizhitzky, "Poly(Ethylene Oxide)-Silicate Intercalation Materials", *Chem. Mat.*, **4**, 1395-1403 (1992).

26. J. H. Fang, X. X. Guo, S. Harada, T. Watari, K. Tanaka, H. Kita, and K. Okamoto, "Novel sulfonated polyimides as polyelectrolytes for fuel cell application. 1. Synthesis, proton conductivity, and water stability of polyimides from 4,4 '-diaminodiphenyl ether-2,2 '- disulfonic acid", *Macromolecules*, **35**, 9022-9028 (2002).

27. J. K. Wolterink, J. van Male, M. A. C. Stuart, L. K. Koopal, E. B. Zhulina, and O. V. Borisov, "Annealed star-branched polyelectrolytes in solution", *Macromolecules*, **35**, 9176-9190 (2002).

28. M. C. Borghini, M. Mastragostino, and A. Zanelli, "Reliability of lithium batteries with crosslinked polymer electrolytes", *Electrochimica Acta*, **41**, 2369-2373 (1996).

29. L. Albertin, P. Stagnaro, C. Coutterez, J. F. Le Nest, and A. Gandini, "A novel approach to crosslinked polymer electrolytes based on polyethers: network formation via photochemistry", *Polymer*, **39**, 6187-6189 (1998).

30. R. V. Morford, E. C. Kellam, M. A. Hofmann, R. Baldwin, and H. R. Allcock, "A fire-resistant organophosphorus gel polymer electrolyte additive for use in rechargeable lithium batteries", *Solid State Ion.*, **133**, 171-177 (2000).

31. M. Popall, R. Buestrich, G. Semrau, G. Eichinger, M. Andrei, W. O. Parker, S. Skaarup, and K. West, "New polymer lithium secondary batteries based on ORMOCER (R) electrolytes-inorganic-organic polymers", *Electrochimica Acta*, **46**, 1499-1508 (2001).

32. K. Asaka, N. Fujiwara, K. Oguro, K. Onishi, and S. Sewa, "State of water and ionic conductivity of solid polymer electrolyte membranes in relation to polymer actuators", *J. Electroanal. Chem.*, **505**, 24-32 (2001).

33. "SKS-21 Synthetic Hectorite, Preliminary Data Sheet," Hoechst Celanese, 1996.

34. K. Mystkowski, J. Srodon, and F. Elsass, "Mean thickness and thickness distribution of smectite cystallites", *Clay Min.*, **35**, 545-557 (1999).

35. J. F. Alcover, Y. Qi, M. Al-Mukhtar, S. Bonnamy, and F. Bergaya, "Hydromechanical effects: (I) on the Na-smectite microtexture", *Clay Min.*, **35**, 525-536 (2000).

36. M. Dijkstra, J. P. Hansen, and P. A. Madden, "Statistical model for the structure and gelation of smectite clay suspensions", *Phys. Rev. E*, **55**, 3044-3053 (1997).

37. H. van Olphen *An Introduction to Clay Colloid Chemistry*; John Willey & Sons: New York, 1977.

38. R. Krishnamoorti and K. Yurekli, "Rheology of polymer layered silicate nanocomposites", *Current Opinion in Colloid and Interface Science*, **6**, 464-470 (2001).

39. R. Krishnamoorti, J. Ren, and A. S. Silva, "Shear response of layered silicate nanocompostites", *J. Chem. Phys.*, **114**, 4968-4973 (2000).

40. R. J. Xu, E. Manias, A. J. Snyder, and J. Runt, "New biomedical poly(urethane urea) - Layered silicate nanocomposites", *Macromolecules*, **34**, 337-339 (2001).

41. E. Manias, "A Direct -Blending Approach for Polypropylene/Clay Nanocomposite Enhances Properties", *MRS Bulletin*, **26**, 862-863 (2001).

42. M. Al-Mukhtar, Y. Qi, J. F. Alcover, J. Conard, and F. Bergaya, "Hydromechanical effects: (II) on the water-Na-smectite system", *Clay Min.*, **35**, 537-544 (2000).

43. J. Conard, H. Estradeszwarckopf, A. J. Dianoux, and C. Poinsignon, "Water Dynamics in a Planar Lithium Hydrate in the Interlayer Space of a Swelling Clay - a Neutron-Scattering Study", *Journal De Physique*, **45**, 1361-1371 (1984).

44. C. Poinsignon, H. Estradeszwarckopf, J. Conard, and A. J. Dianoux, "Structure and Dynamics of Intercalated Water in Clay-Minerals", *Physica B*, **156**, 140-144 (1989).

45. A. C. Balazs, C. Singh, and E. Zhulina, "Modeling the interactions between polymers and clay surfaces through self-consistent field theory", *Macromolecules*, **31**, 8370-8381 (1998).

46. Y. Lyatskaya and A. C. Balazs, "Modeling the phase behavior of polymer-clay composites", *Macromolecules*, **31**, 6676-6680 (1998).

47. J. Kwiatkowski and A. K. Whittaker, "Molecular Motion in Nanocomposite of Poly(ethylene oxide) and Montmorillonite", *J. Polym. Sci. Pt. B-Polym. Phys.*, **39**, 1678-1685 (2001).

48. F. L. Beyer, N. C. B. Tan, A. Dasgupta, and M. E. Galvin, "Polymer-layered silicate nanocomposites from model surfactants", *Chem. Mat.*, **14**, 2983-2988 (2002).

49. Q. Y. Zhou, X. W. Fan, C. J. Xia, J. Mays, and R. Advincula, "Living anionic surface initiated polymerization (SIP) of styrene from clay surfaces", *Chem. Mat.*, **13**, 2465-2467 (2001).

50. T. L. Porter, D. Pace, R. Whitehorse, M. P. Eastman, and E. Bain, "Formation of poly(methylmethacrylate) layers on the surface and intergallery regions of Cu2+-, Fe3+-, and VO2+-exchanged hectorite thin films", *Mater. Chem. Phys.*, **76**, 92-98 (2002).

51. S. K. Lim, I. Chin, J. W. Kim, and H. J. Choi, "New Type of Polymer Nanocomposite with Montmorillonite and the PEO/PMMA Blends", *Polymer Materials: Science & Engineering*, **84**, 555-556 (2001).

52. G. Schmidt, A. I. Nakatani, P. D. Butler, A. Karim, and C. C. Han, "Shear orientation of viscoelastic polymer-clay solutions probed by flow birefringence and SANS", *Macromolecules*, **33**, 7219-7222 (2000).

53. C.-H. Pons, C. Tchoubar, and D. Tchoubar, "Organisation des molecules d'eau a la surface des feuillets dans un gel de montmorillonite-Na", *Bulletin de mineralogie*, **103**, 452-456 (1980).

54. Y. Nakashima, "Self-diffusion of H_2O in stevensite gel: effects of temperature and clay fraction", *Clay Min.*, **37**, 83-91 (2001).

55. J. M. Saunders, J. W. Goodwin, R. M. Richardson, and B. Vincent, "A Small-Angle X-Ray Scattering Study of the Structure of Aqueous Laponite Dispersion", *Journal of Physical Chemistry, B*, **103**, 9211-9218 (1999).

56. T. Aubry, F. Bossard, and M. Moan, "Laponite Dispersion in the Presence of an Associative Polymer", *Langmuir*, **18**, 155-159 (2001).

57. J. H. Wu and M. M. Lerner, "Structural, Thermal, and Electrical Characterization of Layered Nanocomposites Derived from Na-Montmorillonite and Polyethers", *Chem. Mat.*, **5**, 835-838 (1993).

58. V. Krikorian, M. Kurian, M. E. Galvin, A. P. Nowak, T. J. Deming, and D. J. Pochan, "Polypeptide-based nanocomposite: Structure and properties of poly(L-lysine)/Na+-montmorillonite", *J. Polym. Sci. Pt. B-Polym. Phys.*, **40**, 2579-2586 (2002).

59. H. W. Chen and F. C. Chang, "The novel polymer electrolyte nanocomposite composed of poly(ethylene oxide), lithium triflate and mineral clay", *Polymer*, **42**, 9763-9769 (2001).

60. H. Chen, L. T., and F. C. Chang, "Ionic conductivity enhancement of the plasticized PMMA/$LiClO_4$ polymer nanocomposite electrolyte containing clay", *Polymer*, **43**, 5281-5288 (2002).

61. H. W. Chen, C. Y. Chiu, and F. C. Chang, "Conductivity enhancement mechanism of the poly(ethylene oxide)/modified-clay-LiClO4 systems", *J. Polym. Sci. Pt. B-Polym. Phys.*, **40**, 1342-1353 (2002).

62. H. W. Chen, C. Y. Chiu, H. D. Wu, I. W. Shen, and F. C. Chang, "Solid-state electrolyte nanocomposites based on poly(ethylene oxide), poly(oxypropylene) diamine, mineral clay and lithium perchlorate", *Polymer*, **43**, 5011-5016 (2002).

63. J. J. Hwang and H. J. Liu, "Influence of Organophilic Clay on the Morphology Plasticizer-Maintained Ability, Dimensional Stability, and Electrochemical Properties of Gel Polyacrylonitrile (PAN) Nanocomposiye Electrolytes", *Macromolecules*, (2002).

64. L. Fan, C.-W. Nan, and Z. Dang, "Effect of modified montmorillonites on the ionic conductivity of $(PEO)_{16}LiClO_4$ electrolytes", *Electrochimica Acta*, **47**, 3541-3544 (2002).

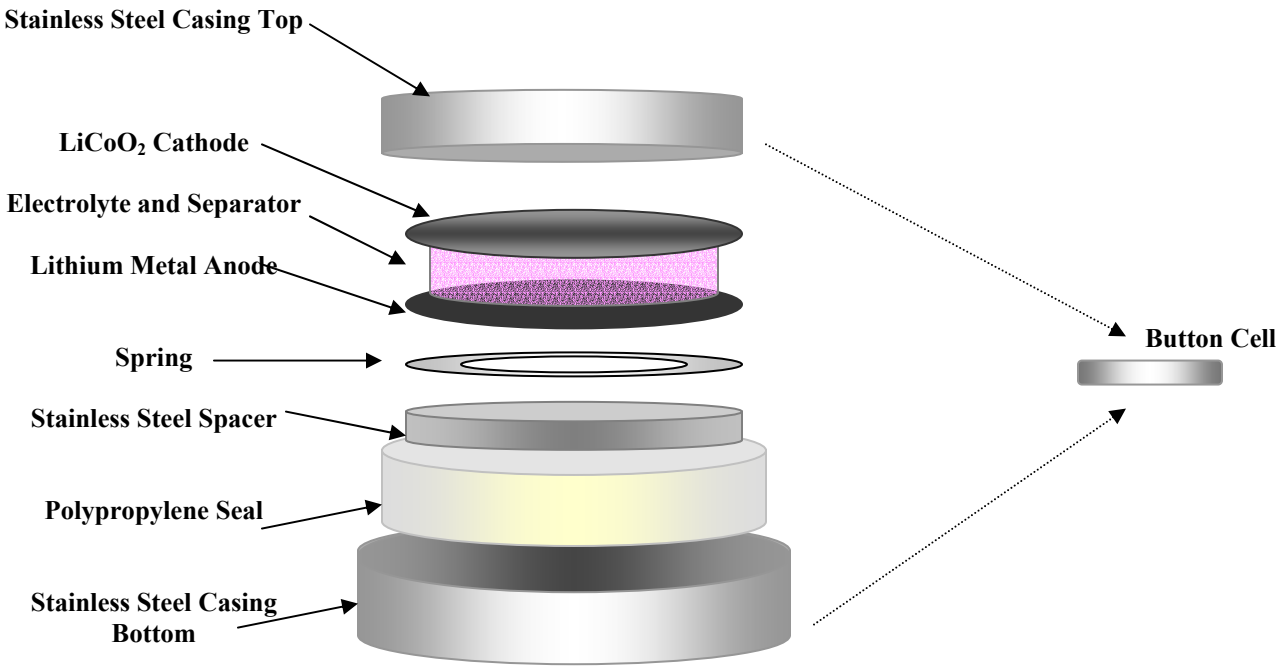

Figure 2.1. Button cell configuration for a lithium metal battery (not to scale).

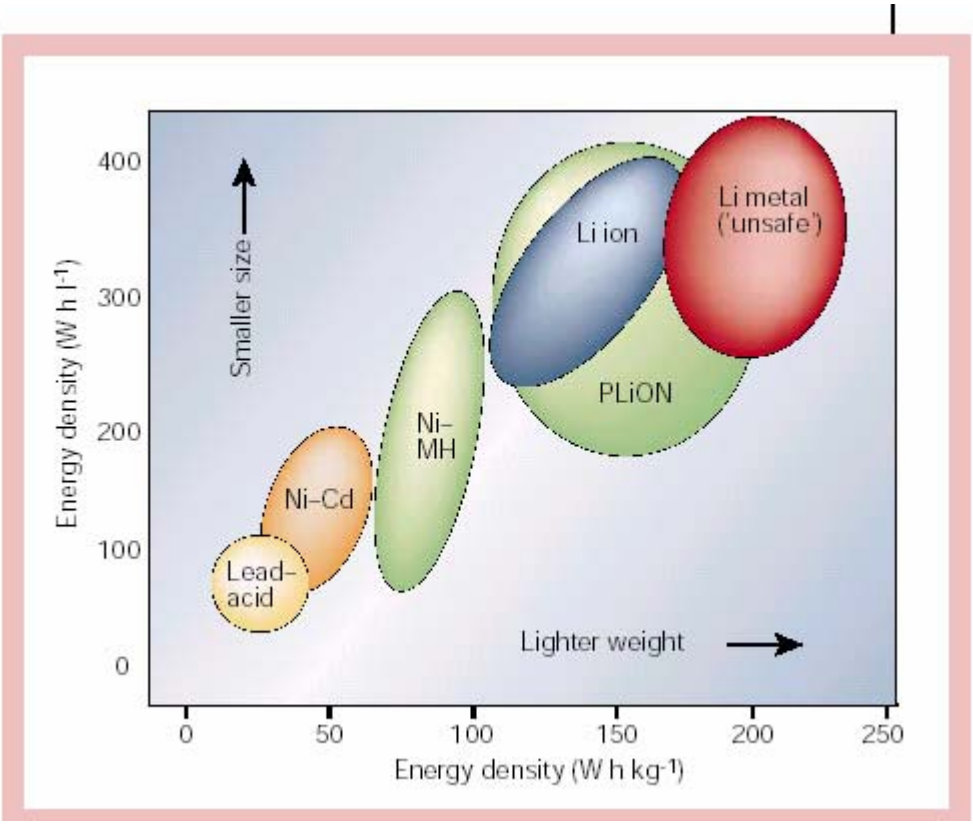

Figure 2.2. Comparison of the different battery technologies in terms of volumetric and gravimetric energy density[6].

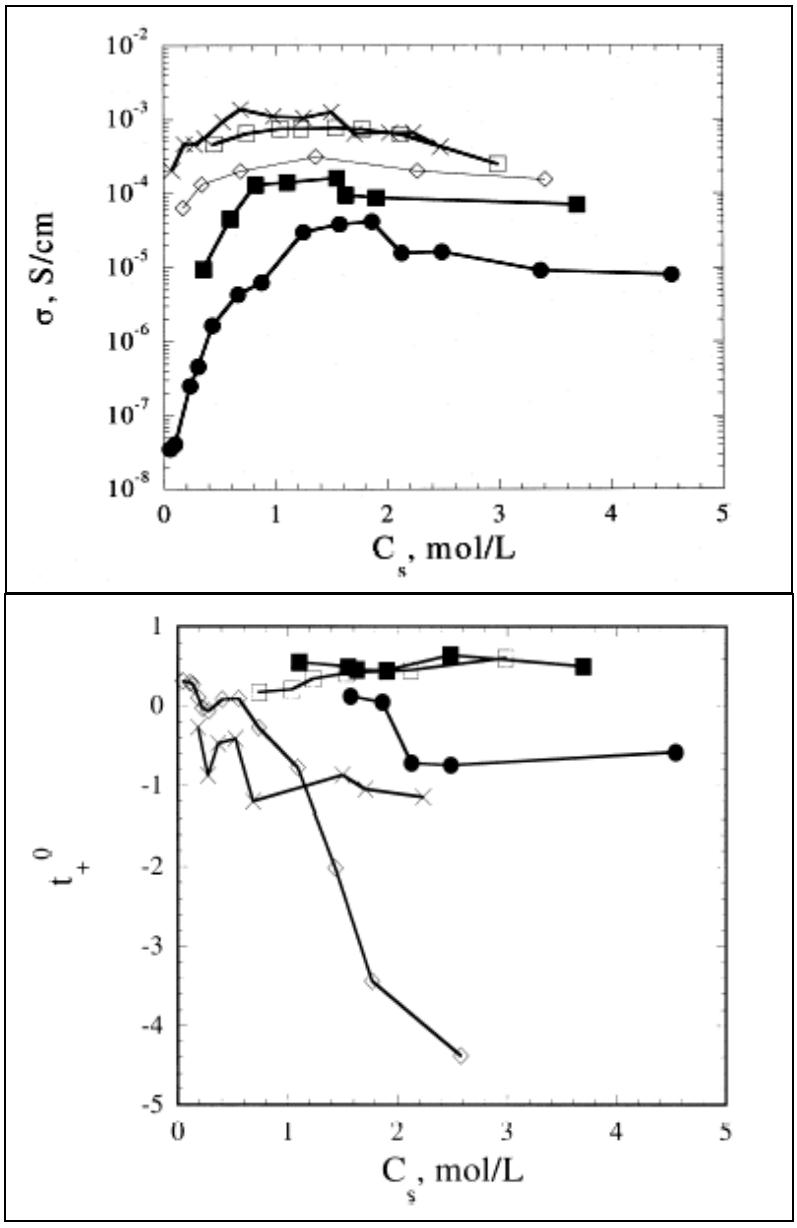

(a)

(b)

Figure 2.3. (a) Conductivities at 85°C as a function of salt concentration for the PEO/NaTFSI (×), PEO/NaTf (◇), PPO/LiTf (-), PPO/LiTFSI (■), and PEO/LiTFSI (□), polymer electrolyte system; (b) t_+^o values at 85°C as a function of salt concetration for the PEO/NaTFSI (×), PEO/NaTf (◇), PPO/LiTf (-), PPO/LiTFSI (■), and PEO/LiTFSI(□) polymer electrolyte systems[13].

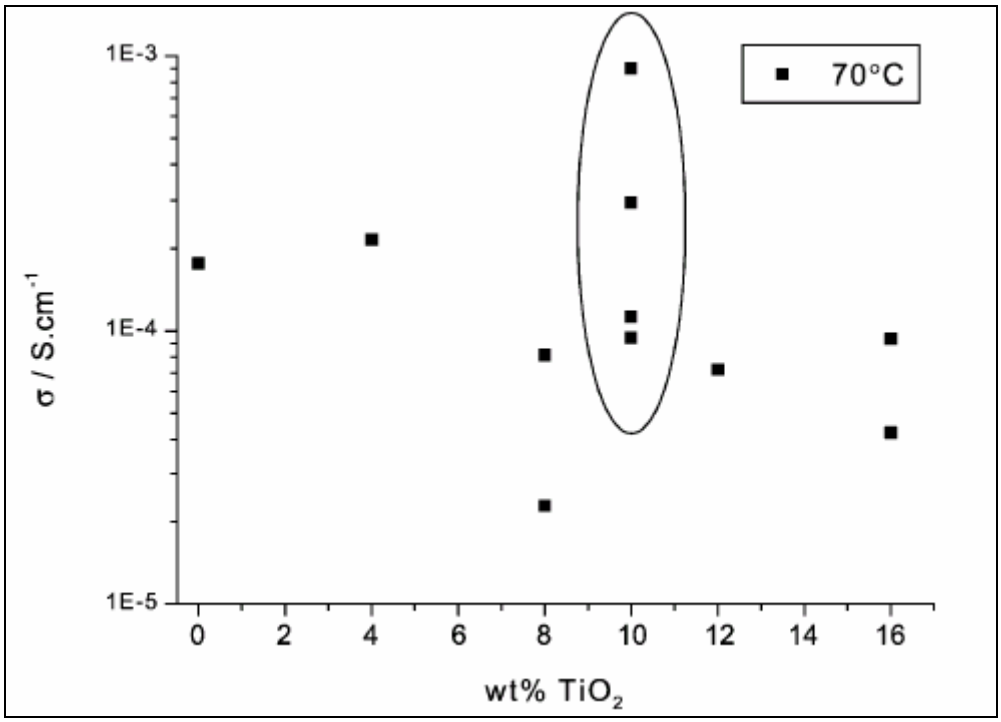

(a)

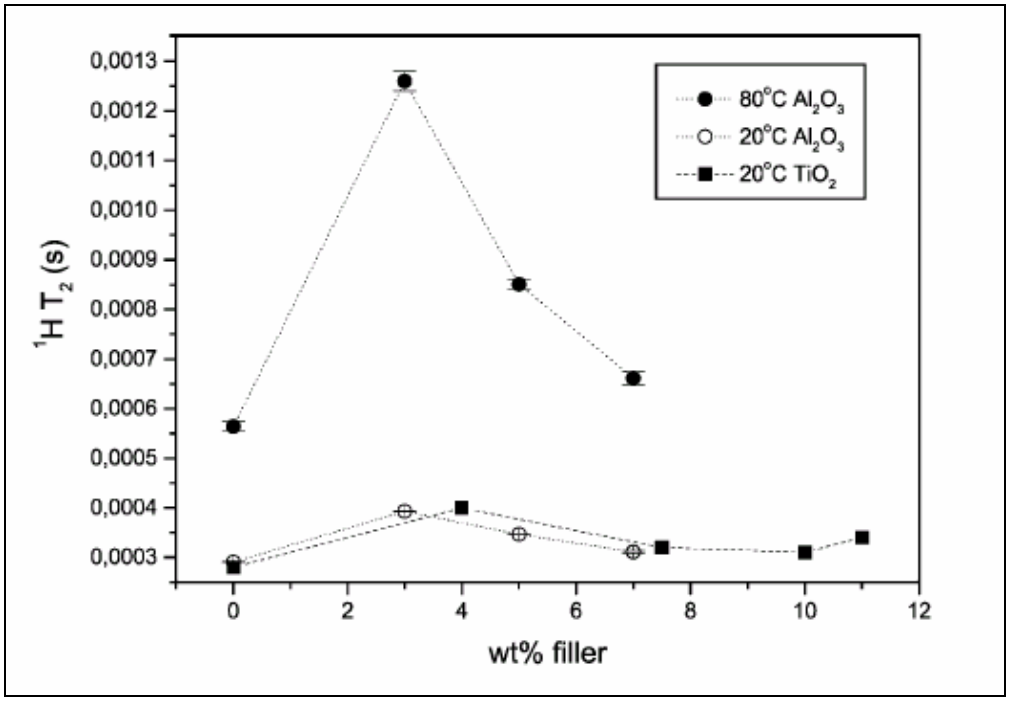

(b)

Figure 2.4. (a) Conductivity as a function of filler content at 70°C for 3PEG (trihydroxypoly(ethylene oxide-co-propylene oxide) at 3:1 ratio and MW 5000 g/mol) /$LiClO_4$/TiO_2 samples. Multiple samples at certain TiO_2 concentrations are shown to illustrate scatter, at 10% TiO_2 (indicated by the ellipse) the most scatter was noticed; (b) ^1H NMR T_2 relaxation measurements as a function of filler content, a comparison of TiO_2 filler versus Al_2O_3 is also made[21].

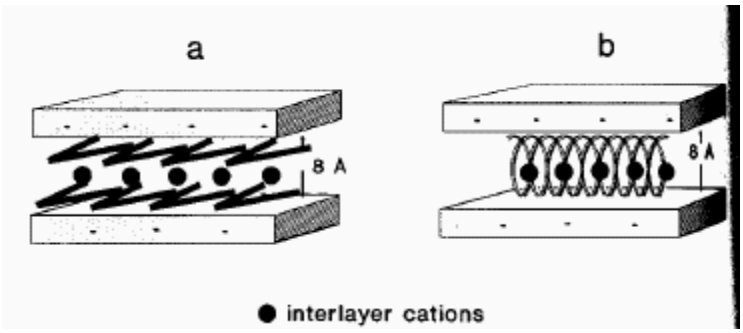

Figure 2.5 Schematic representation of PEO intercalation models in phyllocilicates: (a) double layer planar zig-zag disposition: (b) heliocoidal conformation of PEO chains[25].

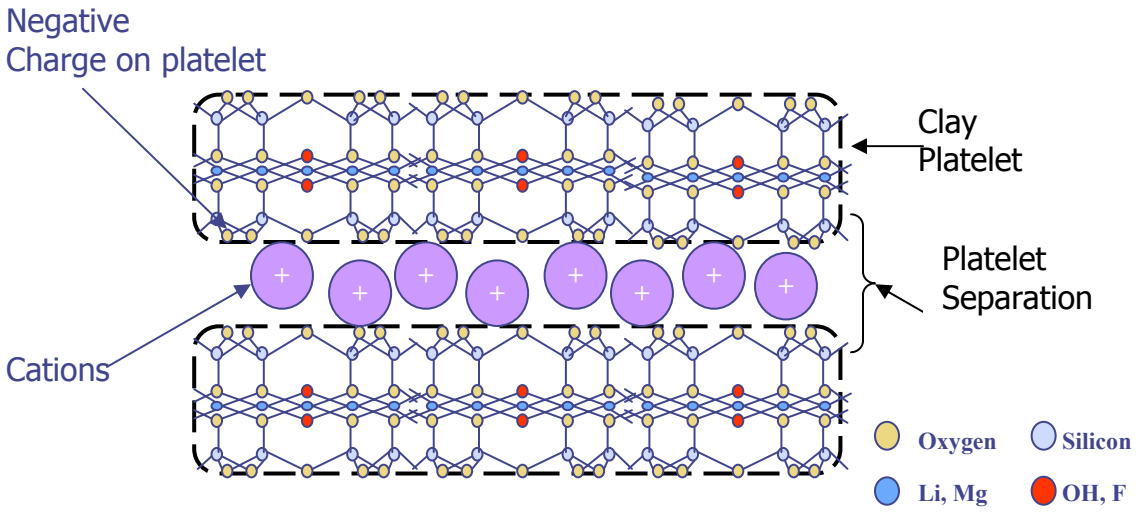

Figure 2.6. Hectorite platelet structure

Figure 2.7. A TEM image of Black Jack beidellite illustrating the counting technique. Cyrstallites are marked with arrows and the numbers of layers are given (scale marker not provided)[34].

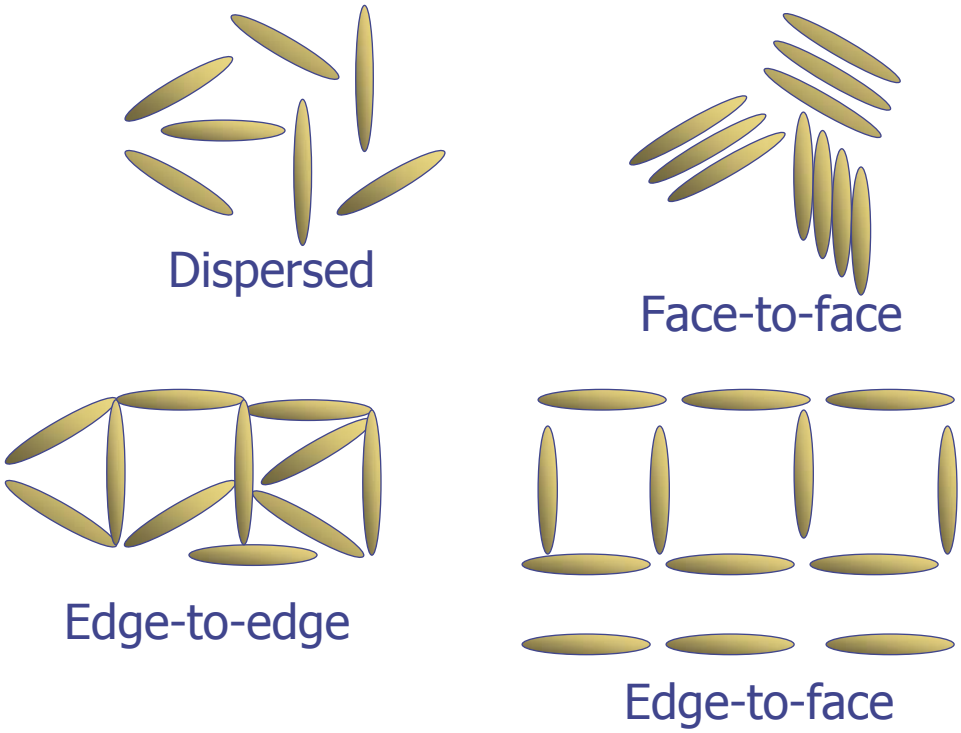

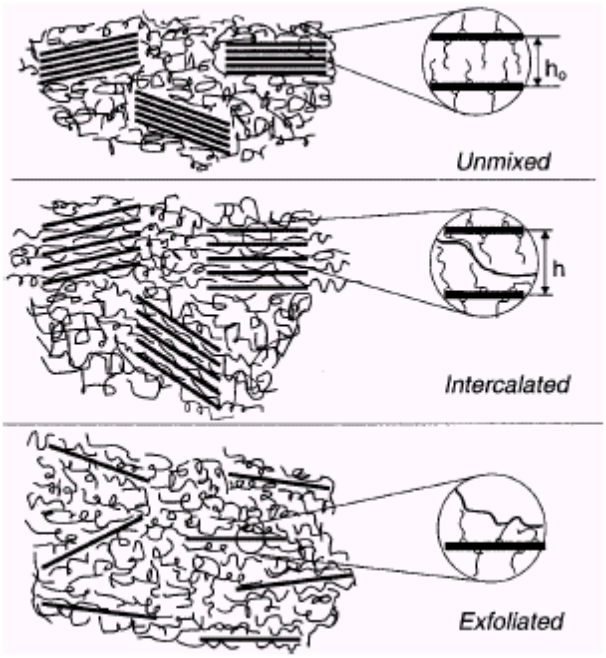

Figure 2.8. Clay platelet interaction using various terminology[39]

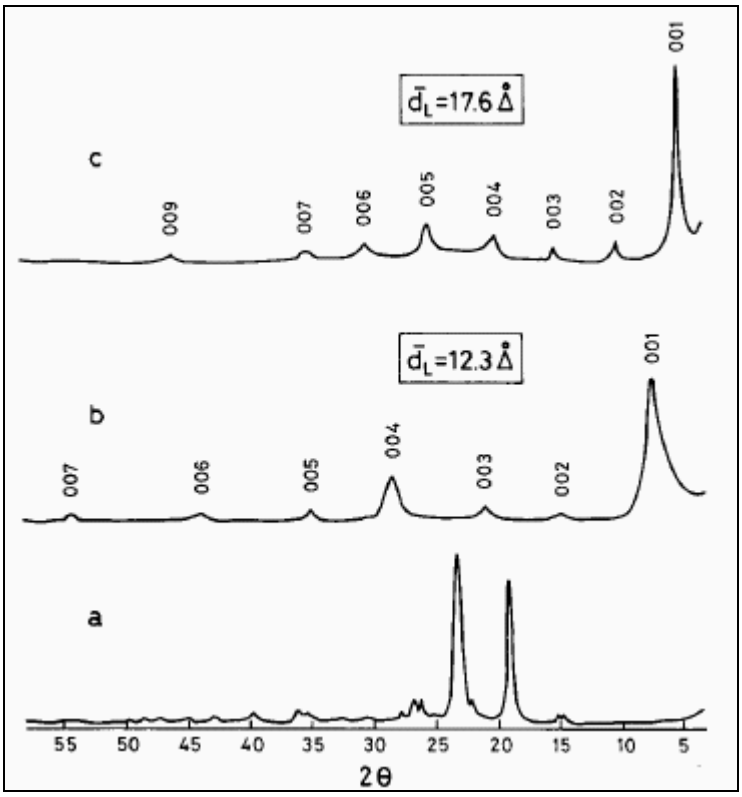

Figure 2.9. X-Ray diffraction patterns of (a) pure PEO; (b) hydrated Na^+-montmorillonite, and (c) PEO/Na^+-montmorillonite compound[25].

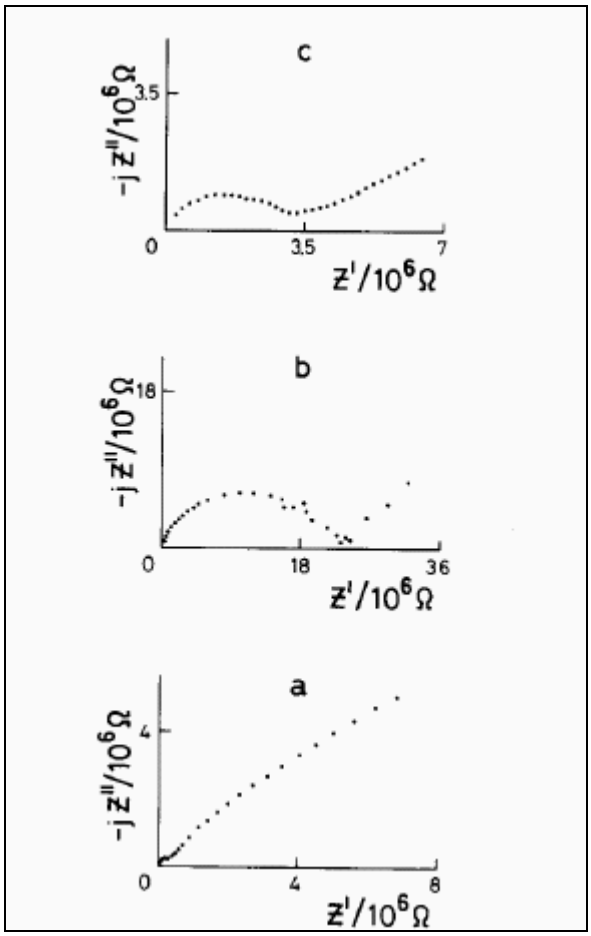

Figure 2.10. Impedance plots and ionic resistance (R_i) values corresponding to the following samples: (a) hydrated Na^+-montmorillonite (293 K), $R_i = 1.26 \times 10^5\ \Omega$; (b) heated Li^+-montmorillonite (700 K), $R_i = 2.5 \times 10^7\ \Omega$; (c) PEO/$Na^+$-montmorillonite (504K), $R_i = 3.47 \times 10^5\ \Omega$[25].

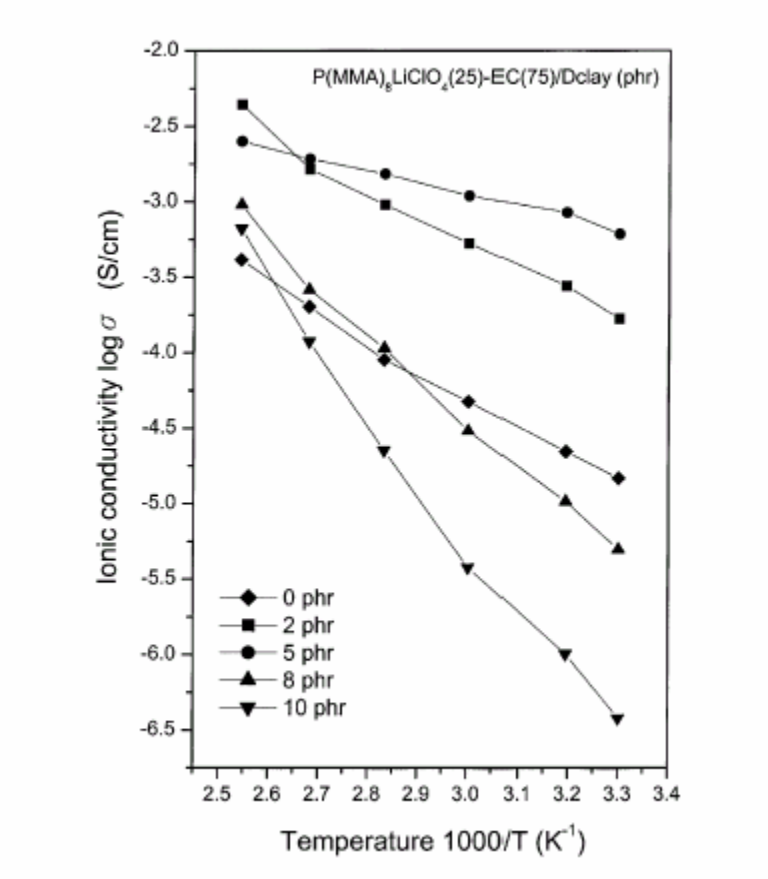

Figure 2.11. Arrhenius conductivity plots for $P(MMA)_8LiClO_4$ and EC (at 25:75 ratio) with dimethyldioctadecylammonium chloride (Dclay) composite electrolyte containing various Dclay part per hundred (phr)[60].

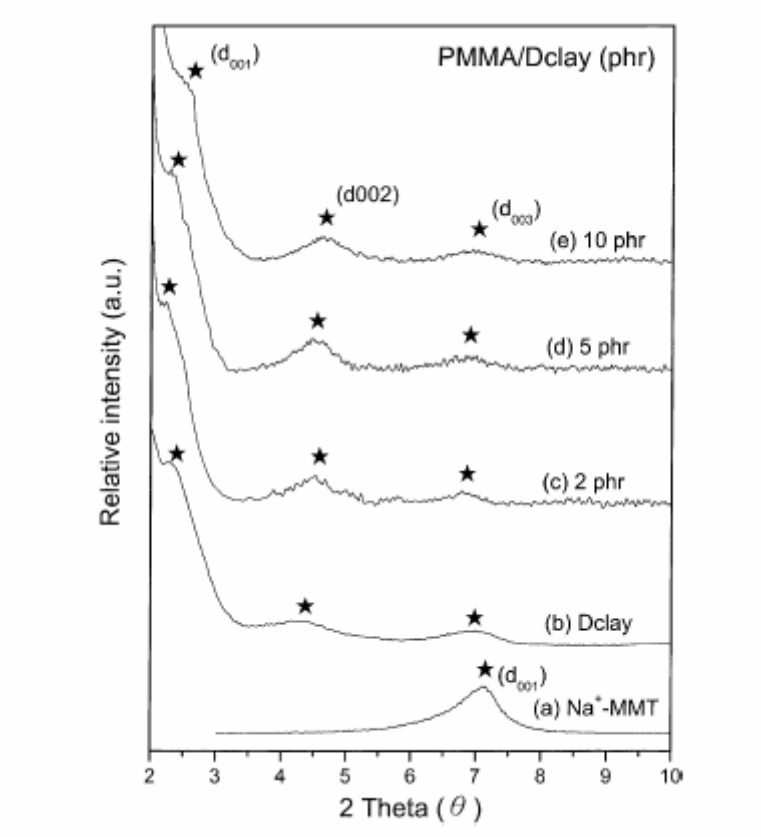

Figure 2.12. XRD patterns of PMMA/Dclay hybrids containing various Dclay part per hundred (phr): (a) Na^+-MMT, (b) DDAC-MMT (Dclay), (c) 2 phr, (d) 5 phr, and (e) 10 phr[60].

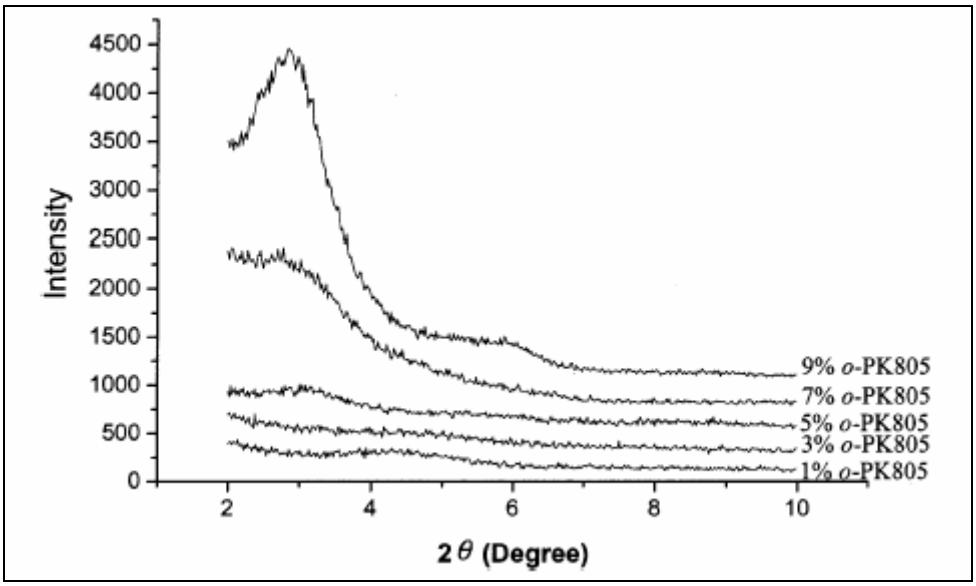

(a)

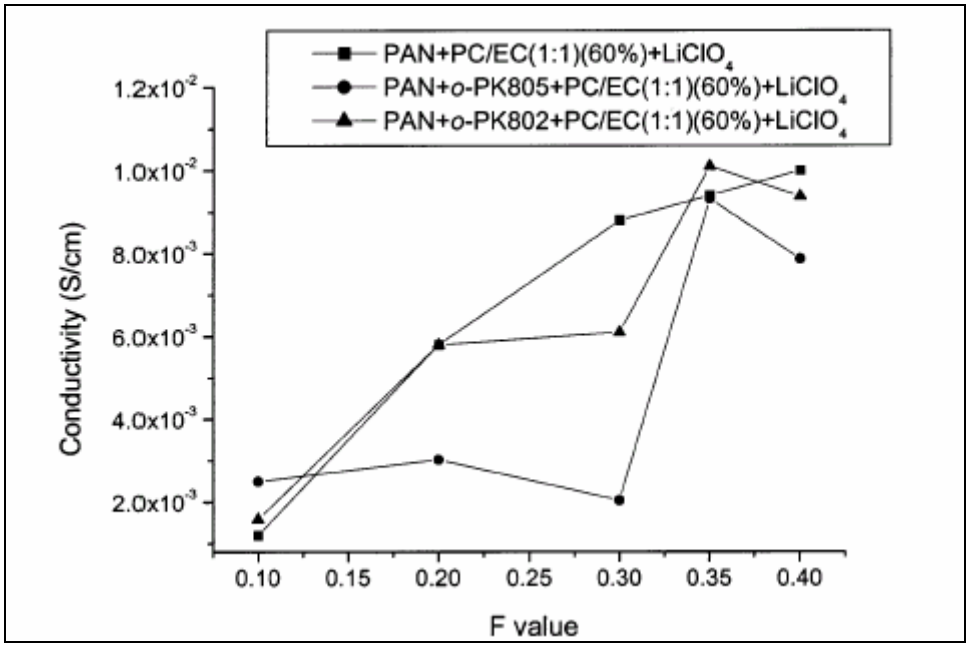

(b)

Figure 2.13.(a) Various X-Ray diffraction patterns by adding different amounts of alkylammonium-modified montmorillonite (o-PK805) into polyacrylonitrile (PAN); (b) Conductivities versus [$LiClO_4$] / [CH2CH(CN)] (F value) for gel PAN nanocomposite electrolytes containing various organophilic clays at room temperature[63].

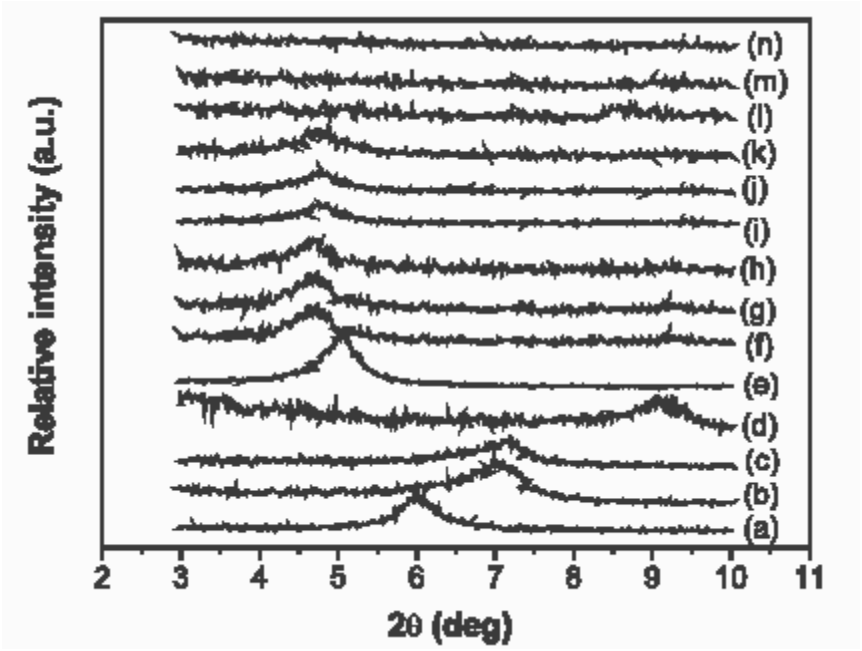

Figure 2.14. WAXRD patterns of (a) Parent montmorillonite, (b) Na-mont, (c) Li-mont, (d) 250-Li-mont (250 represents the temperature in ^{o}C at which the clay was heated to), (e) Org-mont, (f) PEO/Org-mont =95/5, (g) PEO/Org-mont =90/10, (h) PEO/Org-mont =80/20, (i) PEO/Li-mont =95/5, (j) PEO/Li-mont = 90/10, (k) PEO/Li-mont =80/20, (l) PEO/250-Li-mont =95/5, (m) PEO/250-Li-mont =90/10, and (n) PEO/250-Li-mont =80/20[64].

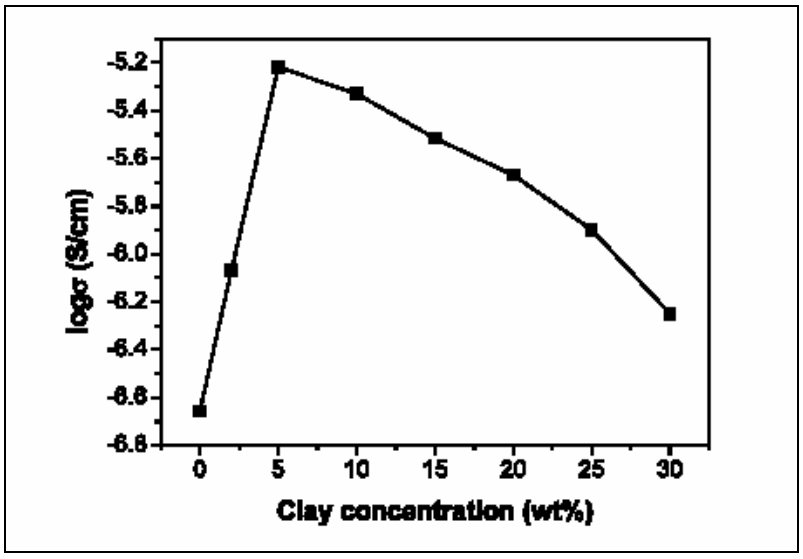

Figure 2.15. Effect of 250-Li-mont (heated at 250^{o}C for 2 days) concentration (wt%) on the ionic conductivity for $(PEO)_{16}LiClO_4$/250-Li-mont composite electrolytes at 30^{o}C[64].

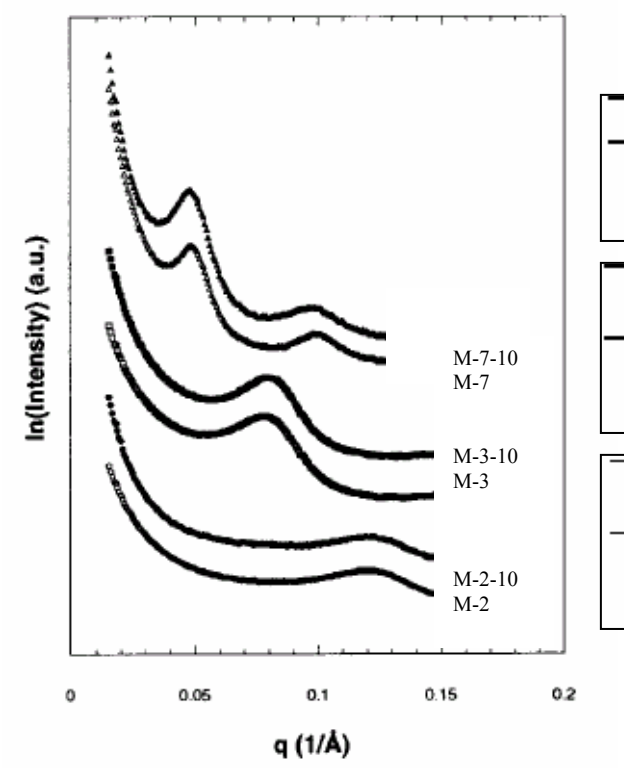

Polystyrene modified surfactants

surfactant	M_n (g/mol)
QPSt-16	1735
QPSt-15	2700
QPSt-14	6800

sample	surfactant
M-2	QPSt-16
M-3	QPSt-15
M-7	QPSt-14

sample	wt of PS homopolymer (g)
M-2-10	0.243
M-3-10	0.253
M-7-10	0.125

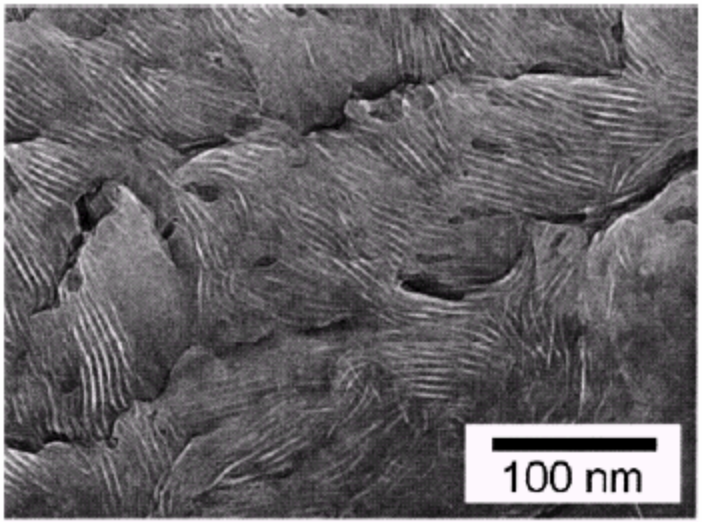

Figure 2.16. (a) SAXS data for polystyrene (PS) modified montmorillonite alone (M-7, M-3, M-2) and nanocomposites after addition of polystyrene homopolymer 10,000 MW (M-7-10, M-3-10, M2-10); (b) Representative TEM micrograph showing the separation of silicate layers after modification with PS-based surfactant. No PS homopolymer is present in this sample[48].

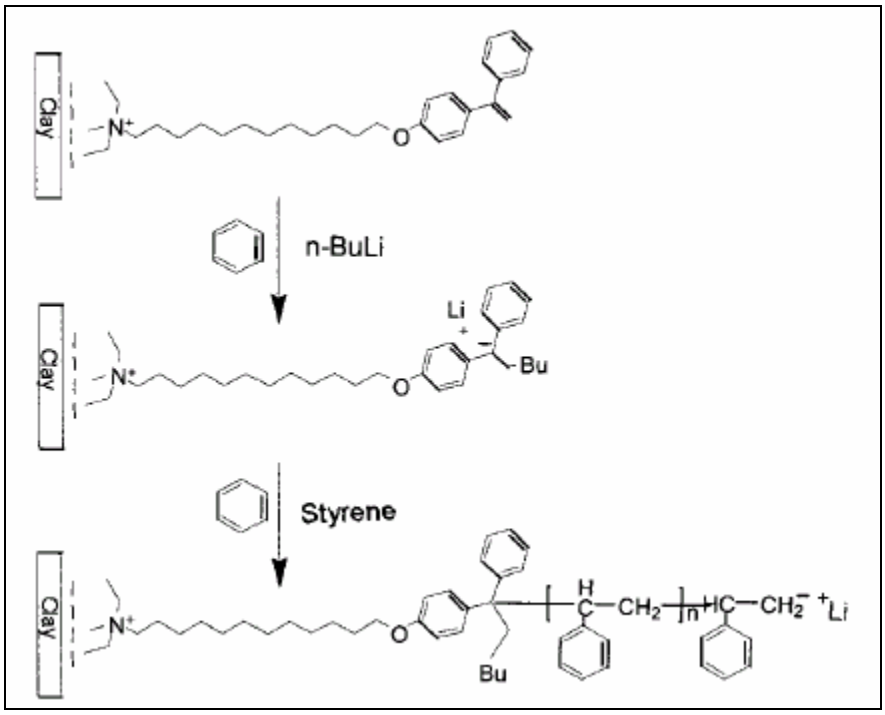

Figure 2.17. Procedure for immobilization of cationic 1,1- diphenylethylene (DPE) initiator and polymerization of styrene on the clay surface. In order to immobilize DPE, the clay surface was reacted with n-BuLi, then styrene was reacted to induce polymerization. Basal spacing of DPE modified clays increased by 1.2 nm when compared to pure clay[49].

Chapter 3: Experimental Materials and Methods

3.1 Electrolyte Preparation

3.1.1 Hectorite Cation Exchange

The first step toward making samples was to exchange sodium ions on synthetic hectorite with lithium ions. These lithium ions serve as the only source of lithium in the electrolyte; no additional salt is added. The native sodium cations were exchanged for lithium ions at a cation-exchange capacity of 88 meq/100 g hectorite[1]. To begin this process, Na-hectorite was dispersed in water using a *Hamilton Beach 7 speed* kitchen blender on speed 4 for 4-5 minutes. The standard initial amount of ingredients used was 20 g hectorite and 850 mL water. After blending the water and clay, 0.75 mol of lithium-chloride (LiCl) dissolved in 150 mL of de-ionized (DI) water was slowly poured in clay/water mixture while blending. This mixture was then transferred into four centrifuge bottles (250 mL each bottle), and centrifuged in a *RC5C Sorvall Instrument* for 30 minutes at 10,000 rpm. This led to a separation between a solid and liquid phase. The liquid supernatant contained water, LiCl and sodium-chloride (NaCl) and the solid was a mixture of Na-hectorite, Li-hectorite, water, LiCl, and NaCl. The solid was transferred into the blender and the supernatant was discarded. To the solid, DI water was added so that the total volume became 850 mL. Then the above procedure was repeated two more times starting with the LiCl addition. After each addition of LiCl but before the centrifuging, the mixture was allowed to rest for one day, to ensure ion-exchange upon adding the lithium salt. Then, a similar procedure was repeated three times omitting the addition of LiCl, and only washing the mixture with DI water. NaCl and excess LiCl were removed through the washing step, which only required one day for the three

washes. After the last centrifuge run, the solid was placed in 100°C oven for 3 days or longer. The remaining solid was dispersed in 100 mL of methanol and filtered in a glass frit under vacuum. The methanol rinse procedure was repeated three times. The filter and clay were put in a 70°C oven for 24 hours minimum time, at which point the clay had a cake-like appearance. The cake was crushed in a crucible until the final form of lithium-exchanged hectorite resembled a white powder, similar to the initial sodium-hectorite.

3.1.2 Hectorite Dispersion and Electrolyte Preparation

A matrix of experiments and samples were investigated in order to understand the effect of low molecular weight polymer as a support solvent in Li-hectorite/carbonate solutions. In this study, two variables were adjusted: solvent volume ratio and hectorite weight. The two solvents used were ethylene carbonate (EC) and polyethylene glycol dimethylether (PEG-dm), and the volume ratios of EC:PEG-dm investigated were 1:1 and 2:1. Control samples were also made where no polymer was added to the EC. Polymer only control samples were not made because hectorite did not disperse in the polymer. Hectorite loading in each electrolyte was determined by a percentage of solvent weight. For example, a 5% hectorite sample based on 17 grams of solvent would require 0.85 grams of hectorite. The data presented in this report are labeled as either hectorite % or mol hectorite/ kg solvent. The hectorite loadings investigated were 5, 10, 15, 20, 25, 30, and 40 % hectorite (0.044 – 0.352 mol hectorite/ kg solvent).

Li-hectorite was used in all of the samples investigated in this research. The solvents, EC (at 70°C) and PEG-dm (at room temperature), were pre-mixed to the desired

volumetric ratio (1:1 and 2:1) at room temperature. Finally, anhydrous ethanol (denatured) was added to separate clay platelets and assist EC/PEG-dm – hectorite intercalation. Order of addition is important to note, the following order was kept consistent: 1) Li-hectorite, 2) EC/PEG-dm mixture, 3) ethanol.

A Silverson L4RT high-shear mixer with a micro mixing head (3/8-inch diameter) was used to combine the components. A *tall-form Kimax* 100-mL beaker was used to hold the solution while mixing and heating. The mixer was operated at 6100 rpm and the mixing head was positioned on the right side of the beaker to induce more agitation. The mixture was brought to 70°C using a heating plate in order to accelerate ethanol removal. When the contents of the mixing vessel reduced to approximately 20 mL (initially the total was around 60 mL), the heat was turned off although mixing was continued. The sample was transferred into a *Pyrex* 100 x 20 mm (diameter x height) petri dish for vacuum drying. The open surface area of the petri dish allowed for more uniform removal of ethanol and trace water from the electrolyte gel while in the vacuum oven. Sets of samples were dried simultaneously for 30 – 60 minute increments in the vacuum oven at 100°C under ~ –30 in Hg pressure. The sample was then transferred to a high purity argon atmosphere glove box (H_2O = 5 ppm, O_2 = 3 ppm, N_2 = 8 ppm, CO/CO_2 = 2 ppm, and THC = =2 ppm). Any EC that was evaporated in the vacuum oven was calculated by comparing the weight difference before and after drying. The weight difference was recorded and the same EC weight was added to the sample in the glove box. In addition, conductivity vials, XRD and rheology samples are prepared in the glove box. A schematic of the overall dispersion procedure described above is shown in Figure 3.1.

Samples were first tested for water content using a *Mitsubishi Karl-Fisher* titrator. Small amounts of each sample (~0.04-0.1 g) were taken from the glove box in glass vials and tested for water content. Samples with water content between 200ppm to 300ppm were considered satisfactory; samples that were higher than 300 ppm were dried again in a vacuum oven. Additional drying steps were performed until the moisture level was between the appropriate range. It was found from Riley[2] that conductivity altered very little for hectorite electrolytes between 200 –600ppm water. Specific dispersion techniques are summarized further in Appendix A.

Conductivity was measured following the water content measurement in glass cells with platinum electrodes (Figure 3.2). Rheological properties were measured on all electrolytes that were in the range of 5 – 20 % hectorite. Electrolytes at higher hectorite concentration i.e., 25 – 40% hectorite would not be measured as they overloaded the rheometer transducer. Some samples were only tested for rheological properties and were made outside of the glove box and with Na-hectorite as opposed to Li-hectorite. In addition, the vacuum oven-drying step was avoided to save considerable time. In addition to saving time, lithium hectorite was conserved, as rheological measurements do not vary significantly with the choice of cation on clay surface (Figure 3.4).

3.2 Conductivity Measurements

Ion movement in the electrolyte was quantified by means of ionic conductivity measurements using electrochemical impedance spectroscopy (EIS). Within electrolytes, ion motion is caused by potential and concentration gradients[3]. The mobility of charge carriers in electrolytes is hindered by the large size of the ions and the low concentration.

Ionic conductivity is the measurement of total charge species in the electrolyte. High conductivity electrolytes are desired because they have lower ohmic potential losses.

Conductivity measurements were made using a PAR 273 potentiostat and *5210 lock-in amplifier (Princeton Applied Research)* or a *BAS-Zahner IM6e Impedance Analyzer (Bioanalytical Systems, Inc.)*. A cell consisting of two platinum electrodes, a thermocouple opening, an o-ring seal, and glass vial was used to find electrolyte conductivity. The design of the cell was developed by Riley[2], and a schematic of the conductivity cell Figure 3.2. Samples were added to these cells within the glove box to ensure low moisture content.

Alternating current (AC) impedance measurements were made using *PowerSine* software, by applying a controlled sinusoidal voltage to an electrochemical sample and recording the response of the current excitation. AC data carries more information than direct current (DC) measurement; however the equipment required, and the theory needed to interpret the results, are more sophisticated. AC measurements are preferred to DC measurements because AC data describes not only ion migration but also the ionic polarization that occurs within the cell. The current response is compared to the input voltage and certain parameters are noted for impedance calculations (Figure 3.2). First, the ratio of maximum voltage (V_{max}) and maximum current (I_{max}) yield a value similar to resistance in DC measurements.

$$|Z| = \frac{V_{max}}{I_{max}}$$

Second, the phase difference (θ) is another important parameter used to find the total impedance of the cell.

$$|Z|\cos q \rightarrow x \text{ component}$$

$$|Z|\sin q \rightarrow y \text{ component}$$

$$Z^* = Z_{RE} - jZ_{IM}$$

As shown in the equations above, impedance can be represented in three different manners: by magnitude ($|Z|$) and phase (q), its x and y components, or by real and complex quantities (Z_{RE} and Z_{IM}). The later representation is the most useful, and is generally how data is depicted in impedance spectroscopy[4]. Typically in experiments, the complex impedance is recorded as a function of signal frequency and a complex impedance plot, Nyquist plot, is generated. From this plot, electrical information of the cell is derived using a circuit model. Within the circuit model, resistors and capacitors represent the migration and polarization of ions. There are three basic impedance components for most batteries connected in series: (i) anode/electrolyte interface, (ii) cathode/electrolyte interface, and (iii) bulk electrolyte. The impedance response of the bulk electrolyte can be represented by a simple resistor (R_E) however, electrode/electrolyte interface impedance requires a more complicated arrangement of components. A parallel circuit model comprised of electrode double-layer capacitance (C_{dA}, C_{dC}), Warburg impedance element, which represents resistance from mass transfer at each electrode ($Z_{W\,A}$, $Z_{W\,C}$), and interfacial reaction impedance at each electrode ($R_{CT\,A}$, $R_{CT\,C}$) is shown in Figure 3.3.

For a resistor, the impedance simply equals R as it is considered independent of frequency. Capacitance impedance is dependent on frequency (w), $1/wC$, and would be a spike on a complex plot. Admittance (Y^*) of a resistor and capacitor are the reciprocal of

the impedance relationships when the resistor and capacitor are in parallel. The relationship of total admittance (Y^*_{total}) and consequently the total impedance (Z^*_{total}) in terms of *R*, *w*, and *C* is given below.

$$Y^*_{total} = Y^*_1 + Y^*_2$$

$$Y^* = \frac{1}{Z^*}$$

$$Y^*_{total} = \frac{1}{R} + jwC$$

$$Z^* = R\left[\frac{1}{1+(wCR)^2}\right] - jR\left[\frac{wRC}{1+(wCR)^2}\right]$$

In a complex impedance plot, the above equation represents a semicircle. Bulk electrolyte resistance and interfacial reaction impedance are labeled as intercepts on the plot (Figure 3.3). The plot also shows the relationship of frequency to impedance, $w \rightarrow$ towards the bulk electrolyte intercept and $w \rightarrow 0$ towards the interfacial reaction intercept. Circuits that are more complicated have been developed to fit the added impedances due to other various impedances within a cell.

3.2 Rheology Experiments

Dynamic rheological measurements were taken on a Rheometrics Dynamic Stress Rheometer (DSR II) using Virtual Instrument RSI Orchestrator software and 25 mm parallel plate geometry. Additional experiments were conducted for high clay concentration samples (above 20 weight %) on a TA Instrument Dynamic Stress Rheometer (Advanced Rheometer 2000) using Rheology Advantage Data Analysis

software and a 20 mm parallel plate geometry (with sandpaper).

3.3.1 Dynamic Measurements

Rheological properties are important in understanding the mechanical stability, processability, and microstructure of a sample. For our electrolytes, rheological properties were used to obtain insight into the stability of clay the electrolyte. In this regard, intrinsic properties of a gel, such as elastic modulus (*G'*) and viscous modulus (*G"*), were measured. Measurements using stress sweeps of Na-hectorite/PEG-dm/EC electrolytes made outside of the glove box. Finally, Creep measurements were taken on the same electrolytes plus Li-hectorite/poly-ethylene oxide (PEO)/EC and Li-hectorite/PEG-dm/EC (the later two were made inside the glove box).

In our studies, we looked at dynamic oscillatory spectrum, where *G'* was plotted versus frequency (*w*). Sinusoidal strain oscillated at a range of frequencies, however the amplitude of the strain was constant.

$$g = g_0 \sin wt$$

$$t = t_0 \sin(wt + d)$$

The equation above shows the response of stress to an oscillating strain, where *d* is the amount *t* is out of phase. Stress is further decomposed to two waves of same frequency, τ' which is in phase with the strain and τ" which is 90^o out of phase.

$$t = t_0' \sin wt + t_0'' \cos wt$$

$$G' = \frac{t_0'}{g_0} \qquad G'' = \frac{t_0''}{g_0}$$

$$t = G'g_0 \sin wt + G''g_0 \cos wt$$

G' and G" are the dynamic moduli, G' is the in phase elastic modulus, and G" is the out of phase viscous modulus. Figure 3.5 shows the wave relationships of γ and τ[5].

In a typical experiment, we would first apply a strain and observe G', also known as a dynamic stress or strain sweep. When strain and stress are linear to each other, G' is a flat line. Every material has a different regime of stress/strain linearity, and this regime is called the linear visco-elastic (LVE) region. Dynamic frequency sweeps were performed after the stress sweeps to observe the G' and G" behavior in the LVE regime. During a stress sweep measurement a breaking point occurs following the flat LVE region where G' decreases dramatically. The breaking point stress is called the yield stress, and it represents the minimum shear needed to begin flow of a plastic material. Yield stress can be determined from estimating the starting point of G decline versus stress. However, yield stress can be found quantitatively from the same stress sweep data, when analyzed as G x Strain versus Strain. The maximum of the G x Strain vs. Strain curve represents yield stress.

Parallel plate geometry was used in this study for ease in sample loading. Figure 3.5 is an illustration of the parallel plate geometry. We used a 25mm radius plate and adjusted gap height (*h*) to around 1mm. Parallel plate geometry fits our systems because the samples used in this study have small strain and solid-like features. Some errors with this geometry are nonhomogeneous strain field and edge effects.

3.3.2 Creep Measurements

Creep is an especially good technique for identifying long time relaxation. Various materials behave differently during stress and relaxation, and thus creep can be useful way to assess a material. During a creep measurement, an instantaneous stress is applied for a length of time (t) to a material, and strain was recorded. Creep compliance $J(t) = \gamma(t) / \tau_o$ is common form to express creep data. For polymeric solutions, deformation can continue for long periods, however the composition of the solution influences the time and amount of recovery. Creep was helpful in understanding the subtle mechanical differences in our clay/polymer electrolytes that could not otherwise be seen by frequency sweep data.

3.4 X-Ray Crystallography - Diffraction

X-Ray Diffraction (XRD) is a method used to explore crystal structure at an atomic level. Although XRD is used to discover minerals and pure crystals, we used powder XRD to find the basal spacing between sheet-like structures of hectorite clay platelets. Unlike single crystal x-ray diffraction, powder XRD does not give exact atom positions in a crystal structure, but rather gives information on different planes within a crystal's unit cell, which can be used to determine basal spacing. Data in this research was collected on an Inel XRG 3000 X-Ray Diffractometer that employed a Cu-Kα radiation (λ = 1.5405 Å), and were performed at 35 kV and 30 mA. All samples were loaded into a 0.7mm quartz capillary tube and data was collected for four hours using a stationary detector that gathers signal over the entire 2 theta range (0-120). Using a

rotating capillary rather than a flat plate as a sample holder ensures that none of the x-rays diffracted at low angles will be blocked by the sample.

Within an XRD instrument, X-rays are produced via an X-ray tube. When a large voltage difference applied between the cathode, a filament, and an anode, a metal target, electrons begin to travel at high velocity toward the cathode. At the cathode, electrons bombard metal atoms and cause their outer shell electrons to shift to lower energy states. These shifting transitions generate X-rays that travel through the instrument window and hit the sample at a range of angles θ. Figure 3.6 shows an example of two X-rays entering a sample at the same incident angle, however the second ray travels a distance *2a* longer than the first ray. Below is the condition needed in order to have constructive interference among X-rays[6,7].

$$n\lambda = 2a$$

Where, λ is the X-ray wavelength and *n* is the integer number of wavelength out of phase. At $n\lambda$ the waves are completely constructive, as opposed to *n/2* λ where the waves are completely destructive. In Figure 3.6, *d* represents basal spacing between crystal lattices, and can be related to *a* as shown in Equation 2.

$$a = d\sin\theta$$

From both equations above we can generate Bragg's Law, which is more commonly used to find basal spacing.

$$d = \frac{n\lambda}{2\sin\theta}$$

3.5 References

1. "SKS-21 Synthetic Hectorite, Preliminary Data Sheet," Hoechst Celanese, 1996.

2. M. Riley, P. Fedkiw, and S. Khan, "Transport Properties of Lithium Hectorite-Based Composite Electrolytes", *Journal of Electrochemical Society*, (2001).

3. G. Prentice *Electrochemical Engineering Principles*; Prentice Hall: Englewood Cliffs, NJ, 1991.

4. P. G. Bruce *Electrical Measurements of Polymer Electrolytes*; Elsevier Applied Science: New York, 1987.

5. C. W. Macosko *Rheology: Principles, Measurements, and Applications*; VCH Publishers, Inc.: New York, NY, 1994.

6. S. A. Nelson *X-Ray Crystallography*; http://www.tulane.edu/~sanelson/geol211/x-ray.htm Tulane University, 2001.

7. Q. Y. Zhou, X. W. Fan, C. J. Xia, J. Mays, and R. Advincula, "Living anionic surface initiated polymerization (SIP) of styrene from clay surfaces", *Chemistry of Materials*, **13**, 2465-2467 (2001).

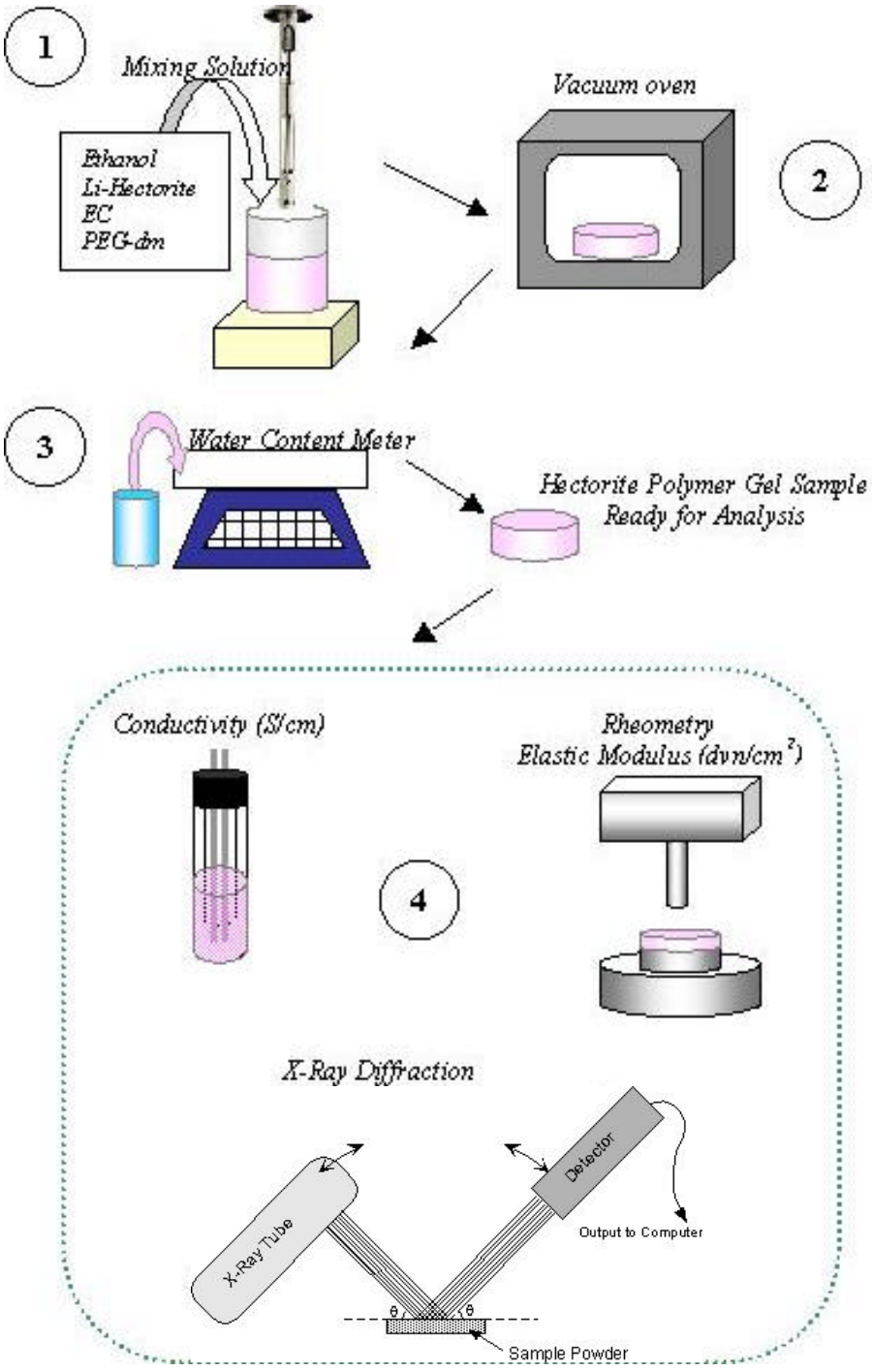

Figure 3. 1. Dispersion schematic for hectorite electrolytes: 1) dispersion with a high shear mixer, 2) drying process in vacuum oven, 3) water content measurement in Karl Fisher titrator, 4) conductivity, rheology, and XRD testing with prepared sample

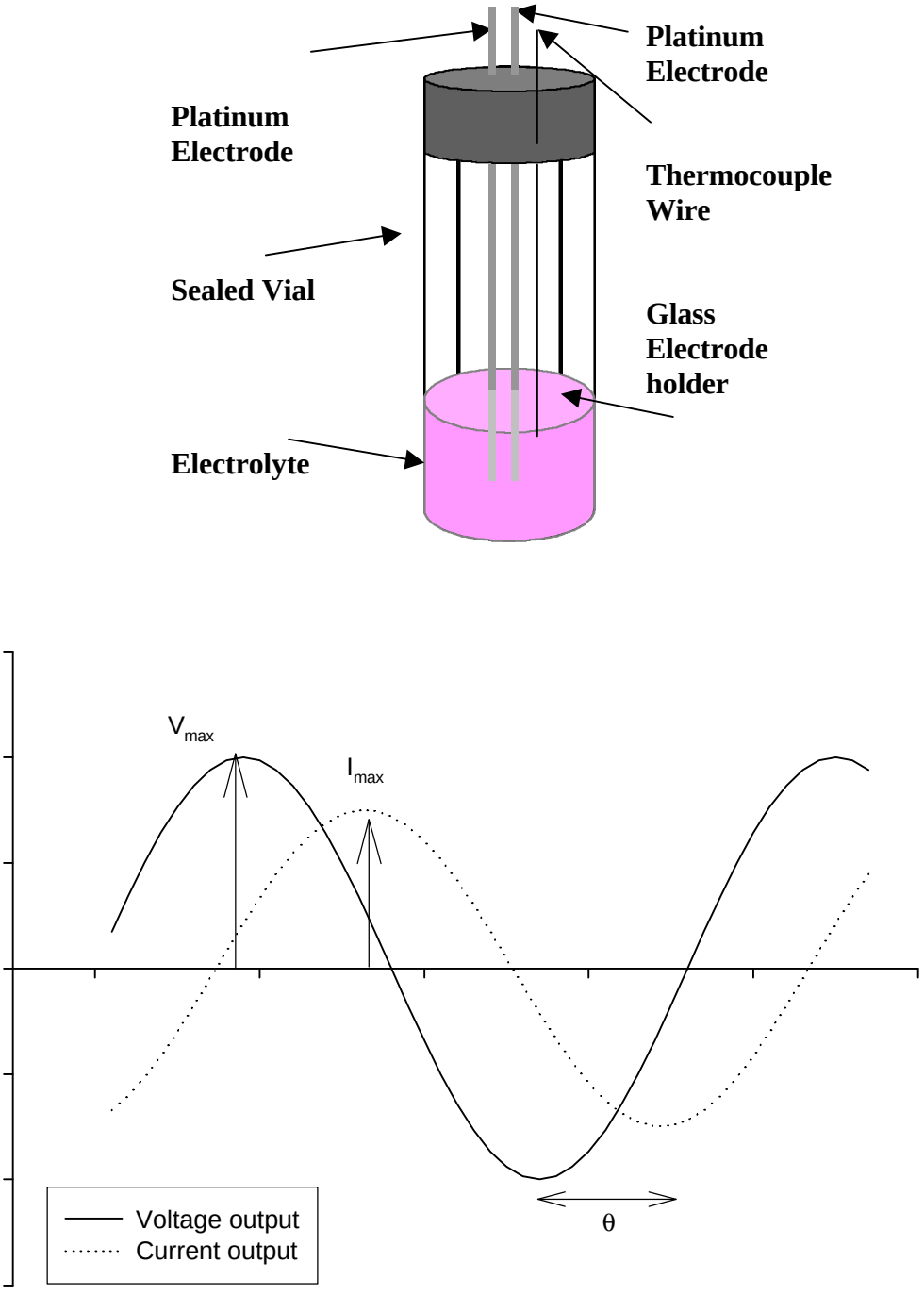

Figure 3. 2. Conductivity cell configuration and sinusoidal current and voltage at a given frequency.

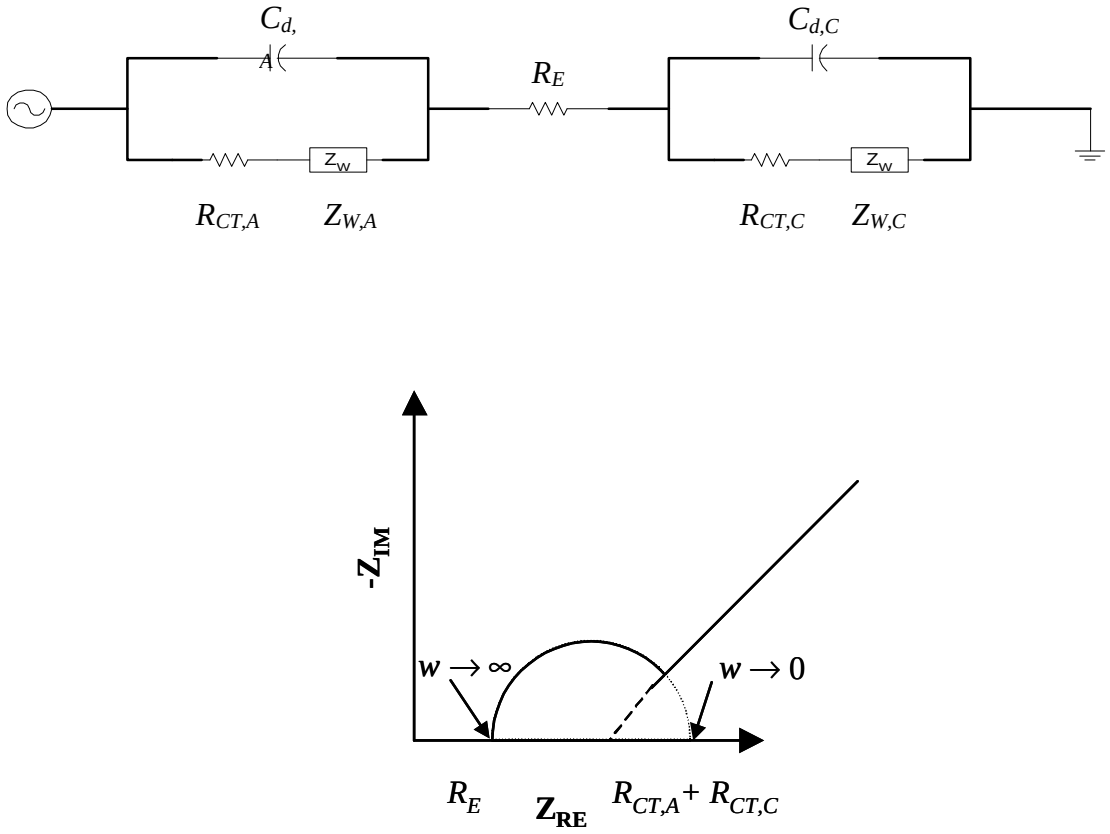

Figure 3. 3 Equivilant circuit for a typical battery with double layer electrode capacitance ($C_{d\,A}$, $C_{d\,C}$), interfacial reaction impedance at electrodes ($R_{CT\,A}$ $R_{CT\,C}$), bulk electrolyte resistance (R_E), and Warburg impedance at electrodes (Z_W).

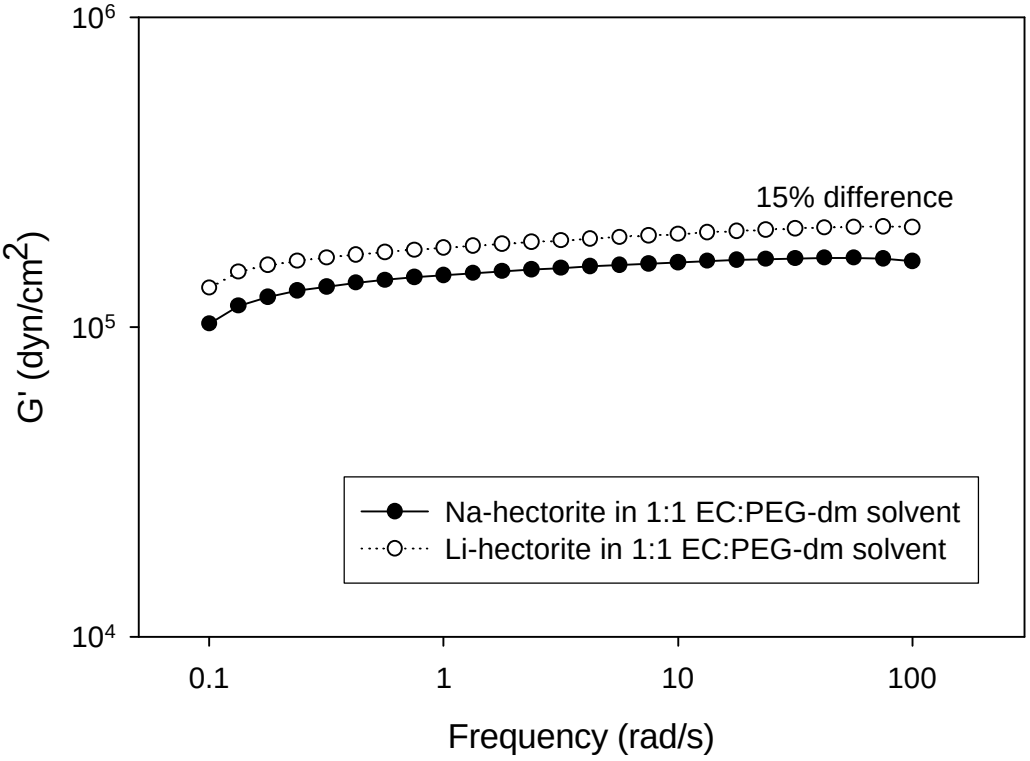

Figure 3.4. Elastic modulus, G′, comparison of Na-hectorite and Li-hectorite (15% clay) in 1:1 EC:PEG-dm solvent.

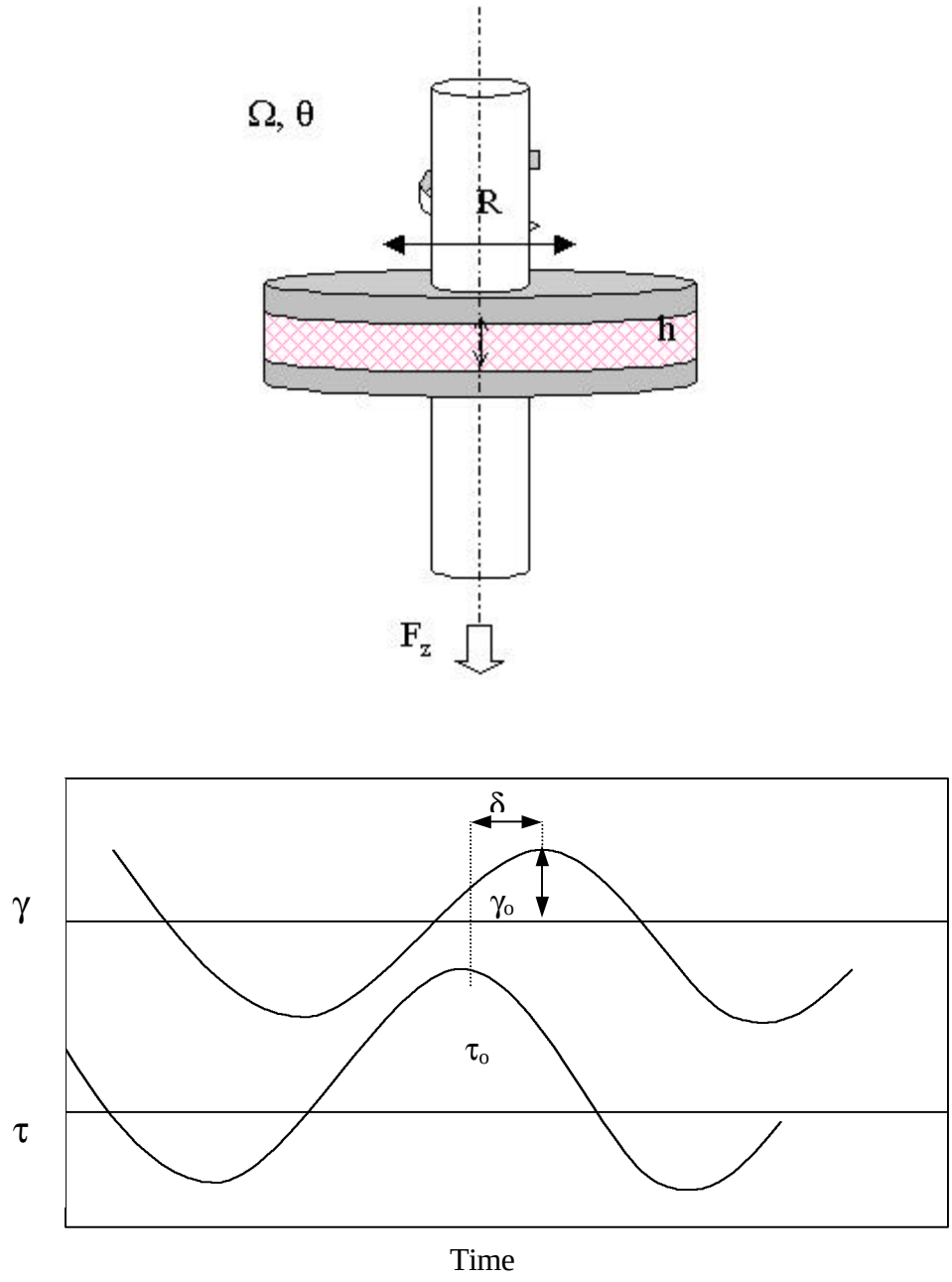

Figure 3. 5. Parallel plate geometry for rheological measurements and sinusoidal strain and stress comparisons showing stress amplitude (τ_o) and strain amplitude (γ_o) with phase shift of δ.

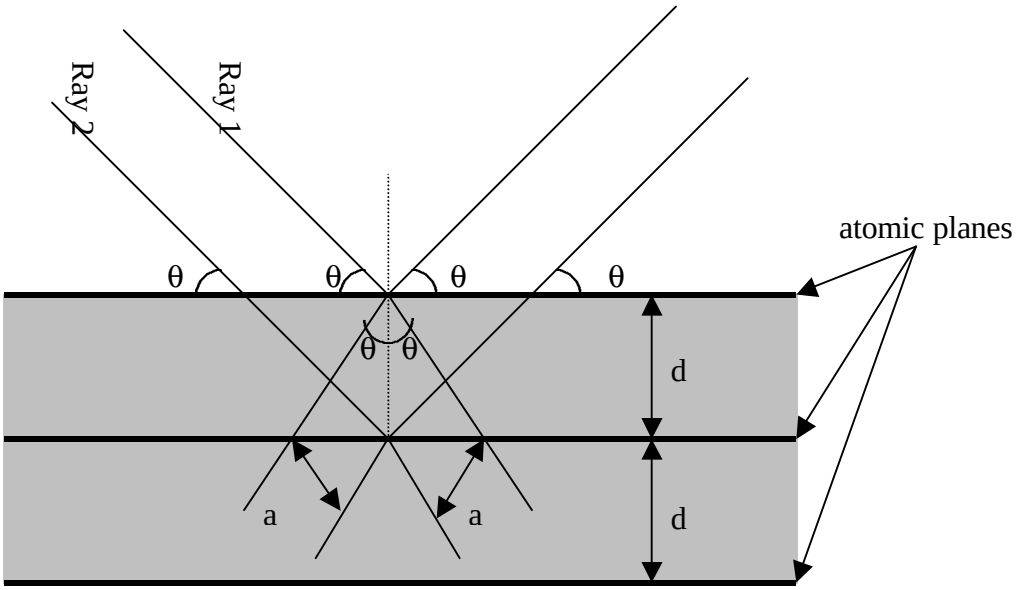

Figure 3. 6. X-Ray diffraction (XRD) schematic where Ray 1 and 2 come in at angle θ across atomic planes that are d distance apart.

Chapter 4: Transport Properties of Hectorite Based Nanocomposite Single-ion Conductors

4.1 Introduction

Rechargeable lithium-ion batteries are an important component in today's small-electronics technology because of desirable characteristics that include high energy density, low weight, and excellent cycle performance. For instance, in 1997 alone, worldwide sales of rechargeable lithium-ion batteries exceeded 1.6 billion dollars[1]. Because of government mandates for electric vehicles and the ever-increasing demand for portable power sources, rechargeable lithium batteries are expected to grow more than 20% per year[2,3]. Lithium-ion batteries in particular are predicted to last the lifetime of a car because of their high energy and power density[4,5]. However, several factors in lithium-ion batteries, especially in the electrolyte, have limited commercial usage. Most lithium-ion batteries use a liquid electrolyte, which requires the use of a microporous polymeric membrane to separate the electrodes. As an alternative, our group[6] is attempting to avoid a separator by using a gel electrolyte with high-mechanical strength. These gel electrolytes must still possess comparable electrochemical properties to liquid electrolytes such as conductivity, lithium transference number, and electrode/electrolyte interfacial stability. The technological impact of developing an electrolyte with improved conductivity and strong mechanical strength is significant and warrants further exploration.

The study of composite polymer electrolytes (CPE) is increasing considerably because they possess desirable properties of both liquid and solid electrolytes. Nano-size fillers such as TiO_2, SiO_2, or Al_2O_3 have shown many advantageous effects on

electrochemical properties, (e.g., conductivity and transference number) of CPEs[7-9]. The benefit of fillers when added to a liquid solvent is their ability to create a gel-like matrix making an open-channel structure for ion transport. However, most fillers are passive, and contribute only to the battery electrolyte as a structural skeleton. We focus on an active filler, lithium hectorite, where the nano-material participates in the ion-transport and improves mechanical strength.

Hectorite and other 2:1 layered clays (smectites) are unique in that they are characterized by a large negatively charged plate-like structure (~250-nm diameter) with exchangeable counter cations sandwiched between thin platelets (~1 nm). For lithium battery application, the native sodium cations on hectorite are exchanged for lithium ions and the plate-like particles are dispersed in high-dielectric solvents (e.g., ethylene carbonate (EC) and propylene carbonate (PC)) to create a physically gelled structure. The cation mobility is considerable relative to the mobility of the large anion clay platelets.

Lithium-ion transference numbers in carbonate solvents with hectorite were shown to be near unity, which indicates predominantly lithium-ion mobility[10]. Conductivity at room temperature, however, in these electrolytes is around 10^{-4} S/cm, whereas the conductivity in a typical non-polymeric Li-ion battery electrolyte ($LiPF_6$ + EC + PC) is around 10^{-2} S/cm. The use of high-molecular weight polyethylene oxide (PEO) has been shown to increase basal spacing of clay platelets[11], however, the ionic conductivity (10^{-6} S/cm) remains several orders of magnitude below non-polymer electrolytes. We hypothesize to show that low-molecular weight methyl terminated PEO, polyethylene glycol di-methyl ether (PEG-dm), with a carbonate co-solvent and Li

hectorite will yield higher ionic conductivities than carbonate electrolytes without PEG-dm; that is, the low-molecular weight PEG-dm (250 MW) will increase basal spacing of the clay platelets and thereby permit lithium ions to travel more freely through the electrolyte.

We report our investigation of the effect of PEG-dm on conductivity, basal spacing of platelets, and rheological properties in hectorite/carbonate electrolytes. Conductivity is measured using impedance spectroscopy to quantify ion motion. The microscopic structure of hectorite clay platelets is analyzed using low angle x-ray diffraction (XRD) to find platelet spacing after dispersion into solution. Rheological properties are investigated to find intrinsic mechanical properties such as gel modulus and yield stress of the electrolyte. Several combinations of clay and polymer loading are studied in an attempt to find an electrolyte with the highest conductivity. A preliminary comparison of rheological properties between hydroxyl terminated PEO (PEG) and PEG-dm as a polymer co-solvent with EC is also made.

4.2 Experimental

ELECTROLYTE PREPARATION

Sodium hectorite, provided by Hoechst (SKS-21, 88 meq/100 g), was mixed with LiCl to exchange sodium with lithium. The lithium counterion of the platelet was the only source of lithium in the electrolyte; no additional salt was added. De-ionized (DI) water (850 mL) and Na-hectorite (20 g) were blended with 150 mL of 0.75 M LiCl solution. The mixture was allowed to equilibrate for one day, and then centrifuged. The supernatant was discarded and the process was repeated twice. After the final LiCl exchange, the clay solids were mixed with 1000 mL of DI water and centrifuged

immediately. The DI water rinse process was repeated two more times. The hectorite mixture was then placed in a 100^{o}C oven for a minimum of three days during which the gel became a solid. The clay was subsequently rinsed with 100 mL methanol (denatured, Aldrich) in a glass frit filter three times to remove residual salts (LiCl and NaCl). Finally, the hectorite was dried at 70^{o}C and atmospheric pressure for at least one day to remove methanol. Li hectorite was sent to Quantitative Technologies Inc. (Whitehouse, New Jersey) for elemental analysis. Table 4.1 has the weight percents of the elements analyzed and the expected weight percents calculated from the chemical formula of Li hectorite ($Mg_{5.3}Li_{0.7}Si_8O_{20}(OH,F)_4Na_{0.7}$). Aluminum was found in our sample, which was not expected in the Hoechst SKS-21 hectorite, but is seen in saponite, another smectite clay made by Hoechst. Discrepency in values could occur because of incomplete cation exchange, impurities (saponite and other compounds), and elemental analysis error.

A matrix of experiments and samples were investigated in order to understand the effect of polymer addition in the Li hectorite/carbonate mixture. In this study, the amount of hectorite and polymer were adjusted. The ethylene carbonate solvent (EC, Aldrich) and the polymer co-solvents (PEG-dm 250 MW and PEG 200 MW, Aldrich) were made at three volume ratios 1:1 EC:PEG-dm, 2:1 EC:PEG-dm, and 1:1 EC:PEG. Control samples were also made where no polymer was added to the EC. Polymer-only control samples (both PEG-dm and PEG) were not because hectorite did not disperse in the polymer solvent. Hectorite loading in each electrolyte was determined as a percentage of solvent weight. Conductivity data is presented in this report with hectorite concentration reported as either hectorite % or mol hectorite/ kg solvent. The Li hectorite

loadings investigated were 5, 10, 15, 20, 25, 30, and 40% hectorite (0.044 – 0.352 mol hectorite/ kg solvent). The solvents, EC (at 70^{o}C) and PEG-dm (at room temperature), were pre-mixed to the desired volumetric ratio (1:1 and 2:1). Anhydrous ethanol (Aldrich) was added to separate clay platelets, which assisted solvent intercalation. Since the order of addition had an effect on the quality of the hectorite dispersion, the following sequence was kept consistent: 1) Li hectorite, 2) EC/PEG-dm mixture, 3) ethanol. When solvent was slowly added to the clay, instead of clay added to the solvent, the platelets absorbed the solvent and created a gel matrix.

The technique for dispersing clay platelets in the solvents was critical to ion mobility. Ethanol was used, instead of water, to exfoliate the clay platelets in order to reduce additional water removal steps. Li hectorite + 15 mL EC/PEG-dm solvent + ~ 40 mL ethanol were mixed at 6100 rpm using a Silverson L4RT high-shear laboratory mixer with a 3/8-inch mixing head. The mixture was brought to 70°C while mixing, using a heating plate, in order to accelerate ethanol removal. When the volume of the mixing vessel was reduced to approximately 20 mL from its initial volume of approximately 60 mL, the heat was turned off but mixing continued. Sets of samples were dried simultaneously for 30 – 60 minute increments in the vacuum oven at 100°C under at least 1 kPa pressure. The sample was then transferred to a high-purity argon (99.998%) atmosphere glove box. The weight of EC that was evaporated in the vacuum oven was calculated by comparing the weight difference before and after drying, and was typically ~30% of the initial EC amount. This amount of EC was then added back to the sample through hand mixing. The sample was hand mixed until the added EC was uniformly distributed. Water content of the electrolytes was measured using a Mitsubishi Karl-

Fisher CA-06 titrator with vaporizer VA-06. Small amounts of each sample (~0.04-0.1 g) were taken from the glove box in sealed glass vials and tested for water content. Samples with water content between 200 to 300 ppm were considered satisfactory, while samples with water content higher than 300 ppm were dried again in a vacuum oven. Additional drying steps were performed until the moisture level was in the appropriate range.

CONDUCTIVITY

Conductivity measurements were made using a PAR 273 potentiostat and 5210 lock-in amplifier (Princeton Applied Research) or a BAS-Zahner IM6e Impedance Analyzer (Bioanalytical Systems, Inc.). A cell consisting of two platinum electrodes in a capped glass vial was used[10]. A cell constant was determined for each cell using a standard KCl solution. Samples were added to these cells in the glove box to ensure low-moisture content. Conductivity was measured between 25 and 100^{o}C and the average of two runs is reported.

X-RAY DIFFRACTION (XRD)

Basal spacing was determined using an Inel XRG 3000 X-Ray Diffractometer that employed Cu-Kα radiation (λ = 1.5405 Å). The measurements were performed at 35 kV and 30 mA. All samples were loaded into a 0.7-mm quartz capillary tube and data was collected for four hours using a stationary detector that gathers signal over the entire 2 theta range (0-120^{o}). The non-uniform surface of gel samples when placed on a flat plate sample holder makes collecting grazing angle (small angle) diffractions difficult. The use of a rotating capillary sample holder helps to alleviate this problem. The x-ray in the

capillary setup transmits through the tube to the sample and diffraction caused by the sample was collected at all possible angles. The beam stop, which protects the detector from the incident beam, produces a peak between 0- 1.9^{o} on the diffractograms.

RHEOLOGY

Dynamic rheological measurements were conducted on a Rheometrics Dynamic Stress Rheometer (DSR II) using Virtual Instrument RSI Orchestrator software and a 25-mm parallel plate geometry for concentrations less than 20% clay. At higher concentrations of clay, a TA Instrument Dynamic Stress Rheometer (Advanced Rheometer 2000) using Rheology Advantage Data Analysis software and a 20-mm parallel plate geometry (with sandpaper) was used because of instrumental limitations of the DSR II. In these experiments, a sinusoidally varying stress was applied to the sample. From the applied stress, the resulting elastic (G′) and viscous (G″) moduli were obtained as either a function of frequency or stress amplitude at a fixed frequency of 1 rad/s. Frequency spectra of G′ and G″ were obtained at a constant stress/strain amplitude in the linear viscoelastic regime. The yield stress was found by applying increasing stress until the elastic modulus decreased precipitously. Creep measurements were recorded to obtain the steady state creep compliance J_e^o and the recoverable creep compliance $J_r\ (t)$. During a creep measurement, stress (t_o = 200 Pa) was applied for a specified time (t = 600 seconds), and strain was recorded. The stress was then removed and the recovery strain was recorded for 3200 seconds. Steady state creep compliance J_e^o was found from the extrapolated point at t = 0 of the linear slope of compliance as a function of time in the initial applied stress regime (the linear slope represents the steady state deformation of sample from the initial stress). Recoverable creep compliance, $J_r\ (t) = g_r\ (t) / t_o$, was

calculated from the recovery strain (g_r) and the applied stress, and represents the recoil of strain after the stress is removed.

4.3 Results

4.3.1 Conductivity Measurements

Figure 4.1 displays the effect of temperature on conductivity for electrolytes containing 5 – 40 % clay. Within the errors of the experiment, most of the samples exhibit an Arrhenius behavior as indicated by the linear relationship between conductivity and 1/T. For one of the samples (2:1 EC:PEG-dm), we observe some slight non-Arrhenius behavior. Conductivity as a function of clay concentration is shown in Figure 4.2 at 25^{o}C for electrolytes with: 1:1 EC:PEG-dm, 2:1 EC:PEG-dm, and 1:1 EC:PC. The conductivity with 1:1 EC:PC solvent was measured by Riley et al.[10] and was mixed slightly different from our samples (water instead of ethanol was used in the initial dispersion and a high-shear mixer was not used). We see an improvement in conductivity for the 2:1 EC/PEG-dm electrolyte when compared to the 1:1 EC:PC and 1:1 EC:PEG-dm solvent. At concentrations above 25% clay, 2:1 EC:PEG-dm and EC solvents displayed a decrease in conductivity. A maximum conductivity at 60^{o}C with concentration of Li hectorite is also seen in Figure 4.3 where EC:PEG-dm solvent mixtures are compared to the EC only control samples. At 60^{o}C the maximum conductivity for both 2:1 EC:PEG-dm and EC electrolytes occurs at 0.22 mol Li hectorite/kg solvent and is 0.60 and 0.49 mS/cm, respectively. The maximum conductivity for 1:1 EC:PEG-dm at 60^{o}C is 0.54 mS/cm and occurs at 0.26 mol Li hectorite/ kg solvent. These results (Figures 4.2 and 4.3) indicate that the concentration

at which maximum conductivity occurs is approximately independent of temperature over this narrow temperture range (25 –60^{o}C). However, the maximum conductivity of 2:1 EC:PEG-dm electrolytes is 10% higher than the maximum conductivity of 1:1 EC:PEG-dm electrolytes at 25^{o}C and is 14% higher at 60^{o}C.

4.3.2 XRD Measurements

Interlayer separation of clay platelets was determined using X-Ray diffraction. Three solvents were investigated: 1:1 EC:PEG-dm, 2:1 EC:PEG-dm, and EC only, at four loadings of clay (5, 15, 25, 40 wt%). The diffraction patterns are shown in Figure 4.4. Two d_{001} peaks are seen for powder Li hectorite, $2\theta = 2.3^{o}$ and 6.9^{o}, which corresponds to a basal spacing of ~3.8 and 1.3 nm, respectively. Previous work[12] has shown a peak for Na hectorite powder around 6^{o}; the peak we notice at 6.9^{o} for Li hectorite is attributed to the same inherent clay platelet spacing. The hectorite used by Cool and Vansant[12] had a platelet diameter of 2000 nm and was found naturally. In our work, we used a synthetic hectorite of 250 nm diameter, which could account for the small 2θ difference between Cool and Vansant's and our XRD patterns. It is conceivable that the low-angle peak at 2.3^{o} is a result of a super lattice structure. If the clay platelets are forming a repeatable n-layer stack through out the powder, then the basal spacing represented at 2.3^{o} is a measure of distance between the stacks. We have ensured that no divalent or stray metal ions are in the powder clay through elemental analysis (Table 4.1). We feel it is possible that bulky organic cations are present, though it is unknown to us, due to the carbon content of around 0.1%. The peak at 2.3^{o} was also seen in Na hectorite diffractograms, which implies that believe methanol used in the exchang process did not cause the large layer spacing, although additives from the manufacturers are unknown. Figure 4.11a is a

pictorial representation of the possible n-layer (for example n=3 in Figure 4.11a) particle relationship to basal spacing.

The hectorite powder diffraction is shown with the electrolyte gel diffractions (Figure 4.4), and the arrows indicate the peaks. The XRD peaks of the composite electrolytes fall between $2\theta = 3.4$ to 4.7^{o}, which represents a downward shift of the 6.9^{o} peak seen in the Li hectorite diffraction pattern. A shift to lower angles indicates clay platelet swelling, i.e., an increase in platelet basal spacing (d).

Using Bragg's law, $d = \lambda/(2 \sin(\theta))$, we calculated the basal spacing (d_{001}) as a function of clay concentration (Figure 4.5). Figure 4.5 displays the basal spacing in 1:1 EC:PEG-dm, EC, and 2:1 EC:PEG-dm solvents as a function of clay concentration. The amount of clay has an influence on the average platelet separation. At 25% clay, basal spacing reaches a maximum (23 – 26 Å) for all three solvents and quickly declines as clay concentration increases.

4.3.3 Rheology Measurements

Figure 4.6 shows a representative plot of the elastic (G′) and viscous (G″) moduli as functions of frequency for a 1:1 EC:PEG-dm solvent mixture at 15% and 5% clay content. At a stress within the linear viscoelastic (LVE) regime, both G′ and G″ are independent of frequency with G′ exceeding G″. These features, which are characteristics of a gel[13], were found for all samples used in this study. Figure 4.6 also shows that G′ and G″ increase with clay concentration. We report the effect of clay concentration in more detail in Figure 4.7, which shows G′ as a function of clay concentration for 1:1 EC:PEG-dm, 2:1 EC:PEG-dm, and 1:1 EC: PEG electrolytes at one

frequency (w = 1 rad/s). Both gels with PEG-dm display similar modulus in the concentration regime measured; however, the PEG gels exhibited lower G′ values. Gel modulus for all samples increase by almost two orders of magnitude over the concentration range studied (5 - 40%).

Apparent yield stress was determined from a plot of G′ as a function of stress amplitude[14,15]. Figure 4.8 shows an example of this procedure for three samples: 10% clay in 1:1 EC:PEG, 5% clay in 1:1 EC:PEG-dm, and 10% clay in 1:1 EC:PEG-dm. Above a certain stress, the sample microstructure is disrupted with a concomitant decrease in G′ and increase in G″ (G″ not shown on figure). The yield stress corresponds to the intersection of extrapolated lines drawn through the stress-invariant and stress-varying regimes, as shown by the arrows. Yield stress obtained using this approach for various samples at different concentrations of clay are provided in Table 4.2. Consistent with the trend in elastic modulus, the yield stress increases with clay concentration and the PEG samples show lower yield stress when compared to PEG-dm samples of the same clay concentration.

The steady state creep compliances J_e^o of samples are tabulated in Table 4.3. The creep compliance decreases with increasing clay concentration, and the PEG samples reveal a higher creep compliance compared to their methyl-capped analog. These results indicate that samples with larger clay content deform (or "creep") less under an applied stress.

The recoverable creep compliances (J_r) of Li hectorite samples in 1:1 EC:PEG-dm and 1:1 EC:PEG solvents at different clay concentrations are shown on a plot of strain normalized with respect to imposed stress (γ/τ_o) as a function of time, Figure 4.9.

While we find clay concentrations to have a large effect on recovery, it is interesting to note that the strain recovery is larger for samples with lower clay concentrations.

4.4 Discussion

4.4.1 Hectorite Concentration Effects

Conductivity in an electrolyte is dependent on both concentration of ions and their mobility. The later, in turn, is affected by electrolyte viscosity and filler dispersion. Increase in viscosity and filler aggregation can impede mobility and lower conductivity. In our research, ion concentration is proportional to clay content, yet the higher the clay concentration the more likely platelet aggregation will occur. This proportionality leads to a maximum conductivity at an optimum clay concentration, which has been shown previously by Riley et al.[10]. We found a broad maxima of conductivity as a function of clay concentration for our PEG-dm electrolytes. We also note a correlation between conductivity and platelet separation maximum with regards to clay concentration.

Nanocomposite clay platelets have been shown by Krishnamoorti et al.[16] and Luckham and Rossi[16,17] to experience interactions with other platelets. In single-ion conductors, these interactions affect conductivity because the platelets create channels for ion movement. Various modes of platelet associations (dispersed, face-to-face, edge-to-face, and edge-to-edge), shown in Figure 4.10, alter the channels for lithium-ion movement and hence conductivity. Clay platelets are stable in suspensions because of electrical double-layer repulsion; at high concentration of clay, however, interlayer repulsion decreases and platelets aggregate. When platelets aggregate, conductivity decreases because lithium-ions become less mobile in between platelets. We found that

25% clay yields the best balance of Li^+ concentration (0.22 mol Li^+/ kg solvent) and clay platelet separation.

The amount of clay has an influence on the average separation distance of platelets, which is verified by XRD measurements. At 25% clay, basal spacing reaches a maximum for all solvent types (23-26 Å) and declines as clay concentration increases (Figure 4.5). The conductivity also follows the same trend, however a less pronounced decrease is seen at high concentration of clay (Figure 4.3). This occurs because of the beneficial effect on conductivity of increased charge-carrier concentration with more clay. The basal spacing and conductivity results indicate that platelets are separated best for single-ion mobility at a concentration of 25% clay (in both 2:1 EC:PEG-dm and EC solvents).

At high concentrations of clay the double-layer collapse leads to closer clay platelets, while at low concentrations (5 and 15% clay) the platelets have a higher degree of random orientation. Randomly orientated clay platelets are unlike the ordered structures in Figure 4.10, and appear as a broad XRD peak of low intensity[12]. A broad peak represents a wide distribution of particle spacing, typical of clay platelets that are near exfoliation (5 and 15% clay samples). TEM images[18,19] show a stacking effect of clay layers when embedded in resin. These stacks of clay layers, ranging from 2-4 in number, constitute one clay particle. High intensity XRD peaks, as seen at 25% and 40% clay concentrations, represent uniform stacks of clay platelets with uniform spacing between the particles ($3.0 < 2\theta < 4.5^o$). A schematic of clay platelets stacks and interplatelet spacing is shown in Figure 4.11. The progression from more clay particles

(Figure 4.11a) to less clay particles (Figure 4.11d) corresponds to a decrease in uniformity of basal spacing.

4.4.2 Polymer concentration effect

One objective of this research was to observe the change in conductivity upon addition of low-molecular weight polymer to a nanocomposite clay-based electrolyte. We found that a EC:PEG-dm (250 MW) solvent mixture, at a 2:1 volumetric ratio, produced electrolytes with the highest conductivity (Figures 4.2 and 4.3). At higher content of PEG-dm, such as 1:1 EC:PEG-dm, conductivity decreased slightly and was similar to the EC only samples. These results indicate polymer addition can be beneficial to ionic conductivity when a small amount is added to the carbonate co-solvent. The dielectric constants for EC and PC[20], $\varepsilon = 89$ and 64, respectively, are greater than that of PEG-dm 250 MW ($\varepsilon = 7.9$)[20], hence PEG-dm is not as conducive to salt disassociation as EC or PC. Surprisingly, the conductivity of 1:1 EC:PEG-dm and 1:1 EC:PC electrolytes are similar despite the high-dielectric constant of the 1:1 EC:PC mixture. We believe that gel formation in our samples is controlled more by the concentration of clay platelets than the solvent type. This is consistent with the rheology results, as discussed later. However, because we observe a slight increase in conductivity when small amounts of PEG-dm are added to EC (2:1 EC:PEG-dm), we expect that interactions (Van der Walls, dipole/dipole, etc.) between PEG-dm molecules and clay platelets exist to affect electrolyte structure.

4.4.3 Rheological Properties of Li hectorite electrolytes

The rheological results indicate that clay concentration plays the most dominant factor in dictating the modulus/strength of the electrolytes. We witness an increase of G′ by almost two orders of magnitude (~10^3 to ~10^5 Pa) as clay weight percent increased from 5 to 15% (Figure 4.7). At concentrations above 15% clay, the elastic modulus plateaus, which represents declining change in particle interactions. The nature or composition of the solvent seems to have a much smaller effect on modulus. For instance, G′ is the same for 1:1 EC:PEG-dm and 2:1 EC:PEG-dm electrolytes. EC only electrolytes had slightly lower G′ in comparison to PEG-dm samples, and at 40 clay %, the modulus was equal to that of both PEG-dm ratios in EC. These results indicate that the clay platelet aggregates are influenced more by platelet/platelet interactions than solvent/clay interactions. The modulus of the EC:PEG samples decreases by only a factor 2-3 from the PEG-dm samples, a difference that is small in comparison to the two orders of magnitude difference observed with changes in clay concentration. Because of the strong electrostatic interactions between clay platelets, the small change in viscosity induced by doubleing the amount of PEG-dm:EC from 1:1 to 2:1, does not affect the overall elastic modulus. In gels using PC:EC solvent mixture shown by Riley et al.[21], the elastic moduli also fall in the range of values presented in this research. Future studies with higher molecular weight PEG-dm is of interest since they may show a greater effect on gel strength because of an increase in polymer viscosity.

The lower elastic modulus observed for the EC:PEG electrolytes compared to EC:PEG-dm electrolytes (Figure 4.7) can be explained in terms of the dispersion of clay in the solvent. Low-molecular weight hydroxyl terminated PEG is more polar than PEG-

dm and would produce a better solvent/clay dispersion. In fact, electrolytes with 1:1 EC:PEG solvent were visually more translucent, or better dispersed, than the PEG-dm mixtures. Because of the relatively more polar nature of the polymer, PEG exfoliates the clay layers compared to PEG-dm, which does not solvate the clay platelets leading to clay aggregation. Such a scenario is consistent with the results of Riley et al.[21], who found G′ and yield stress decrease with enhanced dispersibility. In our case, the yield stress of Li hectorite in 1:1 EC:PEG-dm is also consistently higher when compared to Li hectorite in 1:1 EC: PEG. Our results show that materials with high G′ also have a high yield stress. While these are desirable rheological characteristics for an electrolyte, it is important for an electrolyte to exhibit minimum creep compliance. The steady state creep compliance, J_e^o, shown in Table 4.3, represents the deformation extent of an electrolyte and we find it to decrease with increasing clay concentration. This result is consistent with the modulus data, as we would expect a stronger gel to deform less than a weaker gel when the same stress is applied.

Interestingly though, the opposite trend is noticed in the material recovery, as quantified by the recoverable creep compliance (J_r). The J_r, which reflects the ductile/flexible nature of the sample, increases with decreasing clay concentration. This result indicates that the electrolytes become less elastic with increasing clay concentration. We can rationalize this occurrence by realizing that at high concentrations of clay the matrix of platelets is complex and once altered by stress, the matrix does not recover its original structure. The loss tangent ($\tan \delta \equiv G''/G'$) data from our dynamic experiments is also consistent with the recovery results. For instance, we find that the loss tangent for samples containing 10, 15, and 20% clay in 1:1 EC:PEO, are 0.06, 0.08,

and 0.09, respectively, and in 10 and 15% clay with 1:1 EC:PEG-dm solvent tan δ is 0.06 and 0.10, respectively. This indicates that while addition of clay increases elastic modulus it has a larger effect in enhancing viscous modulus. The relative increase in viscous contribution also manifests itself in the samples by becoming less elastic or ductile with higher clay concentrations.

4.5 Conclusions

In this study, we examine the effects of Li hectorite clay concentration and solvent composition on the conductivity and rheology of nanocomposite single-ion conductors. We find all samples to exhibit gel-like behavior with room temperature conductivities of order 0.1 mS/cm. A maximum in conductivity is observed with clay concentration. A maximum in clay basal spacing is also observed in the same concentration range, suggesting a direct correlation between conductivity and basal spacing. In contrast, the elastic modulus increases with clay concentration and asymptotes to 2×10^5 Pa. These results taken together indicate that while changes in basal spacing are important to conductivity, the rheology is not affected by changes at such a small scale. Solvent composition seems to play a secondary role in terms of affecting both conductivity and rheology. Addition of PEG-dm to the base EC electrolyte produces moderate improvement in conductivity; the elastic modulus also increases by a factor of three. On the contrary, changes in clay concentration over a span of 5 - 15 weight %, enhances G' and yield stress by two orders of magnitude and conductivity by one order of magnitude, indicating clearly clay concentration to be the primary factor in determining the characteristics of these single-ion conductors.

4.6 Acknowledgements

This research was supported by the Department of Education, Graduate Assistance in Areas of National Need (GAANN) Electronic Materials Fellowship. We are thankful for XRD measurements as well as interpretive efforts provided by Professor James Martin's group in the Chemistry Department at North Carolina State University.

4.7 References

1. R. J. Brodd, "Recent Developments in Batteries for Portable Consumer Electronics Applications", *Interface*, **8**, 20-23 (1999).
2. L. Xie, D. Fouchard, and S. Megahed *Material Requirements for Lithium-Ion Batteries*; Mater. Res. Soc. Symp. Proc.: San Francisco, CA, 1995; Vol. 393, pp 285-304.
3. A. Tether *Scientist Helping America*; http://safe.sysplan.com/scihelpamerica/ad.html, 2002.
4. L. Gaines and R. Cuenca, "Costs of Lithium-Ion Batteries for Vehicles", (2000).
5. M. Wakihara, "Recent developments in lithium ion batteries", *Mater. Sci. Eng. R-Rep.*, **33**, 109-134 (2001).
6. S. R. Raghavan, M. W. Riley, P. S. Fedkiw, and S. A. Khan, "Composite Polymer Electrolytes Based on Poly(ethylene glycol) and Hydrophobic Fumed Silica:Dynamic Rheology and Microstructure", *Chem. Mat.*, **10**, 244-251 (1997).
7. Y. X. Li, P. S. Fedkiw, and S. A. Khan, "Lithium/V_6O_{13} cells using silica nanoparticle-based composite electrolyte", *Electrochimica Acta*, **47**, 3853-3861 (2002).
8. J. Fan, S. R. Raghavan, X. Y. Yu, S. A. Khan, P. S. Fedkiw, J. Hou, and G. L. Baker, "Composite polymer electrolytes using surface-modified fumed silicas: conductivity and rheology", *Solid State Ion.*, **111**, 117-123 (1998).
9. H. J. Walls, J. Zhou, J. A. Yerian, P. S. Fedkiw, S. A. Khan, M. K. Stowe, and G. L. Baker, "Fumed silica-based composite polymer electrolytes: synthesis, rheology, and electrochemistry", *Journal of Power Sources*, **89**, 156-162 (2000).
10. M. Riley, P. Fedkiw, and S. Khan, "Transport Properties of Lithium Hectorite-Based Composite Electrolytes", *Journal of Electrochemical Society*, (2001).
11. P. Aranda and E. Ruiz-Hitzky, "Poly(ethylene oxide)/NH^{4+}-smectite nanocomposites", *Appl. Clay Sci.*, **15**, 119-135 (1999).

12. P. Cool and E. F. Vansant, "Preparation and characterization of zirconium pillared laponite and hectorite", *Microporous Mater.*, **6**, 27-36 (1996).

13. C. W. Macosko *Rheology: Principles, Measurements, and Applications*; VCH Publishers, Inc.: New York, NY, 1994.

14. H. J. Walls, B. S. Cains, and S. A. Khan, "Yield Stress and Wall Slip Phenomena in Colloidal Silica Gels", *Rheologica Acta*, (in preparation).

15. M. C. Yang, L. E. Scriven, and C. W. Macosko, "Some Rheological Measurements on Magnetic Iron-Oxide Suspensions in Silicone Oil", *J. Rheol.*, **30**, 1015-1029 (1986).

16. R. Krishnamoorti, J. Ren, and A. S. Silva, "Shear response of layered silicate nanocompostites", *J. Chem. Phys.*, **114**, 4968-4973 (2000).

17. P. F. Luckham and S. Rossi, "The Colloidal and rheological properties of bentonite suspensions", *Advances in Colloid and Interface Science*, **82**, 43-92 (1999).

18. J. F. Alcover, Y. Qi, M. Al-Mukhtar, S. Bonnamy, and F. Bergaya, "Hydromechanical effects: (I) on the Na-smectite microtexture", *Clay Min.*, **35**, 525-536 (2000).

19. H. J. Walls, M. W. Riley, R. R. Gupta, R. J. Spontak, P. S. Fedkiw, and S. A. Khan, "Nanocomposite Electrolytes Derived from Fumed Silica and Hectorites: Passive vs. Active Fillers", *Advanced Materials*, (2002).

20. S. R. Raghavan, H. J. Walls, and S. A. Khan, "Rheology of Silica Dispersions in Organic Liquids: New Evidence for Solvation Forces Dictated by Hydrogen Bonding", *Langmuir*, **16**, 7920-7930 (2000).

21. M. Riley, P. Fedkiw, and S. A. Khan, "Nanocomposite based electrolytes for lithium-ion batteries", *Materials Research Society Symposium Proceedings*, **575**, 137-142 (2000).

Table 4.1. Major elements in Li hectorite found by Quantitative Technologies Inc compared to expected weight percents based on formula of hectorite SKS-21 ($Mg_{5.3}Li_{0.7}Si_8O_{20}(OH,F)_4Li_{0.7}$).

Elements	**Expected Weight %**	**Found Weight %**
Si	29.6	24.5
Mg	17.0	17.6
Li	1.3	0.99
Na	0	0.16
C	0	0.16
Al	0	0.07

Table 4.2. Yield stress (Pa) for 1:1 EC:PEO and 1:1 EC:PEG-dm electrolytes at various clay wt%.

Hectorite %	**1:1 EC:PEG**	**1:1 EC:PEG-dm**
5	160	230
10	1600	3000
15	4000	6000
20	5000	N/A

Table 4.3. Steady state creep compliance, J_e^o (Pa^{-1}), for 1:1 EC:PEG-dm and 1:1 EC:PEO solvent systems at various concentrations of clay

Hectorite %	1:1 EC:PEG-dm	1:1 EC:PEO
10	3.7×10^{-5}	1.0×10^{-4}
15	1.3×10^{-5}	2.6×10^{-5}
20	N/A	1.3×10^{-5}

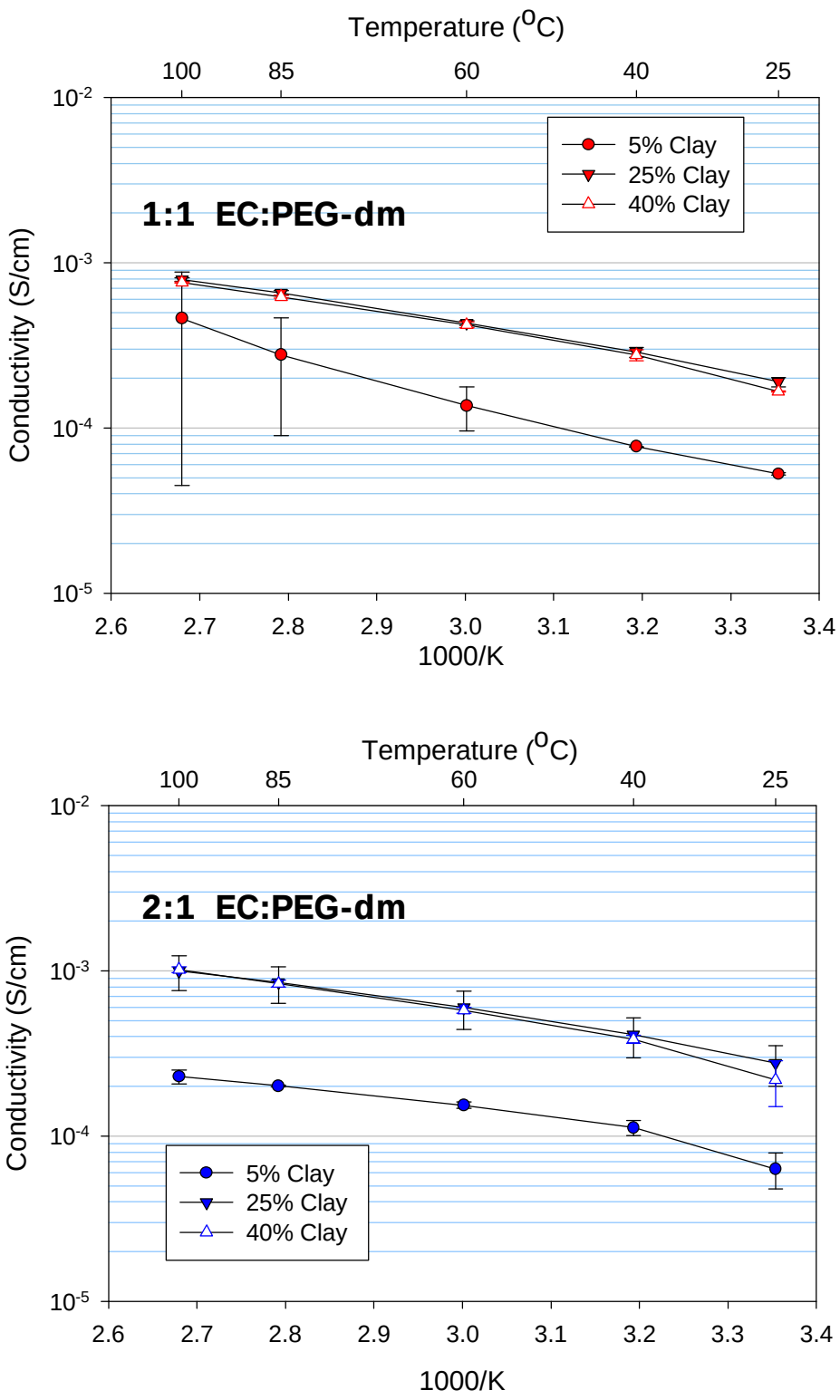

Figure 4. 1. Arrhenius plot of conductivity for 5, 25, and 40% clay electrolytes in 1:1 EC:PEG-dm (top) and 2:1 EC:PEG-dm (bottom) solvent mixture.

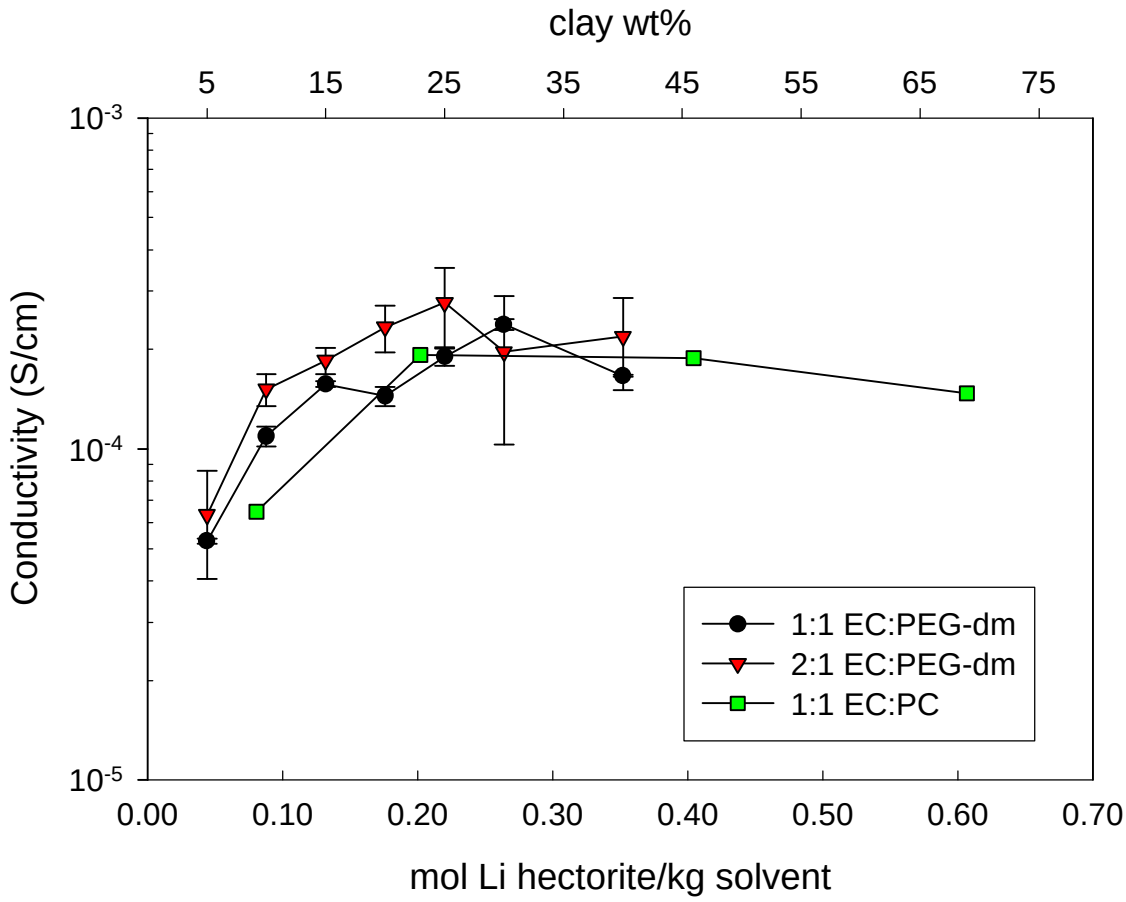

Figure 4. 2. Conductivity at 25°C for three solvent systems: 1:1 EC:PEG-dm, 2:1 EC:PEG-dm, and 1:1 EC:PC (Riley et al.[10]).

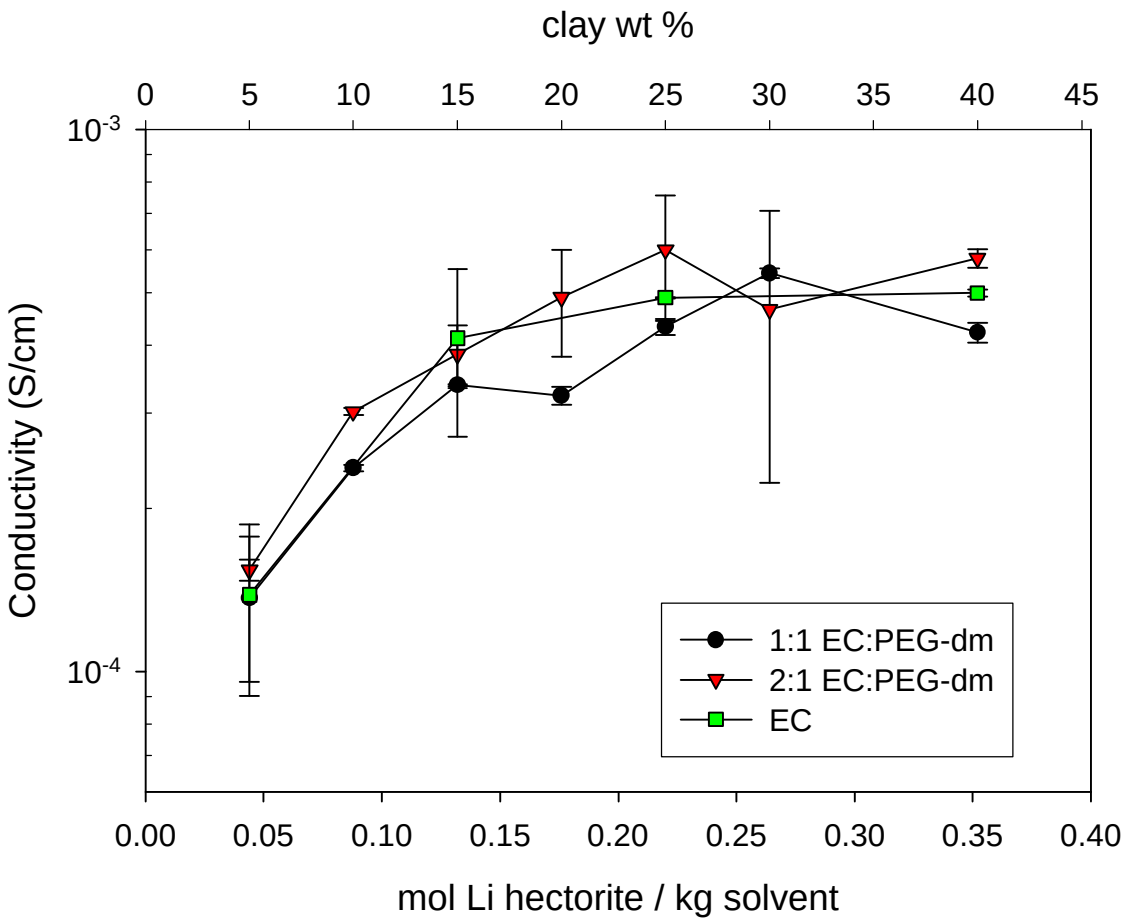

Figure 4. 3. Conductivity at 60°C for 1:1 EC:PEG-dm, 2:1 EC:PEG-dm, and EC only.

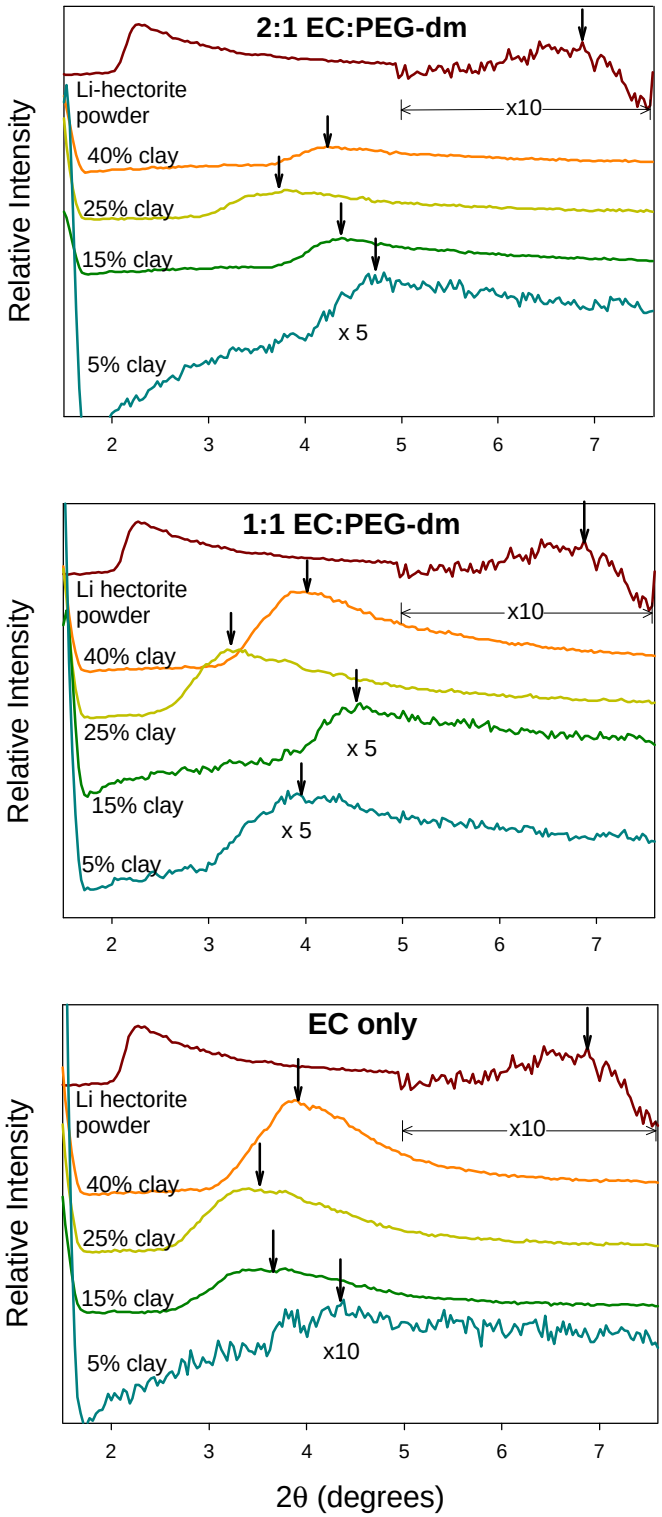

Figure 4. 4. XRD results for 2:1 EC:PEG-dm, 1:1 EC:PEG-dm, and EC only with 5, 15, 25, and 40% clay. Arrows indicate the peaks that represent basal spacing plotted in Figure 4.5. Also shown on each graph is a powder spectrum for Li hectorite, which illustrates the shift of 7^{o} peak position for each of the composite samples.

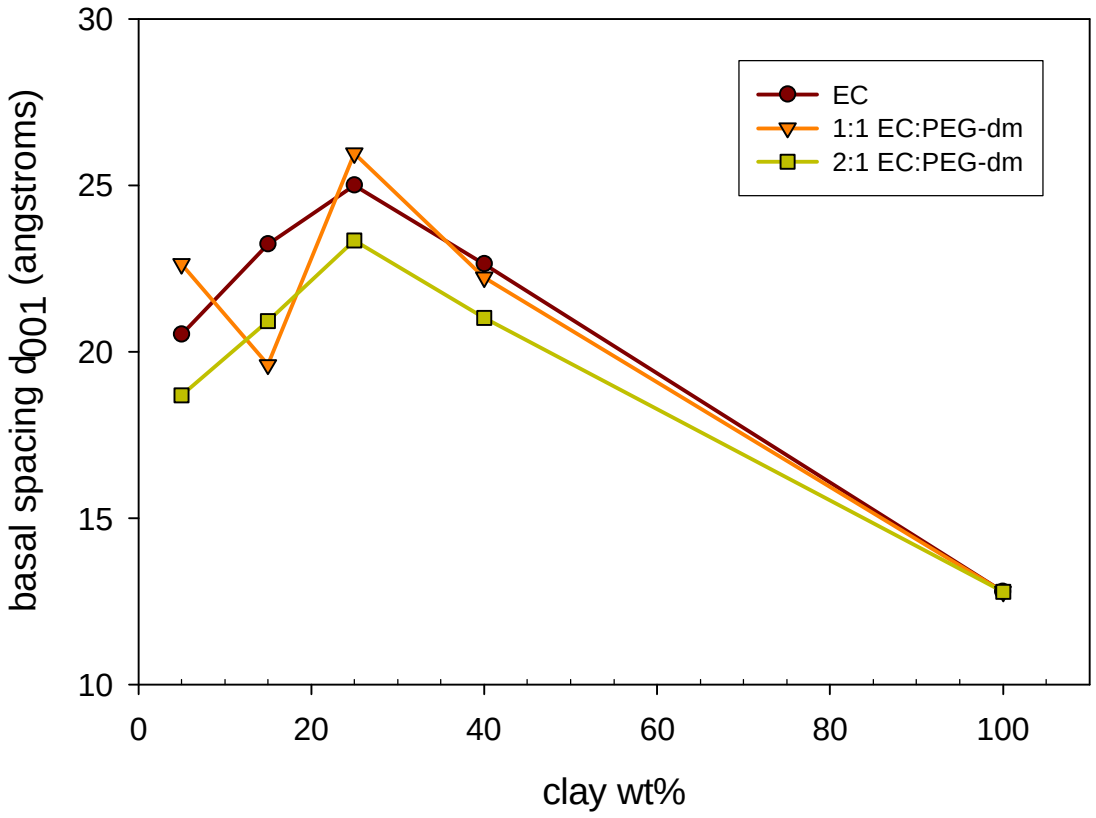

Figure 4. 5. Basal spacing for various clay concentrations in 1:1 EC:PEG-dm, 2:1 EC:PEG-dm and EC only solvents.

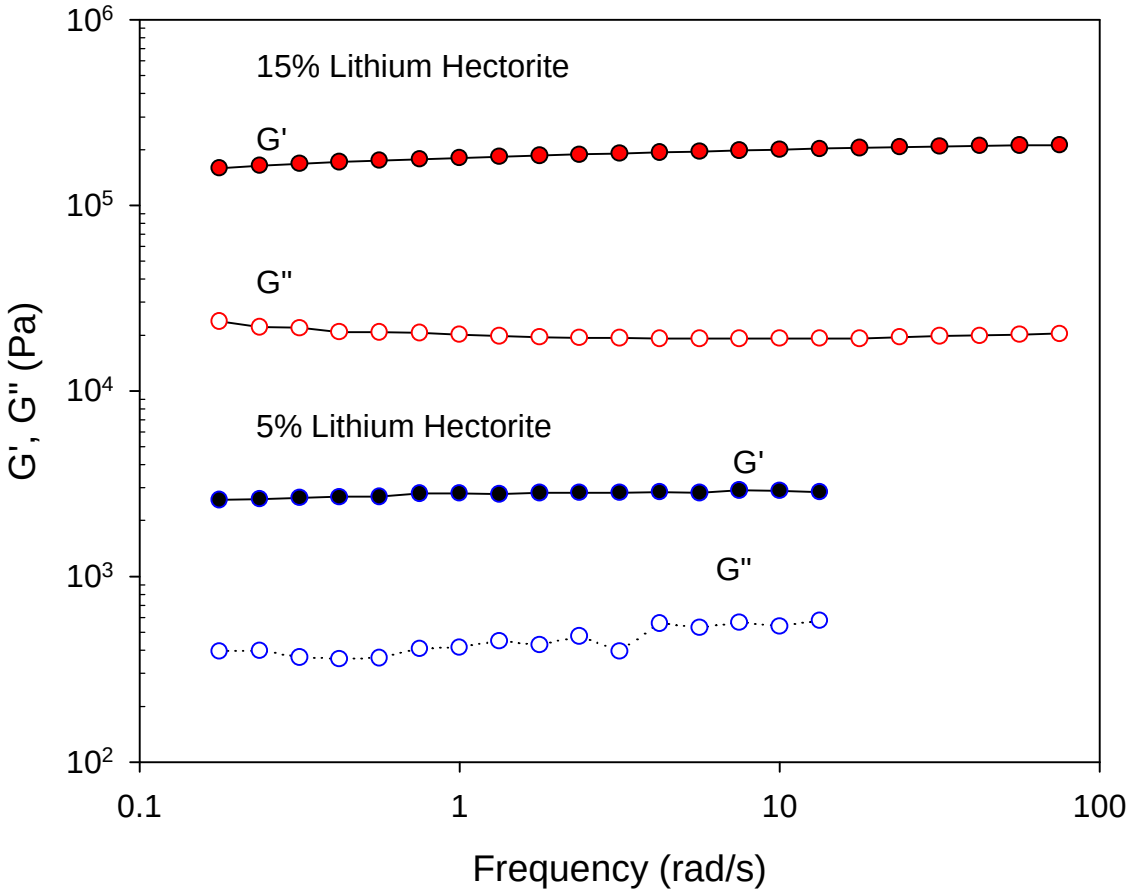

Figure 4. 6. G′ (elastic modulus) and G″ (viscous modulus) as a function of frequency (at a constant stress in the LVE regime) for 15% and 5% clay in 1:1 EC:PEG-dm.

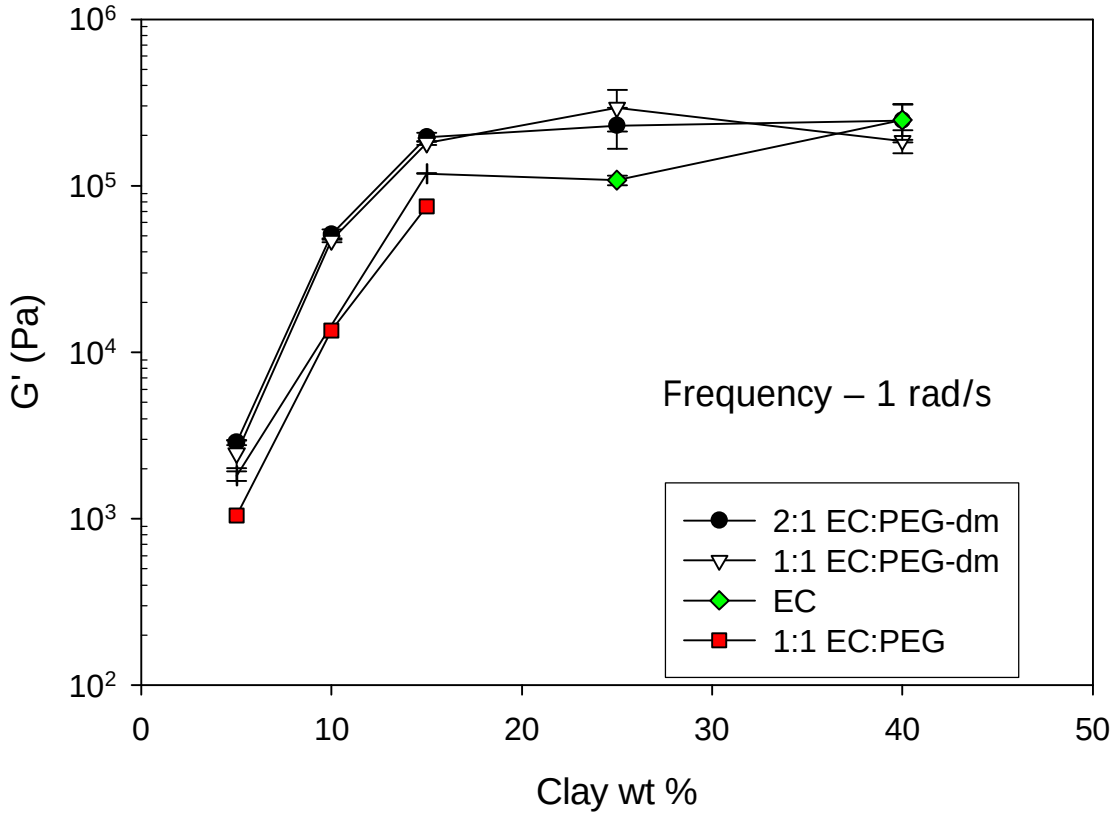

Figure 4. 7. G′ at different clay concentrations for four solvent mixtures (1:1 EC:PEG-dm, 2:1 EC:PEG-dm, EC, and 1:1 EC:PEG).

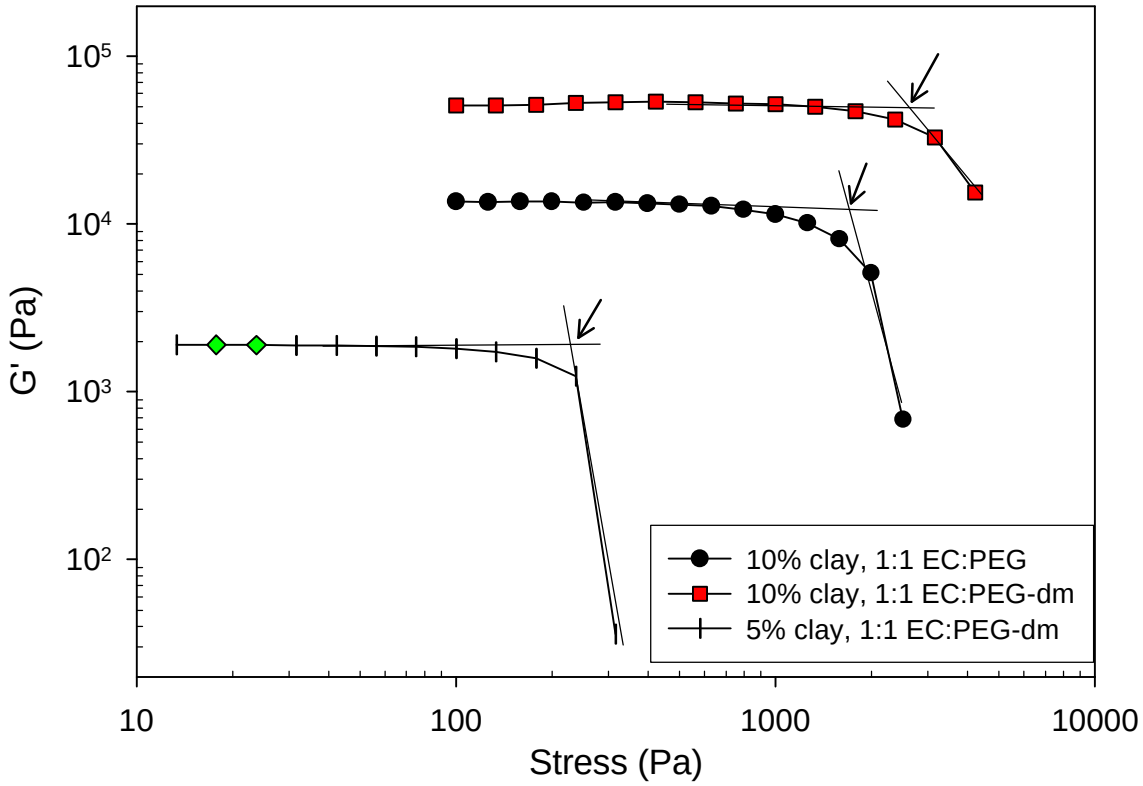

Figure 4. 8. Yield stress (marked by arrow) of 10% and 5% clay in 1:1 EC:PEG-dm and 10% clay in 1:1 EC: PEG.

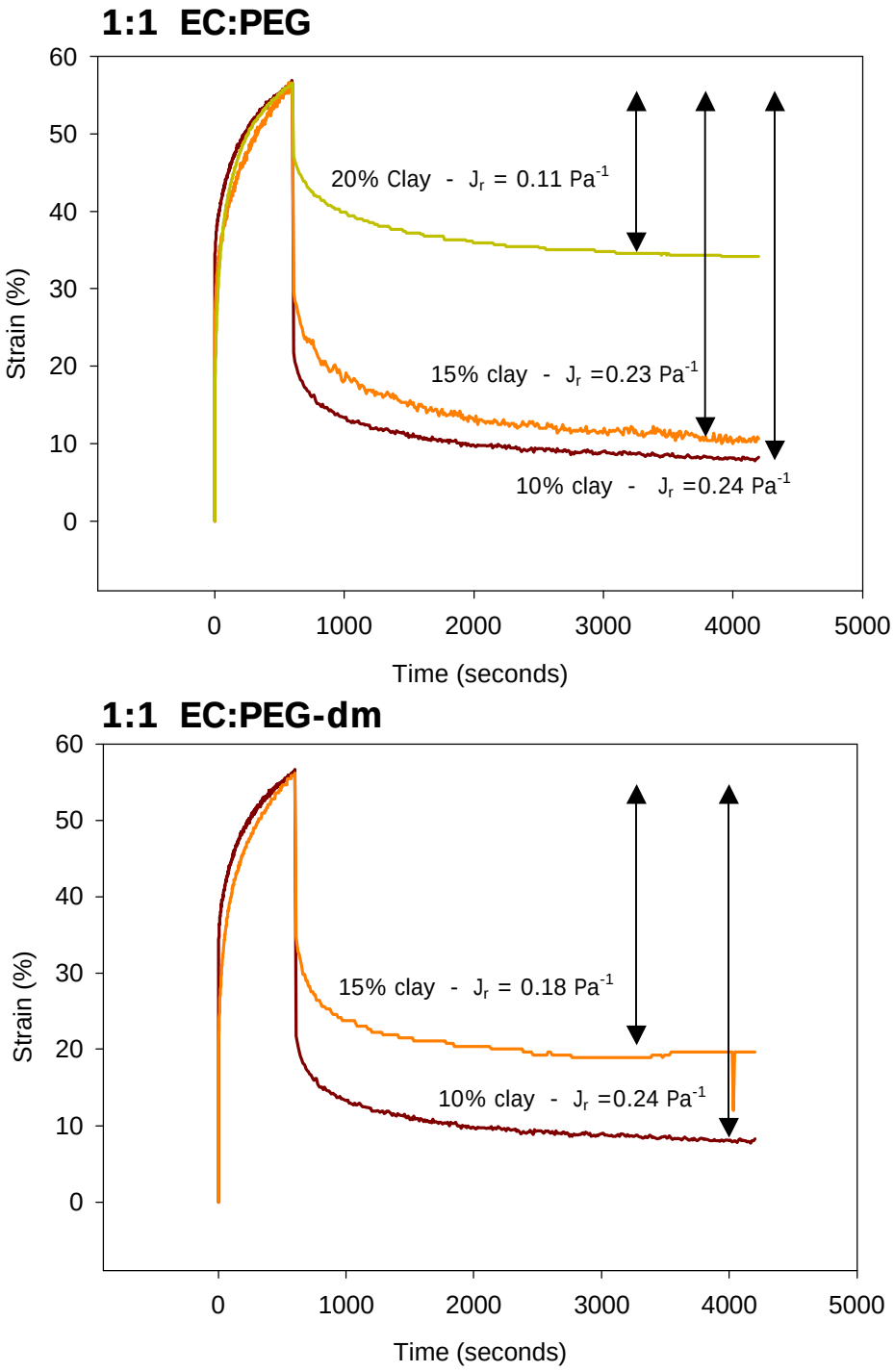

Figure 4. 9. Creep measurements for 1:1 EC:PEG and 1:1 EC:PEG-dm at various loadings of clay. Curves have been normalized to show comparative relaxation extent. The vertical arrows represent the recoverable creep compliance J_r for each sample.

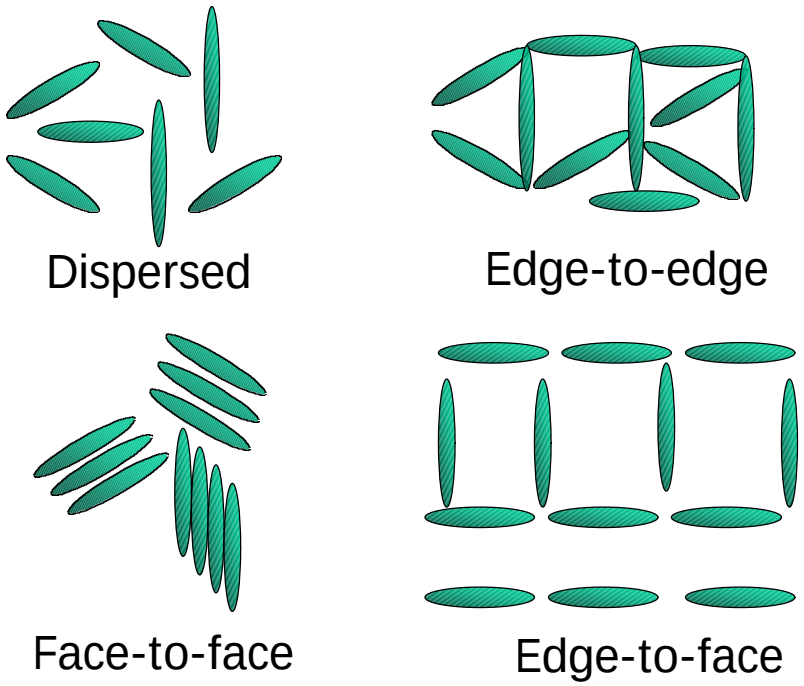

Figure 4. 10. Various clay platelet associations: dispersed, face-to-face, edge-to-face, and edge-to-edge[17].

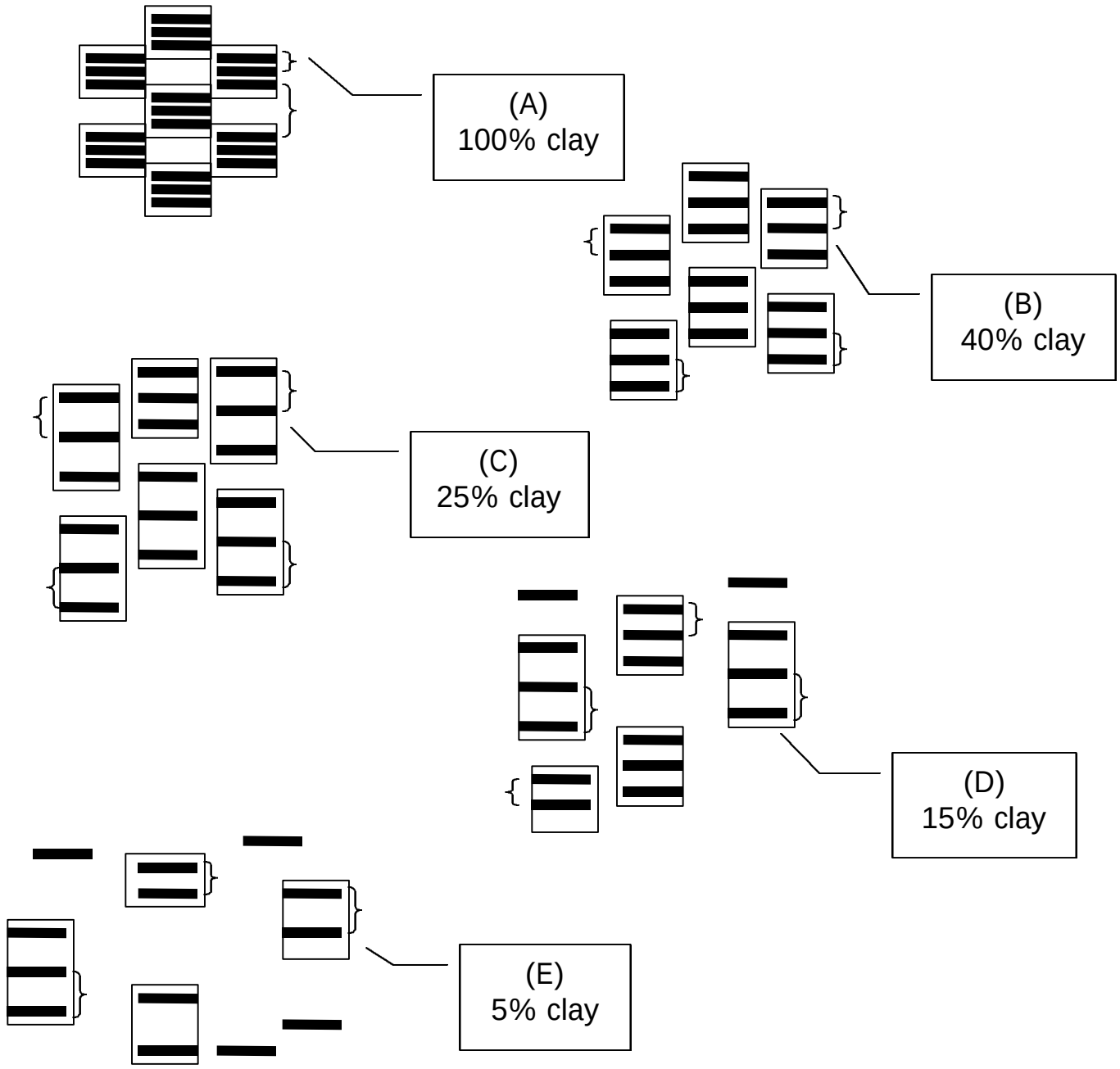

Figure 4. 11. Schematic of clay platelet aggregation. The horizontal bars represent clay platelets. The boxes around platelets represent a collection of platelets that act as a group. Brackets signify examples of spacing that can be detected by XRD. As the clay percentage decreases, A) 100% B) 40%, C) 25%, D) 15%, and E) 5%, and exfoliation increases, the variety of spacing become more apparent, leading to a broader XRD peak (Figure 4.4).

Chapter 5: Conclusions and Recommendations

5.1 Conclusions

5.1.1 Experimental

Adaptations were made from procedures used by Riley et al.[1] to make hectorite based electrolyte gels. Our goal was to minimize the introduction of water to the gels, by using ethanol as a dispersing agent. Ethanol is more volatile than water, which was important during the solvent removal drying process. We also focused on uniform dispersion of clay in the solvent by using a high-shear mixer for all samples as opposed to mixing by hand with a spatula. By using a high-shear mixer, we were able to prepare more consistent samples. We prepared all samples individually to the specifications that we desired instead of making a concentrated stock electrolyte, as Riley had. The purpose of this procedural change was to avoid mixing in the glove-box, which is a confined environment. With samples already made to the correct amount of hectorite and solvent, the only mixing needed in the glove-box was carbonate replacement after drying. This new procedure helped us to study more concentrations of clay at four different solvent ratios: 1:1 EC:PEG-dm, 2:1 EC:PEG-dm, EC, and 1:1 EC:PEG. We also had enough time to make and test two batches of each sample. Although there was a learning curve in creating our samples, the results displayed uniformity. One batch provided enough material for several conductivity, XRD, and rheology runs to be conducted.

5.1.2 Conductivity, XRD and Rheology Results

Low-molecular weight (250 MW) PEG-dm addition to Li-hectorite/EC electrolyte composites had a positive effect on lithium-ion conductivity. We also found an optimum clay concentration and polymer composition, which gave peak conductivity results. Clay concentration had a dominating effect on all results when compared to solvent composition. Conductivity increased by an order of magnitude over the span of clay concentrations we tested (5 – 40% clay), and the elastic modulus increased by two orders of magnitude over the same clay percent range. At 25% hectorite concentration, both conductivity and basal spacing peaked for all solvent mixtures. This was the most significant result in this research, because it confirmed that clay aggregation has a negative effect on the conductivity of ions. At 40% clay, conductivity and basal spacing decreased even though lithium ion concentration increased, signifying the onset of clay particle aggregation.

Addition of PEG-dm to the base EC electrolyte shows moderate improvement in conductivity. Solvent mixtures 1:1 EC:PEG-dm, 1:1 EC:PC, and EC did not show as high conductivity as 2:1 EC:PEG-dm electrolytes, indicating that a small amount of polymer slightly affects the clay platelets to improve conductivity. 1:1 EC:PC and EC solvents had higher dielectric constants, yet showed lower conductivity when compared to 2:1 EC:PEG-dm. This result implied that Li-ion conductivity not only depends on the dielectric constant of the solvent, but overall electrostatic interactions between clay platelets, and dipole interactions between PEG-dm, EC, and the clay surface.

We find all samples to exhibit gel-like behavior with room temperature. The elastic modulus increases with clay concentration and asymptotes to a constant value of

2.0×10^5 Pa. A comparison of elastic modulus, yield stresses, and creep compliance were made for 1:1 EC:PEG-dm and 1:1 EC:PEG electrolytes at different loadings of clay. We found PEG-dm electrolytes to have a stronger gel network, higher G and yield stress, however the PEG samples were more processable and dispersed the clay platelets better. The relaxation properties did not change based on polymer type, however at 10% clay, the recoverable creep compliance was the highest for both PEG-dm and PEG. It is predicted that at higher concentrations of clay, a more complex network of clay platelets is formed that does not recover after stress is applied.

5.2 Recommendations

Hectorite-based electrolytes with low molecular weight polymers (oligomers) have beneficial characteristics, such as high elastic modulus and high basal spacing between platelets. These positive characteristics in addition to improved conductivity when compared to clay electrolytes without oligomers indicate a potential for clay electrolytes in future battery technologies.

5.2.1 Polymer concentration and molecular weight

In this research, we focused on two volume ratios of PEG-dm (250 MW) to EC, one with equal parts (1:1) and one with more EC (2:1). Our results showed a slightly higher conductivity when the polymer amount was less than EC, however we only investigated one ratio where this was true. A future recommendation would be to look at conductivity results for amounts of PEG-dm in between the amounts studied in this research (i.e 3:1 EC:PEG-dm, 5:1 EC:PEG-dm,...). In the same regard, it could be useful

to look at hectorite concentrations between 25% and 40% in order to find a clear maximum conductivity.

The low molecular weight (250 MW) PEG-dm used in this study may have been too low, or the chains were too small, to intercalate between hectorite platelets. It would be beneficial to investigate the interaction of higher molecular weight PEO complexes with hectorite platelets in order to see if the more bulky polymer chains increase the separation of clay layers. Conductivity could be negatively affected by the addition of the low dielectric constant high molecular weight polymer.

5.2.2 Surface initiated polymerization

Surface initiated polymerization (SIP) onto various substrates is an increasing area of research. This novel technology when applied to clay surfaces would be beneficial for permanently separating the clay platelets using anchored polymers chains. However, to induce polymerization, often times the original surface must be modified with self assembled monolayers (SAM), which are more compatible to the SIP initiators. The characteristics of the SIPs and SAMs such as chemical composition, chain orientation, film thickness, and coverage have been measured by Bierbaum et al. and Applelhans et al.[2,3] using many different methods: X-Ray photoelectron spectroscopy (XPS), atomic force microscopy (AFM), ellipsometry, FTIR, contact angle measurements, X-Ray grazing incidence diffraction, and near edge X-ray absorption fine structure (NEXAFS). Important findings have been made by Bierbaum et al. and Applelhans et al. regarding the unique formation of SAM's on the substrate (e.g., island growth of compounds into uniform layers). Appelhans et al. focused on silicon wafers (100) as substrates and thiophene based n-alkyl-trichlorosilane as the surface active

group. Although a clay platelet is inherently different from a silicon wafer, some of the same chemical properties can be used for successful SIP. The hydroxyl group that is present on a clay platelet could react with silane additives that are modified with monomer nucleation sites.

Porter et al.[4] have shown spontaneous surface polymerization on hectorite and montmorillonite using aniline vapors. Using scanning force microscopy (SFM), they studied in-situ nucleation and polymerization on the Cu-exchanged clay surface. They noticed a difference in polymerization between Na-hectorite and Cu-hectorite: Cu-hectorite was found to aid initial reactions of aniline within the micropores of the outermost clay surface.

5.2.3 Hectorite platelet modifications

Varieties of homoionic cations for smectites have been investigated (M^{n+}: Li^+, Na^+, K^+, NH_4^+, Ca^{2+}, Ba^{2+}, Al^{3+}, Cr^{3+}, $CH_3CH_2CH_2NH_3^+$)[5]. Bulky organic cations, such as alkyl ammonium ions and dimethyl-dioctadecyl ammonium ions, on clay platelets make the clay "organophilic", or attracted to polymers. These organically modified clays have been used for clays in polymeric materials in order to improve viscoelastic properties. Highly anisotropic organically modified layered silicates have been shown to orient when shear is applied[6]. This concept could be useful for electrolyte systems in order to create channels for lithium-ion movement. It would be interesting to align the platelets perpendicular to the electrodes and then measure lithium-ion transference number.

In order to enhance hectorite dispersion, ethylenediamine could be uses as an intercalation agent between clay platelets[7]. Ethylenediamine has primarily been used as a

precursor to metal pillaring. However, electronically conductive metals would destroy the battery. Basal spacing, as measured by XRD (X-Ray diffraction), and compositional changes, as measured by TGA (Thermogravimetric analysis) and FTIR (Fourier transform infrared), help characterize amine intercalation. From XRD studies, the basal spacing (d_{001}) between Laponite (synthetic hectorite) clay platelets increased 25-35% from 1 nm, which is found in standard hectorite clay[7]. This larger spacing confirms the adsorption of ethylenediamine. A similar spacing increase was seen in this research with the addition of polymer. However, polymer intercalation was not verified and the spacing was believed to be affected more by clay concentration. With amine intercalation, the amorphous layered clay structure would become a microporous material useable in many applications[8]. Highly porous amine intercalated structures could also have advantages for a battery electrolyte system by providing the needed channels to improve ion transport.

5.2.4 NMR PGSE Studies

Preliminary NMR measurements were taken on hectorite samples, however due to the high viscosity of the sample, the data was unclear. Future studies, on an instrument that can conduct PGSE on high viscosity material should be investigated. From NMR measurements, diffusion coefficient of lithium within hectorite electrolytes can be found. The molecular diffusion coefficient of lithium-ion in an electrolyte expresses the freedom of lithium to move. The self-diffusion coefficient of lithium ion can be found in two different manners, first steady state current analysis and second by pulse gradient NMR spectroscopy. Spin echo experiments developed from the desire to find the true spin-spin relaxation time T_2. A pulse sequence is needed in order to achieve spin echo. One

interesting point of focus is following the 90° pulse and during the off-period of magnetic field $\mathbf{B_1}$. Here, inhomogeneities are created from the dephasing of the individual moments in the magnetic vector **M**. There are fast and slow nuclei precessing in the *y* direction after the 90° pulse causing fanning. Finally, after the 180° pulse, and during a length of time τ, all inhomogeneities collapse and the vector **M** slowly regenerates onto the y-axis. This regeneration is called "spin echo"[9]. Hahn[10] talks about the approach to utilizing the topic of nuclear precession or "spin echoes" by observing the motion of systems under the influence of magnetic fields. He shows the effect of diffusion when spin echoes are in the presence of pulse field gradients, but does not develop techniques for calculating the self-diffusion coefficients. He does however, explain the nuclear induction effect from echo experiments.

5.3 References

1. M. Riley, P. Fedkiw, and S. Khan, "Transport Properties of Lithium Hectorite-Based Composite Electrolytes", *Journal of Electrochemical Society*, (2001).

2. K. Bierbaum, M. Kinzler, C. Woll, M. Grunze, G. Hahner, S. Heid, and F. Effenberger, "A near-Edge X-Ray-Absorption Fine Structure Spectroscopy and X- Ray Photoelectron-Spectroscopy Study of the Film Properties of Self-Assembled Monolayers of Organosilanes on Oxidized Si(100)", *Langmuir*, **11**, 512-518 (1995).

3. D. Appelhans, D. Ferse, H. J. P. Adler, W. Plieth, A. Fikus, K. Grundke, F. J. Schmitt, T. Bayer, and B. Adolphi, "Self-assembled monolayers prepared from omega-thiophene- functionalized n-alkyltrichlorosilane on silicon substrates", *Colloids and Surfaces a-Physicochemical and Engineering Aspects*, **161**, 203-212 (2000).

4. T. L. Porter, M. P. Eastman, D. Y. Zhang, and M. E. Hagerman, "Surface Polymerization of Organic Monomers on Cu(II)-Exchanged Hectorite", *Journal of Physical Chemistry, B*, **101**, 11106-11111 (1997).

5. P. Aranda and E. Ruizhitzky, "Poly(Ethylene Oxide)-Silicate Intercalation Materials", *Chemistry of Materials*, **4**, 1395-1403 (1992).

6. R. Krishnamoorti, J. Ren, and A. S. Silva, "Shear response of layered silicate nanocompostites", *Journal of Chemical Physics*, **114**, 4968-4973 (2000).

7. P. Cool and E. F. Vansant, "Preparation and characterization of zirconium pillared laponite and hectorite", *Microporous Materials*, **6**, 27-36 (1996).

8. N. Maes, I. Heylen, P. Cool, and E. F. Vansant, "The relation between the synthesis of pillared clays and their resulting porosity", *Applied Clay Science*, **12**, 43-60 (1997).

9. R. S. Macomber *A Complete Introduction to Modern NMR Spectroscopy*; Wiley-Interscience Publication: New York, 1998.

10. E. L. Hahn, "Free Nuclear Induction", *Physics Today*, **6**, 4 (1953).

Appendix A: Additional Mixing Techniques

Throughout making of samples, I had help from a very special and smart high school student, Andrew Seltzman. He began work with me in July and continued until the end of December 2002. Andrew and I worked diligently on establishing a procedure for making hectorite electrolytes in an easy and repeatable manner. Chapter 3 has the overall experimental procedure, however Andrew and I implemented additional techniques in making our samples. These subtle techniques not described in Chapter 3 are covered in the bullet points below, as are other important points Andrew noticed during sample making.

- Lithium Chloride is hygroscopic, after it is exposed to the atmosphere it tends to start to get sticky. Try to minimize the time the reagent container is open.

- Adding the Sodium Hectorite to the blender too fast will cause it to blow around.

- Using diluted remains from the blender after the ion exchange can be used to balance the centrifuge bottles.

- After centrifuging the vials and draining out the water use a wide flat spatula to scrape out the Li-Hectorite. Then use DI water to wash out the excess Li-Hectorite.

- Seal the funnel tightly to the vacuum flask when filtering the Li-Hectorite with methanol.

- When weighing the Li-Hectorite hold the container at an angle and tap gently on the side of the container so that the Li-Hectorite is added in small increments.

- When mixing high concentrations of Li-Hectorite / electrolyte mixtures hold the beaker above the hotplate while it mixes for about 30 sec. This is done so the Li-Hectorite does not stick to the bottom and keep the ethanol from boiling.

- As the mixer is run and the Li-Hectorite is broken up, the viscosity decreases and the mixing speed will increase

- The mixer head should have a bronze bushing, not a Teflon one. Use of a Teflon bushing will cause the mixture to darken.

- If the mixer head is washed between cycles it should then be rinsed in acetone and sufficiently dried. Water in the mixture will cause the mixture to darken.

- Running the mixer head in ethanol also clean the head well.

- When the rest of the ethanol is removed by drying in the vacuum oven some of the EC will evaporate as well this should be replaced by dry EC in the glove box.

- When adding EC to the electrolyte in the glove box, the higher concentration electrolytes should be heated so they can be mixed properly.

- When adding the electrolytes to conductivity vials the higher concentration electrolytes should be heated so air bubbles in the electrolyte can be minimized.

Appendix B: Supplemental Data of Na-hectorite Studies

Great care was taken in making electrolytes for conductivity measurements with low moisture. Because a large amount of sample is needed for rheology measurements, we decided to use easier made Na-hectorite electrolytes instead of Li-hectorite electrolytes used for conductivity measurements. Na-hectorite electrolytes were made outside of the glove box in order to save time and use of precious Li-hectorite.

Initial rheological comparisons between sodium hectorite samples and lithium hectorite samples were made. Elastic modulus for Na-hectorite and Li-hectorite (15% clay) in 1:1 EC:PEG-dm is shown in Figure B.1. The data shows error within the allowed 15%, although Li-hectorite has a little higher G . We also compared the yield stress for two different concentrations of clay (5% and 10%) in 2:1 EC:PEG-dm and 1:1 EC:PEG-dm (Figure B.2).

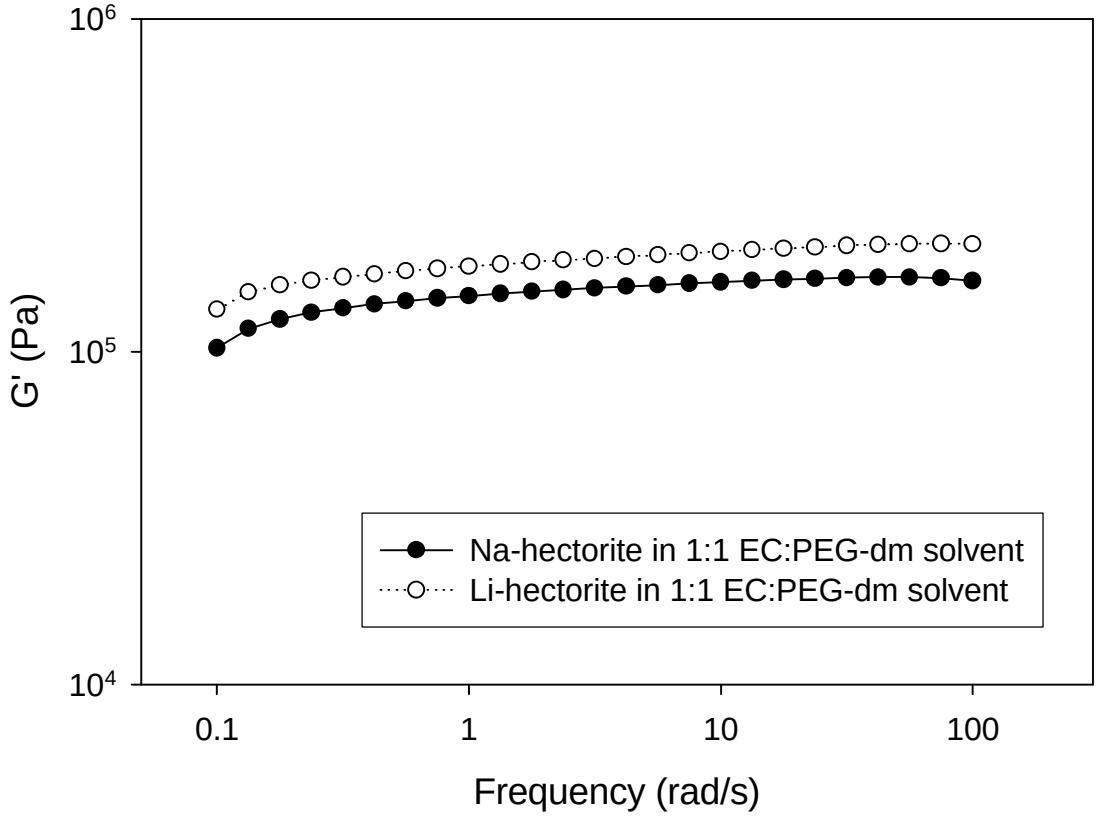

Figure B. 1. Elastic modulus, G′, comparison of Na-hectorite and Li-hectorite (15% clay) in 1:1 EC:PEG-dm solvent.

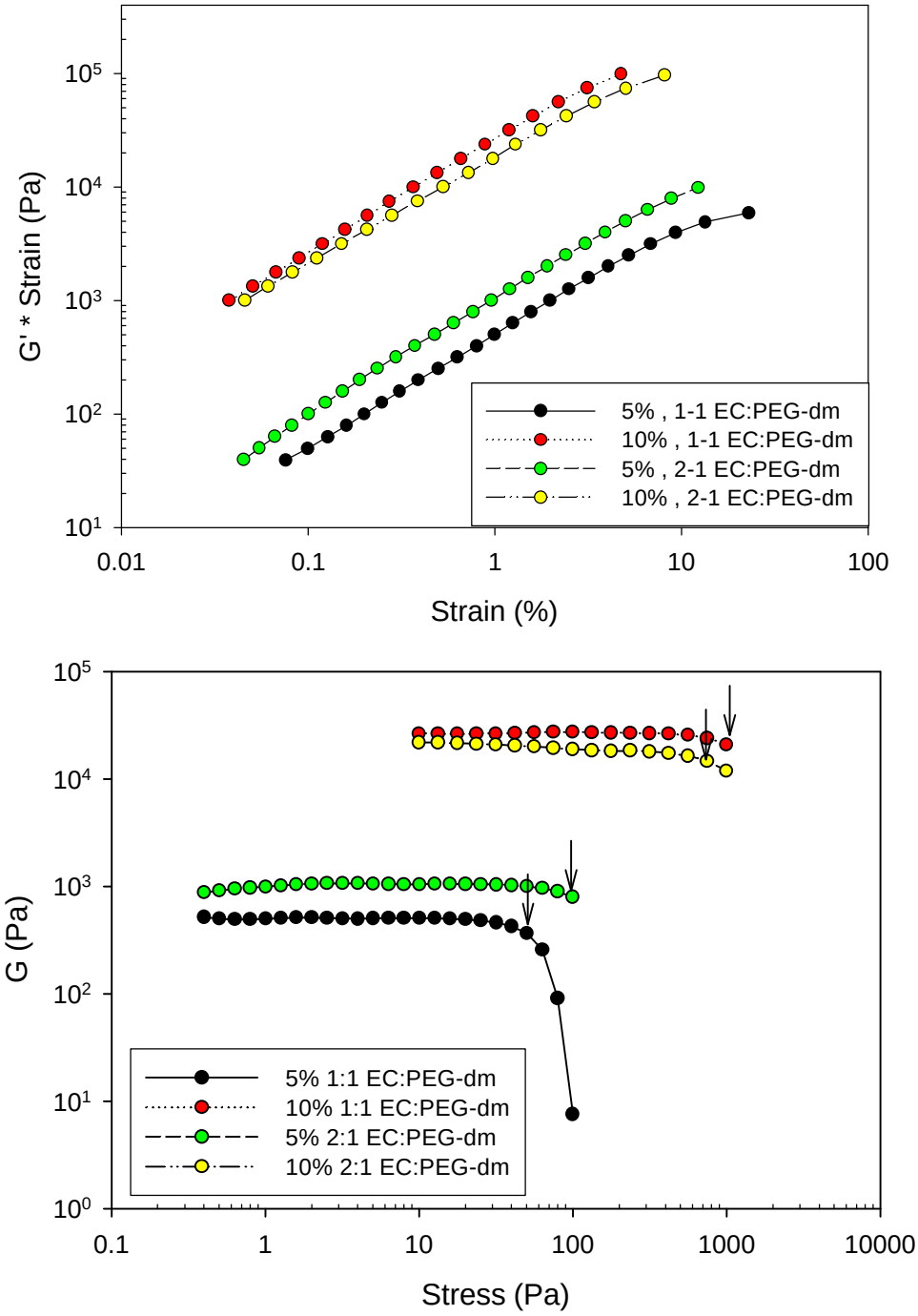

Figure B. 2. Yield stress was estimated from the approximate maximum of G″ x Strain as a function of strain (top) and as the estimated point shown with an arrow on the graph of G′ as function of stress (bottom).

Appendix C: Polymer Coverage Estimate

Studies of PEG-dm 250 MW with fumed silica[6,22,23] have discussed possible interactions between the silica surface and the solvent. Those interactions are due to surface groups on the silica particle. Hydroxyl groups are naturally abundant on the hectorite platelet and hydrogen bonding is a viable interaction between hectorite and PEG-dm. We believe van der Waals attraction forces between the clay surface and PEG-dm molecules aid in stabilizing the clay dispersion. An estimate of area occupied by PEG-dm per area clay platelet was calculated using the polymer radius of gyration of PEG-dm (12 Å) quoted by Walls[24] and the known average platelet diameter of hectorite (250 nm, surface area (SA) = 9.8×10^6 Å^2). The polymer molecule consumes a spherical volume of space due to gyrations. The radius of gyration corresponds to the radius of the sphere, which would project a circular surface area onto a platelet surface (SA = 452 Å^2). For maximum coverage of the platelet, polymer "spheres" were presumed to coat the clay surface in an edge-to-edge fashion, and gaps between projected areas on the clay surface are disregarded. A ratio of estimated total polymer projected area to total platelet area was developed using the calculation below.

y = molecules PEG-dm for Sample A
x = # of platelets for Sample A
$SA_{PEG\text{-}dm}$ = surface area of polymer sphere projection
SA_{clay} = surface area of clay platelet

$$\frac{y \times SA_{PEG\text{-}dm}}{x \times SA_{clay}} = \text{Polymer coverage} \left(\frac{\text{area (polymer)}}{\text{area (platelet)}} \right)$$

Ratios of polymer coverage around the clay platelet for different clay loadings are shown in Table 4.3. At low hectorite concentration, the polymer coverage is greater than at higher concentrations as expected. However, at such low amounts of clay, most of the polymer is in the bulk solution. The ratio of polymer coverage area to hectorite surface area is 44 for the 25% clay in the 2:1 EC:PEG-dm solvent mixture. In the 1:1 EC:PEG-dm electrolyte, twice as much polymer is present, which doubles the possible coverage of clay; however, the conductivity data does not indicate an improvement with this amount of polymer. It would be interesting to find an optimum polymer concentration, which provided the best conductivity, however it was beyond the scope of current investigation.

Table C.1. Ratio of PEG-dm area coverage to total platelet surface area for various amounts of clay in 1:1 EC:PEG-dm and 2:1 EC:PEG-dm solvent mixtures

Hectorite %	1:1 EC:PEG-dm	2:1 EC:PEG-dm
5	428	219
10	214	109
15	143	73
20	107	55
25	85	44
30	71	37
40	56	27

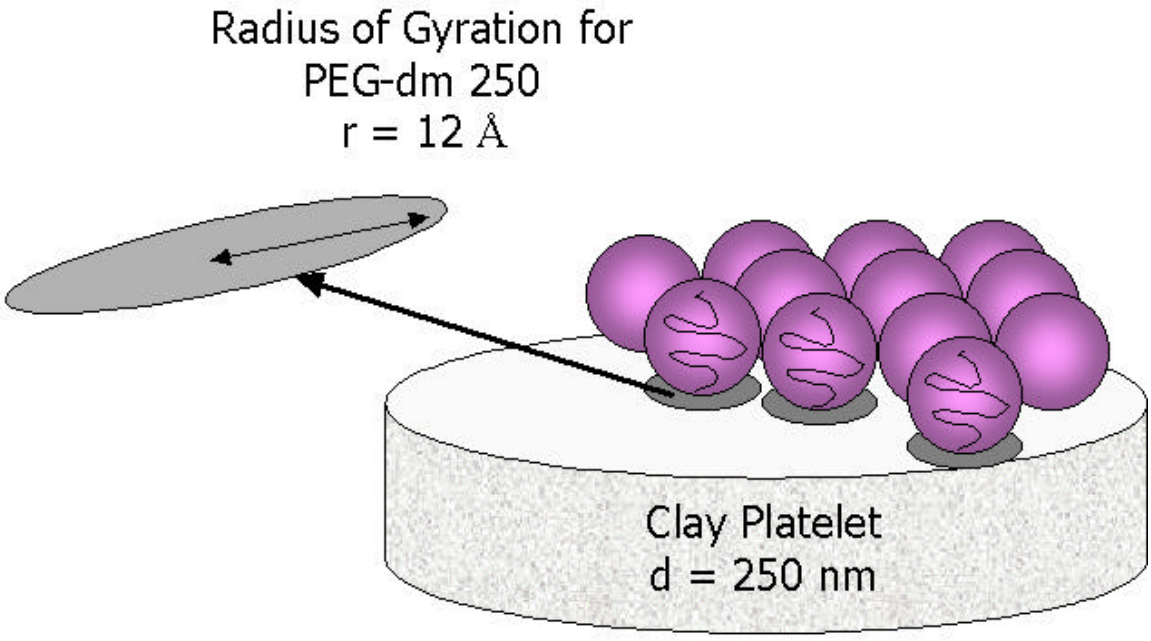

Figure C.1. Schematic of PEG-dm "spheres" on a clay platelet, and the circular projection onto the surface.